UNIVERSIDAD DE EXTREMADURA

TESIS DOCTORAL

Efecto del Recubrimientos en el Comportamiento Mecánico y la Bioactividad de Andamiajes Biocerámicos Fabricados mediante Moldeo Robotizado

Azadeh Motealleh

Departamento de Ingeniería Mecánica, Energética y de los Materiales

Conformidad de los Directores

Fdo: Pedro Miranda González

Fdo: Antonia Pajares Vicente

2015

GRUPO ESPECIALIZADO DE MATERIALES

UNIVERSIDAD DE EXTREMADURA

Este trabajo se enmarca en el contexto de la línea de investigación ***desarrollo de materiales para aplicaciones biomédicas*** desarrollada en el Grupo Especializado de Cerámicos de la Universidad de Extremadura

Dª. Antonia Pajares Vicente, Catedrática de Universidad y **D. Pedro Miranda González**, Profesor Titular de Universidad, pertenecientes al Área de Ciencia de los Materiales e Ingeniería Metalúrgica del Departamento de Ingeniería Mecánica, Energética y de los Materiales de la Universidad de Extremadura

INFORMAN

que la presente memoria **"Efecto del Recubrimientos en el Comportamiento Mecánico y la Bioactividad de Andamiajes Biocerámicos Fabricados mediante Moldeo Robotizado"** ha sido realizada por **Dª. Azadeh Motealleh** en los laboratorios del área de Ciencia de los Materiales e Ingeniería Metalúrgica (Universidad de Extremadura), bajo nuestra dirección.

Y para que conste, en cumplimiento de la legislación vigente, firmamos el presente,

en Badajoz a 9 de octubre de 2015.

Fdo: F. Antonia Pajares Vicente

Fdo: Pedro Miranda González.

TRIBUNAL

Dr. Fernando Guiberteau Cabanillas
Catedrático de Universidad
Departamento de Ingeniería Mecánica,
Energética y de los Materiales
Universidad de Extremadura

Dr. Garrett McGuinness
Lecturer
Mechanical and Manufacturing
Engineering
Dublin City University

Dra. Begoña Ferrari Fernández
Científico Titular
Instituto de Cerámica y Vidrio
Consejo Superior de Investigaciones
Científicas

Dr. Tassilo Moritz
Research group Leader
Departament of Processes/Components
Fraunhofer IKTS

Dr. Ángel Luis Ortiz Seco
Titular de Universidad
Departamento de Ingeniería Mecánica,
Energética y de los Materiales
Universidad de Extremadura

Dedications

To my family
with my warmest affection for their greatest influence on my life

Acknowledgments

I take the opportunity to acknowledge my supervisors Dr. Pedro Miranda González and Dr[a]. Antonia Pajares Vicente for their invaluable guidance and support throughout my PhD experience here in the University of Extremadura.

I also owe much gratitude to my husband, Siamak, for his unwavering love and support in every moment that we have spent together.

A special thanks to Dr. Fidel Hugo Perera for his patience to assist me with this project.

I would also like to acknowledge and thank all the members of our laboratory for their friendship and assistance during my career in Badajoz.

Table of Contents

List of Figures

List of Tables

Summary & Motivation

Bone is one of the most frequently transplanted tissues, and the demand is steeply rising due to the rapidly upward trend of worldwide incidence of bone lesions especially in populations where aging is coupled with increased obesity and poor physical activity. Bone grafts are utilized in a wide array of clinical settings to enhance bone repair and regeneration through osteogenesis, osteoinduction, and osteoconduction. The materials used in bone grafting can be divided into several major categories, including autografts, allografts, and xenografts. Each of these options has its own advantages and disadvantages. Autografts serve as the gold standard in reconstructing small bone defects and possess strong osteoinductive, osteoconductive and osteogenic characteristics. However, autografts are a piece of bone which is transferred from one body site to another of the same patient and thus, requires a second operation and also causes a defect in an otherwise healthy part of the body. Allografts and xenografts are alternative optional treatments which involve transplanting donor bone tissue from another human or an animal. These donor bone grafts have osteoinductive and osteoconductive characteristics but lack the osteogenic properties of autografts. Moreover, using bone obtained from a donor also has side effects, such as immunogenic reactions and disease transmission risks.[1,2]

New methods are thus needed to overcome these problems and meet the growing demand. The field of bone tissue engineering (BTE) was emerged nearly three decades ago as a convenient alternative to promote the regenerative ability of the host body. One of the most important stages of BTE is the design and processing of a porous, biodegradable three-dimensional structure called ‘scaffold’, exhibiting high porosity, high pore interconnectivity and uniform pore distribution, and providing the mechanical support during repair and regeneration of damaged or diseased bone. 3D bone scaffolds can be fabricated from bioceramics, bioactive glasses, biodegradable polymers and their composites.[2–4]

Bioactive glasses are attracting increasing attention for their use as bone tissue engineering due to their high bioactivity.[5,6] Among them, 45S5 bioglass (45 % SiO_2, 24.5 % CaO, 24.5 % Na_2O, 6 % P_2O_5) is probably the most thoroughly studied and most widely used as bone graft substitute in clinical applications,[7,8] being highly bioactive and both osteoinductive and osteoconductive.[9,10]

However, the main disadvantage of bioglass based scaffolds is their high brittleness and, thus, low resistance to crack propagation, which makes most of these scaffolds unsuitable for load-bearing applications. In conventional techniques for manufacturing these bioglass scaffolds such as foam replication, sol–gel processing, thermal bonding of particles or fibers, solvent casting, gas foaming, freeze drying, etc., controlling the pore size, geometry, and spatial distribution is not precisely achievable, which leads to producing scaffolds with very high porosities and consequently very low mechanical properties.[11] More recently, additive manufacturing technologies, such as direct ink writing,[12,13] have been developed, which have led to stronger scaffolds than those fabricated by conventional techniques. Nonetheless, despite the improvement provided by these additive manufacturing technologies, bioglass scaffolds remain too brittle for their application in load bearing regions of the skeleton.

Consequently, the primary objective of this work is to develop novel biomaterials based on 45S5 bioglass scaffolds in combination with synthetic or natural polymers to overcome these obstacles. The specific tasks carried out to achieve this objective include:

The specific tasks carried out to fulfill the above aims include:

(1) Fabrication and characterization of 45S5 bioglass scaffolds by robocasting technique a direct ink writing method which provides a much greater level of control over pore architecture and more regular strut morphologies than conventional techniques. Developing an ink appropriate for robocasting requires careful tailoring of the viscoelastic properties of highly concentrated colloidal suspension through precise control of its composition. In this study, a new and simple formulation has been used for the preparation of the concentrated suspensions required by robocasting from 45S5 powders.

(2) Improving the intrinsic properties of the 45S5 bioglass struts. Since rod microporosity reduces the intrinsic strength of the rods—the micropores act as starting flaws for cracking—dense, defect free struts are desirable. In this study, the microstructure of the rods has been tailored by controlling the sintering parameters. The role of in-rod microporosity on the mechanical performance of the scaffold has been investigated and optimal processing conditions have been determined.

(3) Reinforcement of 45S5 bioglass scaffolds by polymer coatings. Different kind of synthetic polymers such as PCL and PLA, and natural polymers including chitosan, alginate and gelatin have been applied on 45S5 scaffolds by dip coating process in order to improve their strength and toughness. Apart from polymer composition, the effect of other parameters, such as in-rod microporosity, solvent type, solution temperature and polymer concentration, on the mechanical behavior of the developed polymer/bioglass composite scaffolds have been evaluated under compression and, in selected cases, under bending stresses.

(4) Determination of the *in vitro* biodegradability and bioactivity behavior of selected bare and coated scaffolds in SBF. Microstructure evolution and mechanical properties evolution after incubation in SBF have been evaluated, as expected in a study devoted to the development of novel biomaterials.

This manuscript has been organized as follows:

- Chapter 1 provides a brief literature review of biomaterials science and engineering for bone repair. First, a concise description of bone structure and its properties is presented. Next, the main bone regeneration therapies, including conventional clinical treatments with bone grafts and developing alternative treatments with scaffolds, are explored. Subsequently, the requirements for the fabrication of bone scaffolds, the appropriate biomaterials, and the main conventional and additive manufacturing technologies used for this purpose are briefly reviewed. Especial attention is given to robocasting as the fabrication method selected for this study. And finally, polymer infiltration is proposed as an alternative to improve mechanical performance of bioceramic and bioglass scaffolds for bone regeneration, and a summary of exiting literature in this field is provided.

- Chapter 2 describes the materials, experimental procedures and analytical techniques used in this study. First, the materials and processes used for the fabrication of porous 45S5 bioglass-derived robocast structures and their infiltration with different synthetic (PCL and PLA) and natural (chitosan, alginate and gelatin) biodegradable polymers are described. Then, the microstructural and mechanical characterization and *in vitro* testing procedures used in this work are detailed.

- The experimental results obtained in this study are presented and discussed in Chapter 3. This chapter is divided into four sections. First, the results corresponding to the optimization of the robocasting inks and subsequent sintering step used for the fabrication of 45S5 bioglass scaffolds, as well as the microstructural and mechanical characterization of the bare scaffolds are presented and analyzed. Second, the mechanical properties of 45S5 scaffolds coated with synthetic and natural polymers focused on PCL, PLA, chitosan, alginate and gelatin by a dip-coating process are discussed in detail: the effect of various processing parameters on the mechanical properties of the coated scaffolds are analyzed. Third, the results of the *in vitro* characterization performed on bare and coated scaffolds are presented; the bioactivity and biodegradation behavior, and subsequent mechanical evolution are discussed in detail. Finally, a comparison of the mechanical properties of the novel biomaterials developed in this work and natural bone is performed and some implications of this study are discussed.

- The manuscript ends with a brief summary of the main conclusions derived from this study, presented as chapter 4.

Resumen y Motivación

El hueso es uno de los tejidos más frecuentemente trasplantado, y la demanda está aumentando considerablemente debido a que la incidencia mundial de las lesiones óseas está experimentando una tendencia creciente, especialmente en poblaciones donde al envejecimiento se une el aumento de la obesidad y la pobre actividad física. Los injertos óseos se utilizan en una amplia gama de entornos clínicos para mejorar la reparación ósea y la regeneración a través de la osteogénesis, osteoinducción y osteoconducción. Los injertos óseos se pueden dividir en varias categorías: autoinjertos, aloinjertos y xenoinjertos. Cada una de estas opciones tiene sus propias ventajas e inconvenientes. Los autoinjertos son la elección preferida en la reconstrucción de defectos óseos pequeños y poseen buenas propiedades osteoinductivas, osteoconductivas y osteogénicas. Sin embargo, los autoinjertos son un trozo de hueso que se transfiere de una parte a otra del cuerpo del mismo paciente y, por tanto, requieren de una segunda intervención quirúrgica, además, de causar un defecto en una parte sana del cuerpo. Los aloinjertos y xenoinjertos son tratamientos alternativos que implican el trasplante de tejido óseo de otro ser humano o de un animal. Estos injertos óseos tienen características osteoinductivas y osteoconductivas adecuadas, pero carecen de las propiedades osteogénicas de los autoinjertos. Por otra parte, el uso de hueso obtenido a partir de un donante tiene efectos secundarios, tales como reacciones inmunológicas y transmisión de enfermedades.[1,2]

Para superar estos problemas y satisfacer la creciente demanda de tejido óseo se han desarrollado soluciones alternativas. En este sentido, la ingeniería de tejido óseo surgió hace casi tres décadas como una alternativa para promover la capacidad regenerativa del cuerpo del anfitrión. Una de las etapas más importantes de la ingeniería de tejido óseo es el diseño y fabricación de una estructura tridimensional porosa biodegradable llamada "andamiaje", con alta porosidad, alta interconectividad de los poros, distribución de poros uniforme y que sea capaz de proporcionar el soporte mecánico necesario durante la

reparación y la regeneración del hueso dañado. Estos andamiajes 3D pueden ser fabricados a partir de materiales biocerámicos, vidrios bioactivos, polímeros biodegradables y sus compuestos.[2–4]

Los vidrios bioactivos están atrayendo cada vez más atención para su uso en ingeniería de tejido óseo debido a su alta bioactividad.[5,6] Entre ellos, el biovidrio 45S5 (45 % SiO_2, 24.5 % CaO, 24.5 % Na_2O, 6 % P_2O_5) es probablemente el más estudiado y utilizado como sustituto óseo en aplicaciones clínicas,[7,8] ya que es muy bioactivo y tanto osteoinductivo como osteoconductivo.[9,10]

Sin embargo, la principal desventaja de los andamiajes de biovidrio 45S5 es su alta fragilidad y, por lo tanto, baja resistencia a la propagación de grietas, lo que hace que la mayoría de estos andamiajes sean inadecuados para aplicaciones en las que tengan que soportar carga. En las técnicas convencionales para la fabricación de andamiajes de biovidrio 45S5 (solvent casting en combinación con filtrado de partículas, mallado fibrilar, espumado por gas, moldeado fundido, secado por congelación, separación de fases o tecnología supercrítica de fluidos, etc.) es difícil controlar de forma precisa la geometría, tamaño y distribución espacial de los poros. Por ello, para crear canales internos que permitan la vascularización, los andamiajes fabricados mediante técnicas convencionales presentan porosidades muy altas y, en consecuencia, pobres propiedades mecánicas.[11] Recientemente, se han desarrollado tecnologías de fabricación aditiva, como la impresión directa,[12,13] que han permitido fabricar andamiajes con propiedades mecánicas mejoradas. Sin embargo, a pesar de la mejora proporcionada por estas tecnologías de fabricación aditiva, los andamiajes de biovidrio siguen siendo demasiado frágiles para ser utilizados en las regiones del esqueleto sometidas a carga.

En consecuencia, el objetivo principal de este trabajo es el desarrollo de nuevos biomateriales basados en andamiajes de biovidrio 45S5 en combinación con polímeros sintéticos o naturales para superar estos obstáculos. Las tareas específicas realizadas para lograr este objetivo incluyen:

(1) Fabricación y caracterización de andamiajes de biovidrio 5S5 mediante moldeo robotizado (robocasting), un método de impresión directa que proporciona un control de la arquitectura de poros mayor que las técnicas convencionales. El desarrollo de una tinta apropiada para la técnica de moldeo robotizado requiere de un cuidadoso control de las propiedades viscoelásticas de la suspensión coloidal altamente concentrada a través de un control preciso de

su composición. En este estudio, se ha utilizado una nueva formulación para la preparación a partir de polvos 45S5 de las suspensiones concentradas requeridas por la técnica de robocasting.

(2) Mejora de las propiedades intrínsecas de las barras que constituyen los andamiajes de biovidrio 45S5. Dado que la microporosidad de las barras reduce su resistencia intrínseca—los microporos actúan como defectos precursores de la fractura—se requiere que las barras estén libres de defectos. En este estudio, la microestructura de las barras ha sido modificada mediante el control de los parámetros de sinterización. Esto ha permitido estudiar el papel de la microporosidad de las barras en el comportamiento mecánico del andamiaje y determinar las condiciones óptimas de fabricación.

(3) Refuerzo mecánico de los andamiajes de biovidrio 45S5 mediante su recubrimiento con polímeros. Los andamiajes de biovidrio 45S5 se han recubierto con polímeros sintéticos (PCL y PLA) y polímeros naturales (quitosano, alginato y gelatina) mediante su inmersión en una disolución de polímero, con el fin de mejorar su resistencia y tenacidad. Se ha analizado el efecto de la composición del polímero, la microporosidad de las barras del andamiaje, el tipo de disolvente, la temperatura de la solución y la concentración de polímero en el comportamiento mecánico de los andamiajes híbridos mediante la realización de ensayos de compresión y, en casos seleccionados, de flexión.

(4) Determinación de la biodegradabilidad y bioactividad in vitro de los andamiajes de biovidrio 45S5 y de los andamiajes híbridos biovidrio 45S5/polímero. Para ello, se ha analizado la evolución de la microestructura y de las propiedades mecánicas con el tiempo de inmersión en SBF.

Esta memoria se ha estructurado en los siguientes capítulos:

- En el Capítulo 1 se realiza una breve revisión de la literatura sobre biomateriales para la reparación ósea. En primer lugar, se presenta una breve descripción del hueso y sus propiedades. A continuación, se exploran las principales terapias de regeneración ósea, incluyendo tratamientos clínicos convencionales con injertos de hueso y el desarrollo de tratamientos alternativos como los andamiajes. Posteriormente, se revisan brevemente los requisitos para

la fabricación de andamiajes para sustitución ósea, los biomateriales apropiados, y las principales tecnologías de fabricación convencionales y aditivas utilizadas para este propósito. Se presta especial atención a la técnica de moldeo robotizado ya que es el método de fabricación utilizado en este estudio. Y, por último, se propone el recubrimiento con polímero como una alternativa para mejorar la respuesta mecánica de los andamiajes.

- En el Capítulo 2 se describen los materiales, los procedimientos experimentales y las técnicas de caracterización utilizados en este estudio. En primer lugar, se describen los materiales y los procedimientos utilizados para la fabricación de las estructuras porosas de 45S5 mediante moldeo robotizado y para su infiltración con polímeros biodegradables tanto sintéticos (PCL y PLA) como naturales (quitosano, alginato y gelatina). A continuación, se detallan las técnicas de caracterización microestructural y mecánica utilizadas y los ensayos *in vitro* realizados.

- Los resultados experimentales obtenidos en este estudio se presentan y discuten en el Capítulo 3. Este capítulo se divide en cuatro secciones. En primer lugar, se incluyen y analizan los resultados correspondientes a la optimización de las tintas para moldeo robotizado y la sinterización de los andamiajes de biovidrio 45S5, así como los correspondientes a su caracterización microestructural y mecánica. En segundo lugar, se discuten con detalle las propiedades mecánicas de los andamiajes de biovidrio 45S5 recubiertos con polímeros sintéticos y naturales (PCL, PLA, quitosano, alginato y gelatina): se analiza el efecto de varios parámetros del proceso de recubrimiento sobre las propiedades mecánicas de los andamiajes recubiertos. En tercer lugar, se presentan los resultados de la caracterización *in vitro* realizada en andamiajes de biovidrio 45S5 y andamiajes híbridos biovidrio 45S5/polímero; se discuten en detalle la bioactividad y la biodegradación, y la evolución mecánica con el tiempo de inmersión en SBF. Por último, se comparan las propiedades mecánicas de los nuevos biomateriales desarrollados en este trabajo con las correspondientes al hueso natural y se incluyen algunas implicaciones de este estudio

- Finalmente, en el Capítulo 4 se resumen las conclusiones más relevantes que pueden extraerse de este estudio.

Chapter 1

Introduction

In this chapter a brief literature review of biomaterials science and engineering for bone repair is presented. Firstly, a concise description of bone structure and its properties is commented. Secondly, the main bone regeneration therapies, including conventional clinical treatments with bone grafts and developing alternative treatments with scaffolds, are explored. Then, the requirements for the fabrication of bone scaffolds, the appropriate biomaterials, and the main conventional and additive manufacturing technologies used for this purpose are briefly reviewed; especial attention is given to robocasting as the fabrication method selected for this study. And finally, polymer infiltration is proposed as an alternative to improve mechanical performance of bioceramic and bioglass scaffolds for bone regeneration, and a summary of exiting literature in this field is provided.

1.1 Characteristics of bone structure

Natural bone is an exceptional structural material that imparts mechanical support and protection to the vertebrate skeleton. The unique properties of natural bone result from a nanocomposite structure, consisting of a collagen fibre matrix stiffened by well-ordered hydroxyapatite (HA) crystals, with the chemical formula $Ca_{10}(PO4)_6(OH)_2$ and which accounts for 69 % of the weight of the bone.[14]

This combination of the organic and inorganic phases is extremely important, because it gives bone a unique combination of mechanical properties, such as elastic modulus, toughness and strength, which allow it to withstand the various mechanical and structural loads encountered during normal and extreme physical activities.[15]

Another important property of bone is that is a living tissue, which allows it to self-regenerate via the action of osteoblastic cells after, for example, a fracture. However, when the damage produced is severe, bone needs to be artificially repaired or regenerated with external aid.[14]

The hierarchical structure of bone consists of six levels of organization as shown in Figure 1.1. At the largest scale bone macrostructure consists of two different configurations which differ in the level of porosity: cortical (dense, 5-10 % porosity) and cancellous (spongy, 50–90 % porosity) bone; at the second level (10–500 μm), bone microstructure consists of single trabeculae or osteons. The osteon system consists of cylindrical structures composed of concentric layers or lamellae surrounding a central duct called the Haversian canal. This canal delivers the blood supply and provides connection for the nerves in surrounding bone tissue. The next level, sometimes called sub-microstructure (1–10 μm), contains the lamellae which are thin plate like structures, curved into cylinders to form the osteons, that form the basic structural unit of the bone. The lamellae consist of collagen fibre assemblies, which constitute the fourth structural level (500 nm –1 μm). Each fibre is composed at the nanoscale level (< 500 nm) predominantly of collagen fibrils (fifth level) consisting of tropocollagen triple helixes with embedded HA nanocrystals (sixth level)although other non-collagen organic proteins are also present.[16]

The mechanical properties of bone generally depend on its structure and orientation. The typical values of human bone mechanical properties are summarized in Table 1.1.[6,17–21] Due to their evidently different macrostructural features (i.e. porosity), cortical bone has much higher mechanical resistance and stiffness than cancellous bone.[22]

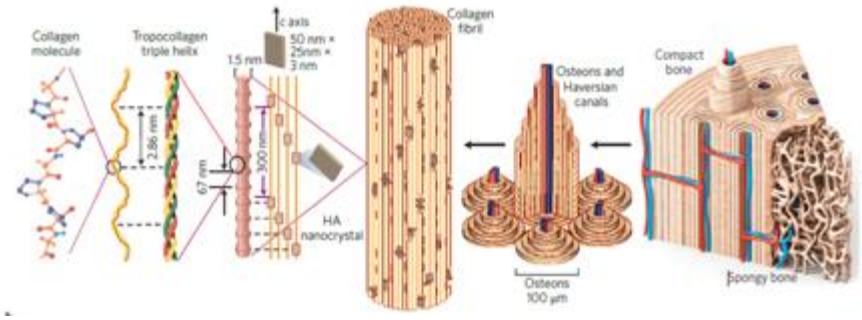

Figure 1.1. The hierarchical structural of bone.[16]

Table1.1. Summary of the mechanical properties of human bone.[6,17–21]

Mechanical property	**Cancellous bone**	**Cortical bone**
Compressive strength (MPa)	2-12	100-230
Tensile strength (MPa)	10-20	50–150
Young's modulus (GPa)	0.05-0.5	7-30
Fracture toughness ($MPa \cdot m^{1/2}$)	0.1-0.8	2–12

1.2 Bone regeneration therapies

The worldwide incidence of bone disorders and conditions is continuously increasing, especially in populations where aging is coupled with increased obesity and poor physical activity.[2] Thereby, the need for therapies to repair and/or regenerate large bone defects is also growing. Although bioinert (e.g. metallic) bone implants are successfully used for the replacement of lost bone, their useful lifetime is often limited and they have a relatively high associated risk of infection. Therefore a preferred treatment would be to heal and regenerate the lost tissue rather than just replace it by another artificial material. The main techniques available to tackle this goal are hereby briefly reviewed.

1.2.1 Bone grafts

Currently, the most routinely used clinical method to reconstruct large bone defects is bone grafting. Bone grafts are utilized in a wide array of clinical settings to augment bone repair and regeneration.[2]

The most common graft is an autograft, whereby bone is taken from the patient's own body and reimplanted.[23] Autografts are biocompatible and non-immunogenic, possess appropriate biomechanical properties and the essential components to achieve osteoinduction (i.e., bone morphogenetic proteins (BMPs) and other growth factors), osteogenesis (i.e., osteoprogenitor cells) and osteoconduction (i.e., porous three-dimensional matrix).[2,24] Although autografts are preferred for faster bone regeneration, this method encounters many challenges inherent to the process, such as the need for an additional surgical site, limitations to harvest the grafts with an appropriate size and shape, and the potential risk of donor site morbidity, which may include infection, fracture, and chronic pain.[24]

An alternative treatment is the use of an allograft whereby bone is removed from an organ donor. Allografts are also likely biocompatible, however, they have reduced osteoinductive properties and no cellular component. In comparison to autografts, allografts have associated risks of immunoreactions and transmission of infections.[2]

1.2.2 Bone tissue engineering: scaffolds

Although clinical bone grafting has been shown to enable bone regeneration, because of the previously mentioned limitations and the high-cost and non-controlled resorption of the grafts,[14] a lot of researches have been directed toward developing alternative biological solutions.[25–27]

Consequently, the field of bone tissue engineering (BTE) was initiated nearly three decades ago with the aim of developing alternative treatment options that will ideally eliminate the previously described issues of current clinically used treatments.[2,28]

For the regeneration of bone in tissue engineering strategies, the most typical approach is to apply a porous 3D structure called 'scaffold' made from

engineered biomaterials, usually in combination with bioactive molecules such as growth factors and relevant cells.[2] Cells and growth factors are seeded into highly porous biodegradable scaffolds, cultured in vitro, and subsequently the scaffolds are implanted into bone defects to induce and direct the growth of new bone. Hence, the main function of a scaffold is to act as the substrate that allows cells to attach, proliferate, differentiate, and organize into normal, healthy bone as the scaffold degrades.[29]

1.3 Bone scaffold requirements

The fabrication of an ideal scaffold for bone tissue engineering is challenging.[14,28,30] The pysico-chemical and biological requirements for a successful BTE scaffold are very stringent, as schematically shown in Figure 1.2. It is necessary for engineered scaffolds to fulfill, to some extent, all these requirements in order to promote bone growth.[31] In addition to porosity, bioactivity, biocompability and mechanical properties requirements, the selected biomaterial should capable of being economically processed into the desired shapes and dimensions.[32]

Some of these requirements for the ideal scaffold biomaterial are now discussed in more detail.

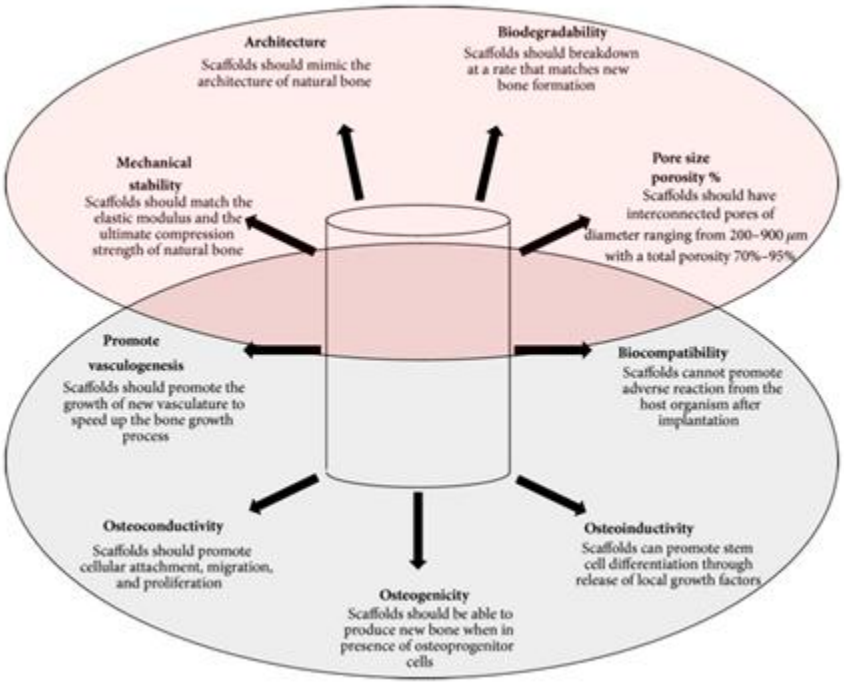

Figure 1.2. Diagram showing physico-chemical (top) and biological (bottom) properties required of bone tissue engineering scaffolds.[31]

1.3.1 Porosity

A common feature of tissue engineering scaffolds is that they are porous structures. Scaffold pore structure (i.e., pore size, volume, and interconnectivity) plays an important role in regulating cell adhesion, growth and migration. Porosity is a measure of the open pore volume within the matrix, often called the void fraction, which can be calculated as follows:

$$Porosity = \frac{open\ pore\ volume}{total\ volume}$$

High porosity is necessary to provide a sufficiently high surface area for cell-scaffold interactions (i.e. increased cell adhesion), sufficient space for

extracellular matrix (ECM) regeneration, and a uniform and efficient cell seeding. A high pore interconnectivity is another requirement of scaffolds in order to facilitate cell in-growthand the deposition of ECM elements.[33]

Although some ambiguity remains about the optimal porosity and pore size for a three-dimensional bone scaffold, studies suggest that scaffolds currently designed with small pore sizes (i.e., < 200 μm) display *in vitro* and *in vivo* osteoblast survival and bone formation limited to the periphery, due to decreased oxygen and nutrient diffusion throughout the scaffolds. On the other hand, scaffolds with a mean pore size of 300 μm display increased osteoblast proliferation and differentiation throughout the entire scaffold, due to enhanced neovascularization and mass transport of oxygen and nutrients.[2] Pore sizes in the range of 200 to 350 μm are found to be optimum for bone tissue in-growth.[34] Furthermore, studies have indicated that multi-scale porous scaffolds involving both micro (pores < 20 μm) and macro (pores > 50 μm) porosities can perform better than only macro porous scaffold.[35] Microporosity is a critical element of the osteoconductive properties of a scaffold material and the resultant bone tissue in-growth and vascularization.[2,35]

1.3.2 Mechanical properties

A key feature of BTE scaffolds is that the need to provide temporary structural support and mechanical integrity at the defect site until the bone tissue is regenerated, and normal biomechanical function is restored.[2] However, as porosity and mean pore sizes increase, mechanical strength is jeopardized, so that a balance between porosity and mechanical performance has to be made for the particular BTE application.[2,6] The broad range of variation in the mechanical properties and porosities of human bone makes it difficult to design a single "ideal bone scaffold".[34] The restorative scaffold's mechanical properties should be modulated or tailored to match the demands of the defect site, to reduce or altogether avoid complications such as stress shielding, implant-related osteopenia, and subsequent refracture.[2,29]

1.3.3 Degradability

Biodegradability (*in vivo* degradability) of scaffold material influences the formation and functionality of new tissues. An appropriate scaffold should exhibit a degradation rate compatible with ongoing bone regeneration at the site of implantation and must maintain the structural stability until the new tissue fully assumes the load-bearing function. The degradation rate of the scaffold can be tailored by varying the material composition, and scaffold fabrication technique.[36,37]

1.4 Bone scaffold materials

A range of different biomaterials have been considered for the preparation of bone scaffolds. However, designing a suitable scaffold with a single biomaterial that fulfills all the relevant criteria still remains a great scientific challenge.[27,38]

Since natural bone matrix is a composite of a biological ceramic (apatite) and a natural polymer (collagen), recent efforts have been aimed in the direction of developing synthetic scaffolds based on two different materials, including bioactive ceramics and glasses, and biodegradable polymers.[6,29,39] The present work can be considered an additional novel contribution to this international effort. Some basic characteristics of these materials are discussed in the following paragraphs, with especial attention to those compositions that are used in the present study.

1.4.1 Bioactive ceramics and glasses

A wide range of bioactive inorganic materials similar in composition to the mineral phase of bone are of clinical interest. For instance, calcium phosphates (CaP) with different Ca/P ratio such as HA (Ca/P ratio of 1.6)[14], TCP (Ca/P ratio of 1.5)[14], and biphasic calcium phosphate (BCP, intimate mixture of HA and β-TCP) are generally considered among the most biocompatible synthetic products used for hard tissue replacement. Although these inorganic ceramics

are not osteoinductive, they are biodegradable, bioactive, and osteoconductive. They have also a remarkable bonding capacity to natural bone after implantation through the release of Ca and P ions.[14,29,40–42] However, CaP have low mechanical strength and brittleness, which limits their application in load-bearing devices.[15]

On the other hand, bioactive glasses are attracting an increasing attention for the fabrication of bone tissue engineering scaffolds due to their high bioactivity and rapid formation of Ca-P layer (in a few hours) in contact with aqueous solutions (e.g. body fluids),[43] which leads to a fast tissue bonding and also their capacity of bonding to soft-tissue, a property that has not been reported for other bioactive materials.[5,14,32,36]

According to the literature, bioactive glasses containing Ca- or Si-based are the most promising for bone scaffolds due to their ions-releasing ability, high osteoconductive and osteoinductive properties, and hydrophilic behavior.[36] Among them, 45S5 bioglass, a silicate-base bioactive glass (45 wt.% SiO_2, 24.5 wt.% CaO, 24.5 wt.% Na_2O and 6 wt.% P_2O_5), is probably the most thoroughly studied and most widely used as bone graft substitute in clinical applications since 1985.[6,8,44]

Regarding their mechanical properties, bioactive glasses are weaker than most other bioactive materials, which restrict their application to non-load-bearing situations. However, bioglasses exhibit a lower elastic modulus, which is desirable to avoid problems related to stress-shielding of surrounding bone.[14]

The insufficient strength of bioglasses in general is exacerbated in 45S5 bioglass due to its poor sintering ability because of its high crystallization tendency. In the fabrication of porous scaffolds for BTE, 45S5 tends to be partially crystalline,[43] which can negatively affect its bioactive performance.

1.4.2 Biodegradable polymers

Over the past 40 years, polymers have been extensively used in biomedical applications.[14] Polymeric biomaterials can be manufactured from many natural sources or from synthetic materials. Natural polymers have attractive properties for the construction of 3D scaffolds, such as biocompatibility and biodegradability. The most commonly used natural polymers for bone tissue engineering are collagen/gelatin, chitosan, silk, alginate, hyaluronic acid, and

peptides.[4,45] On the other hand, synthetic polymers have numerous advantages, such as excellent processing characteristics, biocompatibility and biodegradablilty. Synthetic biodegradable polymers have been fabricated under controlled conditions to produce scaffolds with tuneable, predictable mechanical and physical properties (e.g. tensile strength, elastic modulus, and degradation rate).[15,29] Examples of synthetic biodegradable polymers include, among others, PLA, PGA, PLGA and PCL.[15]

However, polymer-based scaffolds are not generally suitable for bone repair because they do not exhibit osteoconductive properties as bioceramics and bioactive glasses do. In addition, the stiffness and fracture strength of polymers inferior to those of bioceramics and generally insufficient for applications in bone tissue regeneration.[36] This is shown in Figure 1.3 where the elastic modulus versus compressive strength values of various BTE biomaterial classes are compared to human bone.[2]

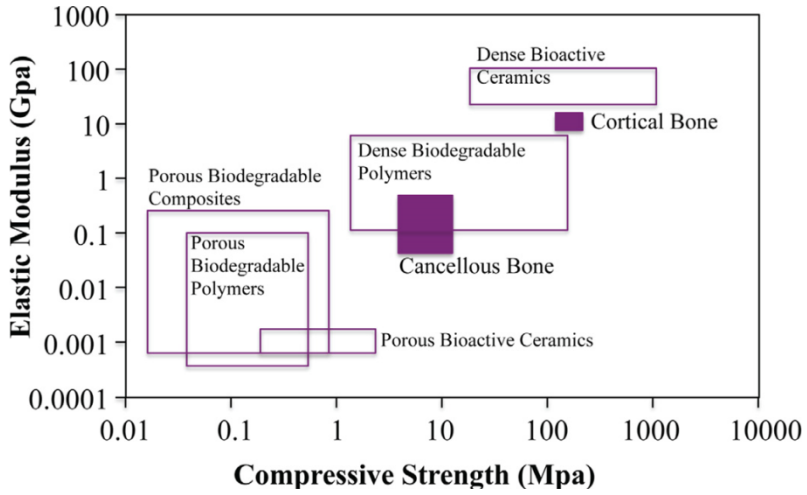

Figure 1.3. Elastic modulus versus compressive strength values of various BTE biomaterial classes compared to human bone.[2]

Some biodegradable polymers, of interest for the present study, are described in greater detail in the following paragraphs:

— Poly(lactic acid) (PLA) is an aliphatic polyester usually obtained from polycondensation of D- or L-lactic acid stereoisomers or from ring opening polymerization of lactide, a cyclic dimer of lactic acid. Polymer derived from pure stereoisomers are called PLLA (obtained from L-lactide or PDLA (from D-Lactide), while blends of both stereoisomers are referred to as PDLLA. Therefore, PLA can be found in different blend compositions, molecular weights and degrees of crystallinity which yield different mechanical properties and degradation rates.[46,47] The chemical structure of PLA is shown below.[48]

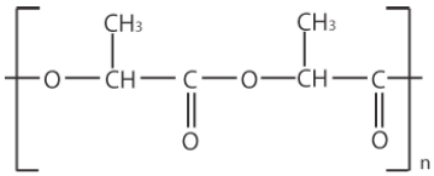

Figure 1.4. Chemical structure of PLA.[48]

PLA is a hard, transparent polymer with an elongation at break of 3-6 % and a tensile strength of 45-60 MPa. It has a melting point of 170-180 °C and a glass transition temperature around 60 °C.[48] PLA is a hydrophobic polymer due to the presence of –CH3 side groups and can be dissolved in various organic solvent, such as chloroform, methylene chloride, methanol, ethanol, toluene benzene, acetone, DMF.[47] PLA is one of the most widely used polymers in tissue engineering applications due to its biocompatibility, biodegradable control and suitable mechanical properties. However, PLA is brittle and this character makes it suitable only for low load bearing applications.[36] PLA can be degraded through hydrolytic and enzymatic pathways, yielding lactic acid as a degradation product,[50] which helps reduce the pH of the environment and induce further degradation.[51] The rate of degradation of PLA depends on the degree of crystallinity.[46] The typical hydrolytic reaction of polyesters degradation is shown below:[50]

$$\text{--}COOR\cdots HOOC\text{--} + H_2O \rightarrow 2COOH + ROH$$

— **Polycaprolactone (PCL)** is an important material in the aliphatic polyesters family,[47] whose structural formula is shown in Figure 1.5.[52] PCL is a good candidate for bone tissue engineering because of its good mechanical properties, biocompatibility, bioresorbability and slow degradation rate.[53] PCL is synthesized by the ring-opening polymerization of cyclic monomer ε-caprolactone in the presence of stannous octoate, serving as a catalyst.[47] PCL is a semi-crystalline polymer with low glass transition temperature around -60 °C and melting temperature around 60–65 °C.[46] The crystallinity of PCL increases with the decrease of its molecular weight. PCL is soluble in tetrahydrofuran, chloroform, methylene chloride, carbon tetrachloride, benzene, toluene, cyclohexanone dihydropyran, and 2-nitropropane; and only partially soluble in acetone, 2-butanone, ethyl acetate, acetonitrile, and dimethyl fumarate. The degradation mechanisms of PCL and its copolymers are similar to PLA, and involve two steps, ester cleavage by random hydrolysis and weight loss through the diffusion of oligomeric species from the bulk.[47] However degradation rate of PCL is typically lower than for PLA.[50] In terms of mechanical properties, PCL is a more ductile polymer (300-500 % elongation at break) with a significantly lower stiffness (elastic modulus of 0.4 GPa) which makes it inappropriate to substitute by itself bone structural function, especially in porous form.[47]

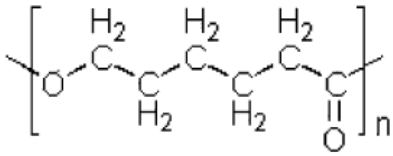

Figure 1.5. Chemical structure of PCL.[52]

— **Alginate** or alginic acid is a a polysaccharide-based polymer found in seaweeds and typically obtained from marine brown algae.[54] Alginate primarily consists of a family of unbranched binary copolymers of (1,4) linked β-D-mannuronic acid (M) and α-L- guluronic acid (G) residues as shown in Figure 1.6.[54–56] Typically, alginate is ablock copolymercomposed of three different polymeric blocks: consecutive G monomers, consecutive M monomers and alternating MG monomers.[57] Alginate is widely used as a biomaterial for tissue engineering, with good scaffold-forming properties that can be useful to treat

the loss or failure of diverse organs. Alginate is biocompatible, non-toxic; non-immunogenic and biodegradable.[54] Tuning the structure and properties of alginate such as biodegradability, mechanical strength, gelation property and cell affinity can be achieved through combination with other biomaterials, and physical or chemical cross-linking.[57] Calcium chloride ($CaCl_2$) is one of the most frequently used agents to ionically cross-link alginate.[55]

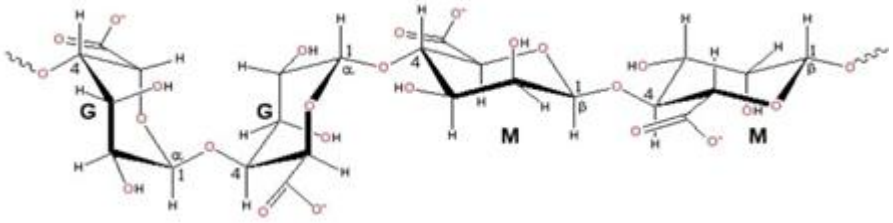

Figure 1.6. Chemical structure of alginate.[54]

— Gelatin is a soluble protein compound obtained by partial hydrolysis of collagen, the main fibrous protein in bones, cartilages and skins; therefore, the source, age of the animal, and type of collagen can influence on the properties of the gelatins. There are two types of gelatin known commercially as type-A gelatin (isoelectric point at pH ~ 8–9) and type-B gelatin (isoelectric point at pH ~ 4–5) obtained under acid and alkaline pre-treatment conditions respectively.[58] A typical structural formula of gelatin is shown in Figure 1.7.[59] Gelatin is an ideal candidate for the design of 3D scaffolds. It is inherently biocompatible and biodegradable, and stimulates proliferation and differentiation of cells as extracellular matrix, however, it has poor mechanical properties as a result of high water solubility.[60] In order to overcome this limitation, Gelatin has been used either in combination with synthetic polymers[61–63] after chemical cross-linking using agents such as glutaraldehyde (GA)[64,65] or genipin (GP),[66,67] which leads to improved mechanical properties and water resistance.

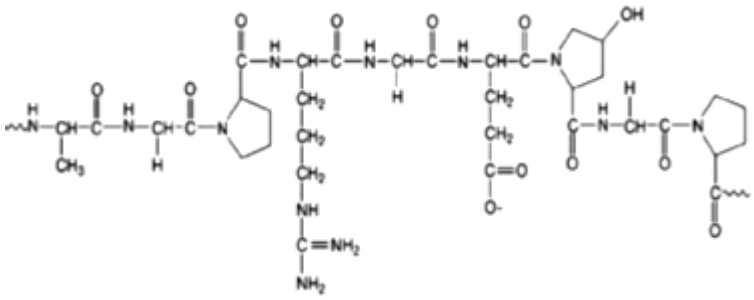

Figure 1.7. Basic chemical structure of gelatin.[59]

— **Chitosan** is a linear polysaccharide of randomly distributed N acetyl glucosamine and glucosamine units (Figure 1.8), derived from chitin by its deacetylation. Chitosan is nontoxic, semicrystalline, biodegradable, and biocompatible.[68] The degradation rate is inversely related to the degree of crystallinity which is controlled mainly by the degree of deacetylation (DD). Highly deacetylated forms (85 %) exhibit a relatively low degradation rate and may take several months *in vivo*, whereas, the forms with lower DD degrade more rapidly. The degradation rates also affect both the mechanical and solubility properties.[60] Chitosan is only soluble in acidic solutions of pH below 6.5,[68] for example in organic acids such as acetic or formic acid. Chitosan has been widely used as films, membranes, fibres and particles.[60]

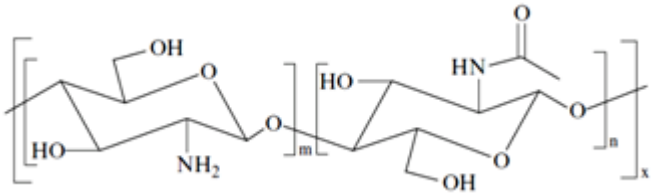

Figure 1.8. Chemical structure of chitosan.[68]

1.4.3 Biocomposites

As already mentioned, both of the materials groups already proposed for the fabrication of BTE scaffolds have their intrinsic limitations. On the one hand, biopolymers are usually not stiff enough to substitute bone structural function and they are not intrinsically bioactive and osteoconductive[69] due, among other things, to their lack of calcium and phosphate ions. On the other hand, it is well known that the main disadvantage of bioceramic and bioglass-based scaffolds is their intrinsic brittleness, and thus low resistance to crack propagation, which makes most of these scaffolds unsuitable for load-bearing applications.[38] For example, the compressive strength of 45S5 scaffolds is normally comparable with that of cancellous bone, but far from cortical bone values.[70,71]

One applicable solution for overcoming the limitations of both groups of materials is to combine them to form a biocomposite structure.[72,73] Polymer-bioceramic composite materials represent attractive candidates for bone tissue engineering because bone is, as we discussed in Section 1.1, a composite material composed of inorganic hydroxyapatite nanocrystals and organic collagen fibers.[2]

Furthermore, polymer-bioceramic composite scaffolds represent a convenient alternative due to the possibility to tailor their various properties (e.g., mechanical and structural behavior, degradation kinetics and bioactivity). Composites made of polymers and bioceramics combine the advantages of their singular components.[2,6] Polymers provide relatively high ductility, toughness, favorable formability as well as processability. The glass or glass-ceramic phase adds stiffness and adequate mechanical strength to the composite.[6]

Much current research is therefore focused on the fabrication of bioactive composite materials particularly development of porous, high-strength composite structures for regeneration of human bone at load-bearing sites with the bioactive phase incorporated as filler or coating into the bioresorbable polymer matrix.[6,74] In addition the polymer can act as a carrier of bioactive molecules such as drugs and growth factors,[75,76] while the ceramic provides a required source of calcium and phosphate ions. A wide variety of polymers have been used for hybridization with bioactive glass and other bioceramic materials. Natural polymers, such as collagen, glycosamino glycan, chitosan, starch, hyaluronic acid, alginate and bacterial sourced poly (hydroxyl alkanoates) offer the advantage of flexibility to adapt their shape to desired

forms and faster biodegradation.[77] However they exhibit very limited mechanical performance, which constitutes a drawback in load bearing applications. On the other hand synthetic bioresorbable polymers such as polycaprolactone (PCL)[76,78–81] and polylactic acid (PLA)[69,82,83] have been regarded as preferable candidates in polymer–ceramics composite system due to their low cost and sufficient mechanical properties..However, some problems have been encountered regarding the use of these polymers in tissue engineering applications due to the release of acidic degradation products which can disturb the cell survival environment and induce host inflammatory reaction.[84,85]

Most current research is focused on the fabrication of bioactive composite materials with the bioactive phase incorporated as filler or coating into the bioresorbable polymer matrix.[6,74] For example, in 2003, Boccaccini *et al.*[86] reported for the first time on the successful fabrication of porous foam-like structures of PLGA containing bioactive glass particle additions, which exhibited well-defined, oriented and interconnected porosity. Since then, a great many studies have been carried out along similar lines to investigate and develop composite scaffolds for bone tissue engineering concerning material combinations, bioactive properties, degradation characteristics, mechanical properties as well as *in vitro* and *in vivo* behavior.[6]

Nevertheless, for the development of porous, high-strength composite structures for regeneration of human bone at load-bearing sites, the use of a polymeric matrix presents limitations, especially in term of stiffness. This has spawned a more recent interest in the development of biocomposite scaffolds where the bioceramic phase is continuous and the polymer is incorporated as an infiltrate or coating. This is the approach that has been adopted in this study and therefore a more extensive review of existing literature in this matter will be carried out later on (Section 1.6).

1.5 Scaffold fabrication technologies

Multiple techniques can be used for the preparation of porous structures to be used as BTE scaffolds. Some of those will be describe in this section, with special attention to those methods applicable to the fabrication of bioceramic and bioglass scaffolds which are used in this study.

Scaffolds fabrication method should enable the preparation of pieces with appropriate external shape, controlled pore architecture. Indeed, the architecture of porous scaffolds (e.g., surface curvature, pore shape, and pore size) that are used for bone tissue engineering has recently been shown to significantly influence the cellular response (e.g., cell adhesion, proliferation and differentiation) and the rate of bone tissue regeneration.[87,88] The appropriate fabrication technique needs to be able to generate a porous scaffold with reproducible architecture and sufficient mechanical performance, especially for load-bearing applications.[36]

Different fabrication routes based on ceramic powder or colloidal processing approaches have been used for three-dimensional (3D) scaffolds with interconnected high porosities suitable for bone tissue engineering.[2,38] The most conventional routes include, for example, foam replication technique (Figure 1.9a),[89–92] sacrificial template (porogen) method (Fig. 1.9b)[92,93] and direct foaming (Fig. 1.9c).[92,94,95] freeze extrusion methods and a variety of rapid prototyping techniques. These conventional methods are simple, but provide only limited control of the scaffold pore architecture.

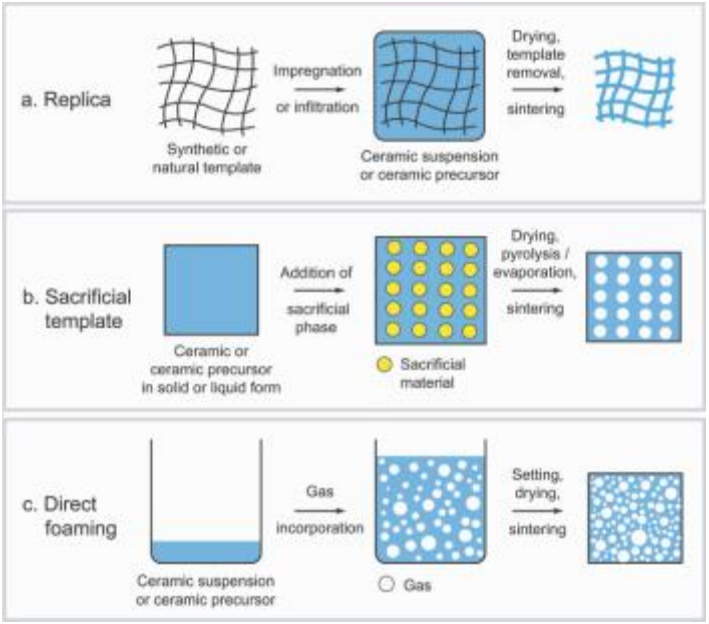

Figure 1.9. Scheme of some processing techniques used for production of macroporous ceramics.[92]

Additive manufacturing (AM) techniques also referred to as Rapid prototyping (RP), solid freeform fabrication (SFF) or 3D printing (3DP) techniques have received significant attention in the field of tissue engineering as an alternative to traditional scaffold fabrication methods.[13,96,97] The main advantage of these manufacturing methods is their ability to produce complex geometries directly from a digital model (CAD file), which yield an unsurpassed control on both the external shape and internal pore architecture of the fabricated scaffolds.[4,98] By using the data from medical scans to produce the scaffold external shape, AM techniques enable the fabrication of customized, patient-specific implants.

Among a broad range of additive manufacturing techniques, a few methods including stereolithography,[99–101] selective laser sintering[102,103], and direct ink writing[104,105] have been used to fabricate bioactive ceramic-glasses scaffolds. The technique used in this study to fabricate bioglass scaffolds belongs to this latter group, which will be now described in greater detail.

1.5.1 Direct ink writing (DIW)

The term “direct ink writing” or ‘‘direct-write assembly’’ describes fabrication methods that use a computer-controlled translation stage, which moves a pattern-generating device to create materials with controlled architecture and composition through the deposition of colloidal or organic-based inks. In common configurations these systems extrude the ink utilizing standard syringes and needles to create structures layer-by-layer.[106 107]

The inks are typically formulated to create a stable, homogeneous suspension with the desired and reproducible rheological behavior. The critical rheological parameters for a given ink formulation include its apparent viscosity, yield stress under shear and compression, and viscoelastic properties (i.e. the shear loss and elastic moduli), which are tailored for the specific direct-write technique of interest.[106] 3D ink-writing techniques can be divided into two approaches: (1) droplet-based or (2) filament-based inks, Figure 1.10.[106]

Several direct ink writing techniques have been introduced that are capable of patterning materials in three-dimensional, including 3D printing, direct ink-jet printing, robocasting, fused deposition, and micropen writing whose characteristics are summarized in Table 1.2.[106,108]

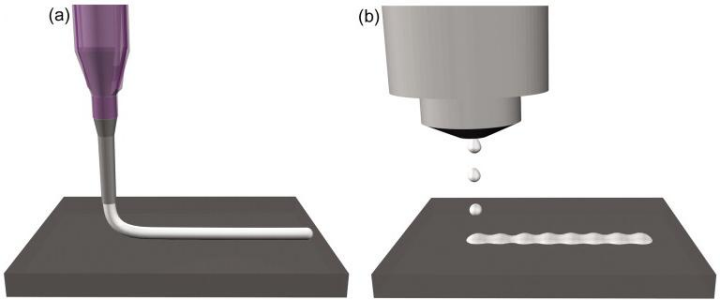

Figure 1.10. Schematic view of ink-based deposition schemes: (a) continuous filament writing and (b) droplet jetting.[109]

Table 1.2. Droplet- and filament-based techniques for DIW.[106,108]

Technique	Ink formulation
Droplet-based	
3D Printing	Binder solution printed on powder bed
Ink-jet Printing	Colloidal fluid
Filament-based	
Robocasting (in air)	Concentrated colloidal gel
Robocasting (in oil)	Concentrated colloidal gel
	Concentrated nanoparticle gel
Fused deposition	Thermoplastic polymer melt
Micropen writing	Concentrated, shear-thinning colloidal fluid

Among all the techniques belonging to this family, robocasting is chosen in this study and reviewed in greater detail in the following section.

1.5.1.1 Robocasting

Robocasting is a filament-based direct ink writing technique consisting on a layer-wise deposition of highly loaded colloidal slurries through an orifice.[110] Cesarano *et al.*[111] were pioneer in using the flocculated colloidal slurries (or gels) as inks for robocasting of ceramics. The process is virtually binderless

since less than 1 vol.% of organic additives are neede. Parts can be fabricated, dried, and sintered in less than 24 hours.[110]

Robocasting requires careful characterization and control of the ceramic paste being deposited. The paste must be viscoelastic so that it yields upon extrusion but sets upon deposition.[112] In addition, it must contain a high solid volume fraction to minimize drying-induced shrinkage after assembly is complete.[113]Ink preparation for robocasting consists of initial dispersion of powders in an aqueous polymer solution followed by controlled coagulation of powders to create a colloidal gel having pseudoplastic behavior with yield stress rheology.[114]

The resulting paste is then loaded into a syringe mounted on a three-axis motion control stage, as illustrated in Figure 1.11,[112] and extruded through a nozzle to construct three-dimensional parts in a layer-by-layer sequence. The motion of the moving stages is controlled by a computer and follows the scaffold/part design created in a CAD program. After deposition, the parts are dried and then sintered to get densified. Figure 1.12 show some optical images of scaffolds fabricated by robocasting.[114]

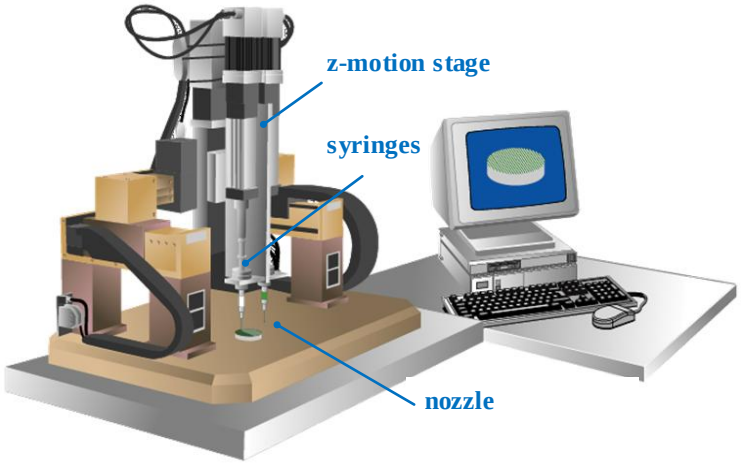

Figure 1.11. Schematic of the robocasting system.[112]

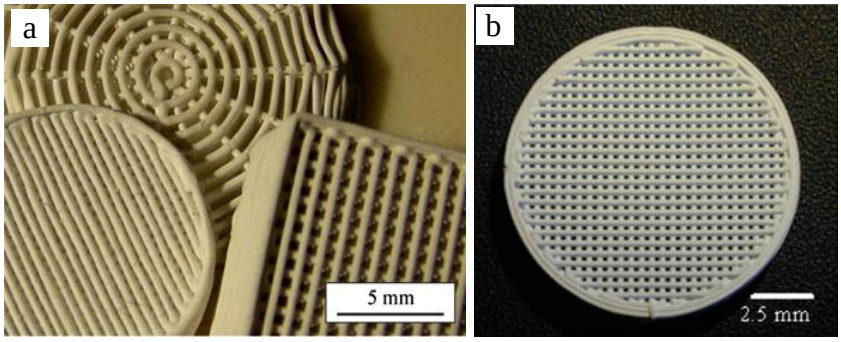

Figure 1.12. (a) 45S5 bioglass scaffolds in this work, and (b) HA scaffold fabricated by robocasting.[114] Visible pores between rods are macropores designed in a CAD program.

This robotic deposition process allows the fabrication of scaffolds with homogeneous struts , which leads to stronger scaffolds than those fabricated by conventional techniques.[12,106] Recent studies have shown that silicate 13-93 and 6P53B bioactive glass scaffolds fabricated by robocasting have compressive strengths comparable to those of human cortical bone (100–150 MPa).[105,116] As in other DIW techniques, robocasting provides also aprecise control of pore size, shape, and alignment, and highly uniform macroporosities can be obtained by varying the rod spacing and size (Fig. 1.12).[112,115] Scaffolds with pore widths and strut diameters covering a wide range, 10-1000 μm, can be created by robocasting.[117]

1.6 Improving bioceramic scaffolds with biodegradable polymer coatings

Various approaches to the development of bioresorbable and bioactive composites for tissue engineering applications are being investigated worldwide. Polymer coating method has attracted considerable attention due to its quick and facile process and the versatility that enable the use of a diversity of polymers in order to meet the clinical demands.[69] In this section, a review is provided of the state of the art on bioceramic scaffolds reinforced by polymeric

coatings to form interpenetrating polymer-bioceramic structures for bone tissue engineering.

1.6.1 Quick review of polymer coating processes

Polymer coating (and infiltration) can be easily achieved by simply immersing a scaffold with a high degree of interconnected porosity into the desired liquid polymer, e.g. previously dissolved in an organic solvent or water, for sufficient time to allow the solution to permeate into the pores.[38] Figure 1.13 shows a schematic of such a dip coating process.[118]

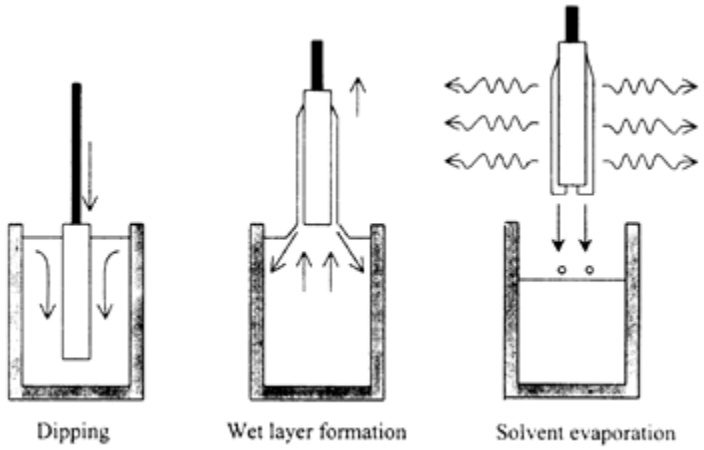

Figure 1.13. Schematic of a dip-coating process.[118]

However, there are other alternative methods for coating bioceramic scaffolds. For example, Martinez-Vazquez *et al.*[119] have infiltrated and coated robocast β-TCP scaffolds by in situ polymerization of ε-caprolactone (ε-CL) monomers in order to enhance their mechanical performance while preserving the predesigned macropore architecture.

Bretcanu *et al.*[120] have fabricated different biodegradable polymeric nanofibrous coatings by electrospinning onto 45S5 bioglass scaffolds. The polymers used were P3HB, PHBV, and a composite of PCL and PEO (PCL–

PEO). In other study, Califano *et al.*[121] coated 45S5 bioglass-based scaffolds with PDLLA by matrix assisted pulsed laser evaporation (MAPLE) technique, a method inspired by pulsed laser deposition (PLD), but well suited for polymeric or organic materials. The polymer was shown to penetrate to some extent from the surface producing a graded composite structure, with a core made fully of bioglass and outer layer made of the polymer coated scaffold. Such a graded scaffold structure can be beneficial for application in osteochondral tissue engineering, which promotes the simultaneous regeneration of articular cartilage and underlining subchondral bone.

1.6.2 Mechanical enhancement provided by polymeric coatings

As already mentioned, one of the main reasons for applying a polymeric coating onto a bioceramic scaffold lies in the mechanical enhancement it can provide. Figure 1.14 clearly shows this by comparing the force–displacement curves for 45S5 bioglass (BG) scaffolds and for polymer-infiltrated structures. The curves for non-coated BG scaffolds exhibit much lower maximum forces (i.e. lower strength) than the curves of the polymer-infiltrated scaffolds.[38]

The strengthening achieved in coated structures is attributed to the mechanism of defect healing. It consist on the impregnation of the micropores or microcracks on the scaffold struts with the polymer, which makes it harder to initiate a crack from these defects.[80] The actual extent of this reinforcing effect will depend on the mechanical properties of the polymer, the quality of the infiltration and the conditions at the polymer–ceramic interface.[38]

On the other hand, coating or infiltrating an inorganic scaffold with a tough polymer leads to enhancement of fracture energy or toughness[38]. This is more clearly shown in Figure 1.15 where the strain energy density, calculated as the area under the force–displacement curve, is plotted versus displacement during compression tests of uncoated and polymer-infiltrated bioglass scaffolds. The energy dissipation of the polymer-infiltrated scaffolds is considerably higher than that of the uncoated scaffolds, which indicates an increased toughness upon polymer infiltration. Such toughening is provided by polymeric fibrils that bridge the crack walls together during crack propagation and need to be stretched and eventually broken for the propagation to continue.[122,123] Of course, the effectiveness of such a crack bridging mechanism depends of the

mechanical properties of the coating material, with ductile, tough polymers being more effective infiltrates in this regard.

Because of this extraordinary enhancement of mechanical properties bone scaffolds reinforced with tough polymers have received an increasing attention.[38,78,81,83,119,124–127] In the following sections, the most significant efforts devoted to analyze the effect of polymeric coatings on the bioactivity and mechanical performance of bioceramic scaffolds is reviewed

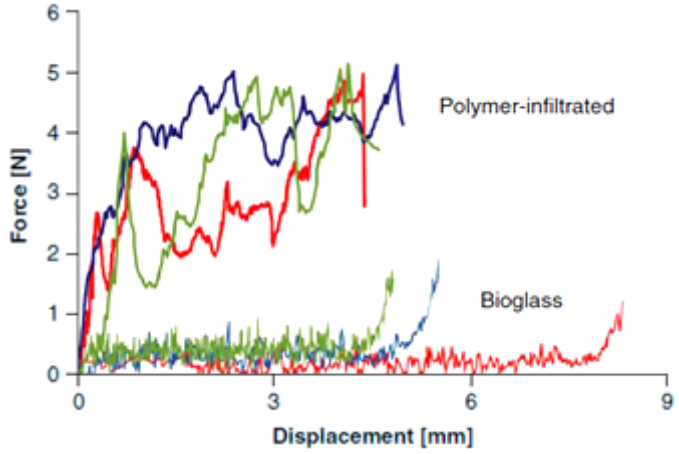

Figure 1.14. Typical force–displacement curves of non-coated and coated bioactive glass scaffolds under compressive loading.[38]

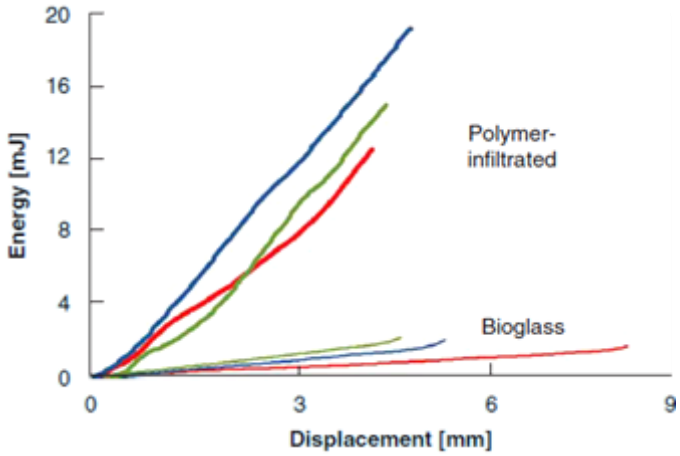

Figure 1.15. Energy consumption versus displacement behavior during compression tests on uncoated and polymer-infiltrated bioactive glass scaffolds.[38]

1.6.3 Coating with synthetic polymers

Coating and infiltration of calcium phosphate (CaP) ceramic and bioglass scaffolds with synthetic polymers, including PCL, PDLLA and PLGA, have been extensively investigated and reviewed by Philippart *et al.*[38]

For example, Miao *et al.*[128] have produced porous calcium phosphate ceramics with interconnected macropores (> 200 μm) and microporosity (~ 5 μm) as well as high porosities (~ 80 %). They have infiltrated the open micropores of the struts with PLGA to achieve an interpenetrating bioactive ceramic/biodegradable polymer composite structure. The PLGA filled struts were further coated with a 58S bioactive glass (33 wt.%)-PLGA composite coating. The bioactive glass-PLGA coating rendered a good bioactivity to the composites, evidenced by the formation of an apatite layer on the sample surfaces immersed in SBF for 5 days. Furthermore, the structure exhibited compressive strengths up to 7.7 MPa and compressive moduli up to 3 GPa, which were comparable to those of natural spongy bones.

In other research done by Kang *et al.*,[129] porous β-TCP scaffolds were infiltrated with a thin layer of PLGA polymer, showing a significant increase in the compressive strength from 2.90 MPa to 4.19 MPa, bending strength from 1.46 MPa to 2.41 MPa, and toughness from 0.17 MPa to 1.44 MPa, while retaining an interconnected porous structure with a porosity of 80.65 %.

In other developments targeted to improve bone ingrowth and osseo integration, polymers combined with ceramic particles, such as HA, can also be applied as coating on porous bioceramic scaffold. For example, HA scaffolds have been coated with PCL and HA particles. The PCL matrix also acted as carrier for the antibiotic drug tetracycline hydrochloride which was entrapped within the coating layer.[76,130]

Roohani-Esfahani *et al.*[124] investigated highly porous (~ 91 %) biphasic CaP scaffolds coated with PCL layer. In addition, hydroxyapatite nanoparticles (30 wt.%) that were added to the coating led to a increase in the bioactivity and osteoblast differentiation profile as well as an almost 20-fold increase in compressive strength, whereby the shape of the HA nanoparticles also had a significant effect on the mechanical strength. In a more recent study by the same group[125], nanosized bioglass was introduced at varying percentages (1–90 wt.%) in the nanocomposite coating layer, and the mechanical properties and in vitro behavior of the scaffolds were comprehensively examined, and compared with

that for BCP scaffold coated with PCL and nano-HA. The maximum increase in compressive strength (~ 14 times) and modulus (~ 3 times), achieved at 30 wt.% nano-BG content, was lower than that with the nano-HA composite layer, but nano-BG induced better bioactivity and a faster degradation rate. In a related study involving biphasic CaP, Peroglio *et al.*[131] have infiltrated the BCP scaffolds with the solution of PCL in chloroform or ethyl acetate of varying concentrations between 3 % and 10 % w/v, in order to determine the best solvent and concentration for a homogeneous coating. They showed that the polymer effectively contributes to energy to failure enhancement in bending, compressive and tensile tests. It was also reported that the presence of fibrils at two different size scales –as found in scaffolds with a bimodal pore distribution– resulted in a more effective toughening effect as compared to scaffolds with a monomodal pore size distribution. Other group[132] has reported the mechanical behavior and cell response of PCL coated α-TCP foams with 80–85 % porosity and 500–700 μm pore size. They have shown that the compressive strength of α-TCP was increased with increasing the PCL concentration from 5 wt.% to 15 wt.% and reached 750 ± 20 kPa when coated with 15 wt.% of PCL solution (~ 25-fold).

In other research, Martinez-Vazquez *et al.*[119] have infiltrated robocast β-TCP scaffolds with in situ polymerization of ε-caprolactone (ε-CL) in order to enhance their mechanical performance while preserving the predesigned macropore architecture. The strength and toughness of PCL-coated scaffolds were significantly increased (two-fold and five-fold increase, respectively) over those of the bare scaffolds as a result of healing the preexisting microdefects in the bioceramic rods.

Another group of polymers selected to coat CaP-based scaffold is the polyhydroxyalkanoate family which was recently studied by Foroughi *et al.*[133,134] They used 50 wt.% natural nano HA to make the scaffolds, as after 30 s infiltration with P3HB, 90 % porous structure with an average diameter of 100–400 μm was obtained, which demonstrated a compressive strength and modulus of 1.46 and 21.27 MPa, respectively.

Bioglass scaffolds have also been coated with synthetic polymers. Chen *et al.*[135] have investigated the mechanical properties and bioactivity of 45S5 bioglass-based foams, before and after applying a PDLLA coating layer on the foam struts. It was shown that the compressive and three-point bending strengths of the bioglass foams were slightly improved by the PDLLA-coating,

while the fracture toughness was considerably enhanced, as a significant 20-fold improvement of work-of-fracture was reported.

After that, Bretcanu *et al.*[136] used biodegradable, bacteria-derived PHB to infiltrate 45S5 bioglass-derived foams. It was found that polymer coating did not affect the interconnectivity of the pore structure. Although the polymer coating was not fully homogeneous, the compressive strength of the scaffolds was considerably increased (from ~ 0.2 MPa to ~ 1.5 MPa at 85 % porosity). Also, the formation of HA crystals on the scaffolds' surface was investigated confirming the high bioactive character of the scaffolds.

In another attempt to develop bone scaffolds with local drug delivery ability, Li *et al.*[137] fabricated PHBV microsphere/45S5 bioactive glass composite scaffolds. In this approach, microspheres loaded with drug (Vancomycin) were used to coat the scaffolds instead of polymer layers. It was reported that the microsphere coating slightly improved the mechanical properties of the scaffolds (2-fold). The limited strengthening and toughening effects, were attributed to the fact that these microspheres did not form a continuous polymer film able to infiltrate the microcracks in the struts, and a crack bridging effect did not occur in the microsphere-coated scaffolds.

In the other system based on phosphate bioglasses and titania, P_2O_5–CaO–MgO–Na_2O–(TiO_2), coated by methacrylate-modified oligolactide polymer, the compressive strength and machinability of the porous glass specimens were significantly enhanced by polymer coating of the inner surface of the porous glasses while the interconnected porosity was maintained

1.6.4 Coating with natural polymers

Synthetic polymeric coatings require the use of organic solvents in the fabrication process, so any remaining solvent may be harmful to transplanted cells or host tissues.[138] Therefore, natural polymers are becoming more widely used to coat bioceramic scaffolds when using an organic solvent is not desirable in the fabrication of composite scaffolds. Different natural polymers including silk,[138,139] chitosan,[140] gelatin,[141–144] collagen,[145] and alginate[143,146] are being increasingly considered for this approach.

For example, Wu *et al.*[139] have coated porous mesopore-bioglass scaffolds with pore sizes ranging from 200 to 400 μm in silk protein solutions (2.5 and 5 % w/v). It is reported that the silk film thickness on the scaffolds was approximately 600 nm, and following silk modification the compressive strength increased from 60 kPa to 250 kPa.

A related study by Li *et al.*[138] shows that coating biphasic calcium phosphate scaffolds (pore sizes of 400−500 μm) with multiple silk layers has significantly improved the mechanical properties of BCP scaffolds. For example the optimal condition of 5-cycle coating led to a significant 6-fold and 12-fold increase in compressive strength and toughness, respectively, and enhanced osteogenic response of hMSCs *in vitro*.

Other group has studied infiltration of 45S5 bioglass scaffolds with alternately alginate and chitosan solutions through layer-by-layer assembly. Three layers of alginate–chitosan couples led to great improvement in compressive strength, almost 4 times higher than that of bioglass scaffold[147] in wet condition. Also, after 48 h immersion in SBF the coated scaffold showed excellent strain tolerance and did not lead to significant strength reduction.

In a relevant investigation, Li *et al.*[148] coated the highly porous 45S5 bioactive glass scaffolds in cellulose nanowhiskers aqueous suspension (0.42 % w/v) by dip coating method. The cellulose coating improved the mechanical properties of the scaffolds and did not hinder their bioactivity in SBF. The coating layer had no negative influence on the behavior of osteoblastlike cells (MG-63). It was also shown that the cellulose coating adhered well to the surface of 45S5 bioglass struts. This qualitative good adhesion is likely due to the hydrophilic character of these two materials.

Gelatin has been also used to infiltrate bioceramic scaffolds. For example in the study done by Liu *et al.*,[149] calcium phosphate porous scaffolds with the porosity of ~ 86 % and pore size ~ 300–500 μm was impregnated in 5 % gelatin solution for three times. It was found that the mean compressive strength of coated scaffolds was improved to 5.17 ± 0.17 MPa compared to non-coated ones (1.04 ± 0.15 MPa), and also the mean elastic modulus was enhanced from 0.1 GPa to 0.3 GPa, without sacrificing their porosity greatly.

Erol *et al.*[141] have shown that Sr-doped bioactive glass scaffold coated with gelatin exhibited improved the mechanical properties without altering its bioactivity and retaining the pore interconnectivity. The results also indicated that scaffolds can deliver controlled doses of strontium toward the SBF medium which is known to positively act on bone remodeling.

In a similar study, Metze *et al.*[144] fabricated highly porous 45S5 bioglass scaffolds by foam replication, and coated with a gelatin layer by dipping method. It was shown that depending on macropore size of the scaffold and gelatin concentration, compressive strength was enhanced in different degreees in comparison with uncoated structure. Also for developing the scaffold with drug delivery capability, gelatin layer was loaded with tetracycline hydrochloride.Since gelatin dissolves quickly in an aqueous environment, cross-linking of gelatin is necessary to overcome this limitation. This can be achieved either using physical methods, such as dehydrothermal treatment (DHT)[150,151] and ultraviolet[152] or gamma[153] irradiation, or chemical methods such as glutaraldehyde (GA)[154,155] or genipin (GP).[156,157]

As an example, Gil-Albarova *et al.*[158] implanted nanocrystalline HA (HABP) scaffolds coated with gelatin crosslinked with glutaraldehyde in the femur of 15 mature male New Zeeland rabbits. Radiographical studies after 4 months implantation showed healing of treated bone defects, with bone integration of the HABP scaffolds and osteoconduction over its surface.

In other study done by Bellucci *et al.*[159], porous 45S5 bioglass scaffolds were infiltrated with 5 % w/v gelatin solution, and after drying immersed in 5 % w/w genipin (GP) solution for 24 h to obtain a stable cross-linked gelatin coating. The mechanical evolution after coating wasn't studied in their work. However, gelatin release tests demonstrated that the coating started to dissolve after just a few days and its degradation was almost completed after 1 week. *In vitro* tests in SBF confirmed the excellent bioactivity of the gelatin-coated samples.

In similar study done by another group, 45S5 Bioglass® scaffolds with high porosity (> 90 %) were coated with genipin cross-linked gelatin and further incorporated with poly(p-xylyleneguanidine) hydrochloride (PPXG) for antibacterial effect. A 26-fold higher compressive strength was provided to 45S5 bioglass scaffolds by coating, which slightly retarded but did not inhibit the *in vitro* bioactivity of 45S5 bioglass scaffolds in SBF.[157]

In some cases, synthetic and natural polymers are coated together to improve the brittleness of bioceramic scaffolds and drug delivery capability at the same time. Recently, Yao *et al.*[160] have reported the incorporation of PCL and chitosan coating in 45S5 bioglass scaffolds for controlled drug delivery. For this purpose, the scaffolds were coated with PCL and vancomycin-loaded chitosan by a two-step procedure. An improvement of the compressive strength, elastic modulus and toughness of PCL/chitosan-coated bioglass scaffolds over uncoated scaffolds was demonstrated.

In another approach by Roohani-Esfahani *et al.*[161], biphasic calcium phosphate (BCP) scaffolds coated with nanostructured silk/PCL were produced. Bioactivity of composite scaffolds was improved while preserving high porosity and interconnectivity. The compressive strength and modulus of BCP/PCL-silk scaffolds reached 0.42 MPa and 25 MPa respectively compared with 0.07 MPa and 5 MPa for uncoated BCP. Attachment, proliferation and differentiation of HOB cultured on the composite scaffold were also greatly enhanced.

As explained in the previous sections, different types of bioceramic and bioglass scaffolds have been coated with biocompatible and biodegradable synthetic (including PLGA, PDLLA, PCL, and PHB) or natural (silk, gelatin, etc.). Significant improvements in mechanical properties were generally observed, particularly in terms of strength and toughness, without strongly affecting the biological performance of the scaffolds The actual extent of this reinforcing effect will depend on the mechanical properties of the polymer, the quality of the infiltration and the conditions at the polymer–ceramic interface.[38] Dip-coating is the most commonly used method for coating deposition, and while this technique is simple to practice, there are some important parameters including polymer concentration, polymer an solvent composition,[162] etc that can affect the coating performance. Despite the diversity of reports existing in the literature on this matter, some of which have just been reviewed, there is a lack of systematic studies aimed at analyzing the role of such processing parameters on the quality and performance of polymeric coatings used to reinforce bioceramic scaffolds.

The present study seeks to redress this deficiency. Different polymeric coatings, from both natural (alginate, chitosan and gelatin) and synthetic (PCL and PLA) polymers, will be deposited under different conditions onto 45S5 porous scaffolds in order to systematically analyze the effect of the different fabrication variables on the mechanical and biological performance of hybrid polymer/bioglass scaffolds.

Chapter 2

Materials and methods

In this chapter, the materials used for the preparation of experimental samples are described and the different steps involved in the fabrication of bare and coated 45S5 bioglass scaffolds are detailed. Also, the procedures followed for the microstructural and mechanical characterization of the samples are described.

2.1 Materials

45S5 bioactive glass powder with the composition of 45 % SiO_2, 24.5 % CaO, 24.5 % Na_2O and 6 % P_2O_5 (wt.%) used for fabrication of scaffolds was supplied by MO-SCI Corporation (USA). The density of the glass, as indicated by the manufacturer, was 2.7 $g \cdot cm^{-3}$.

Carboxymethyl cellulose (CMC, Mw = 250 000, Lamberti Iberia S.A.U., Castellón, Spain) was used as the sole processing additive—as indicated by the supplier, a 2 wt.% aqueous solution of this CMC had a viscosity in the range of η = 1–3 Pa·s.

Two synthetic polymers as PLA in powder form (ICO Polymers, Ecorene™ NW61-100) and PCL beads (Capa™ 6500, Perstorp, UK), were used to infiltrate 45S5 robocast scaffolds. Powders of three natural polymers, sodium alginate (medium viscosity, W201502, Sigma Aldrich), gelatin (from porcine skin, type A-300 bloom, Sigma Aldrich), and chitosan (85/20, Heppe Medical Chitosan GmbH) were used for infiltration of 45S5 scaffolds. Acetic acid

(pharma grade, PRS Panreact) was used to reduce the pH of the aqueous solution before dissolving the chitosan.

Toluene (puriss. p.a., Sigma Aldrich), xylene (puriss. p.a., Sigma Aldrich) and acetone (Panreac AppliChem) were also used as solvents.

2.2 Fabrication of 45S5 bioglass scaffolds by robocasting

45S5 Bioglass-based scaffolds were prepared by robocasting method through several steps that are described in detail in the following sections:

2.2.1 Powder preparation

The particle size of the powder used for ink preparation is a critical factor. Particles between 1 and 10 μm are preferred to facilitate dispersion and avoid clogging.[104] Therefore, the commercial bioglass particles were pre-treated by milling. The as-received 45S5 bioglass powder was milled for 4 h in an attrition mill (Model 01-HD, Union Process, Akron, OH), using high-purity zirconia container and balls (6 mm) as milling media and ethanol as dispersing medium. The resulting slurry was dried at 60 °C and then sieved through 106 and 73 μm stainless steel sieves to eliminate any agglomerates created during the drying step. To make sure that the obtained bioglass particles were in the desired size range (1–10 μm), the particle size distribution of the milled powders was measured using a laser diffraction particle size analyzer (Mastersizer 2000MU, Malvern, UK).

2.2.2 Ink preparation

For preparation of 45S5 colloidal suspensions, carboxymethyl cellulose was used as the sole processing additive, to act simultaneously as dispersant and binder/gelling agent. Concentrated inks containing 45 vol.% solids could be prepared with CMC that exhibited a rheological behavior appropriate for

robocasting. Preparation of colloidal suspensions using different added amounts of CMC ranging from 0.5 to 2 wt.% was attempted. The CMC was first dissolved in deionized water and then 45 vol.% of 45S5 glass powder was added to the suspension in small batches between successive mixing procedures performed in a centrifugal planetary mixer (ARE-250, Thinky, Japan) for a total mixing time of around 20 min. The flow properties of all the colloidal gels were evaluated using a rheometer (Bohlin CVO, Malvern, UK). The measuring configuration adopted was a cone and plate (4°, 40 mm, and gap of 150 μm), and flow measurements were conducted at shear rates between 0.2 and 100 s^{-1}.

2.2.3 Robocasting of 3D bioglass scaffolds

As shown in Figure 2.1, a robocasting device (A3200, 3D inks, Stillwater, OK, USA) was employed to fabricate three-dimensional structures by layer-wise deposition of the optimized 45S5 bioglass ink, containing 1 wt.% of CMC as a single processing additive and a solids loading of 45 vol.%. The ink was housed in a syringe and extruded through a conical nozzle (inner diameter: 410 μm) by the computer-controlled robotic system. The position of the nozzle moved following the CAD model designed previously in the control software (Robocad 3.0, 3D inks, Stillwater, OK, USA). The external dimensions of the scaffolds were set at about $13 \times 13 \times 10$ mm, for the specimens used in the optimization of polymer infiltration processes and the fabrication of compression test samples; or at $40 \times 20 \times 12$ mm for the specimens used in the fabrication of bending test samples. The scaffold design consisted of a tetragonal mesh of cylindrical rods with a center-to-center spacing between adjacent rods within a layer of 820 μm and a layer height of 287 μm. The ink flowed through the nozzle at the volumetric flow rate required to maintain a constant deposition speed of 20 $mm \cdot s^{-1}$.

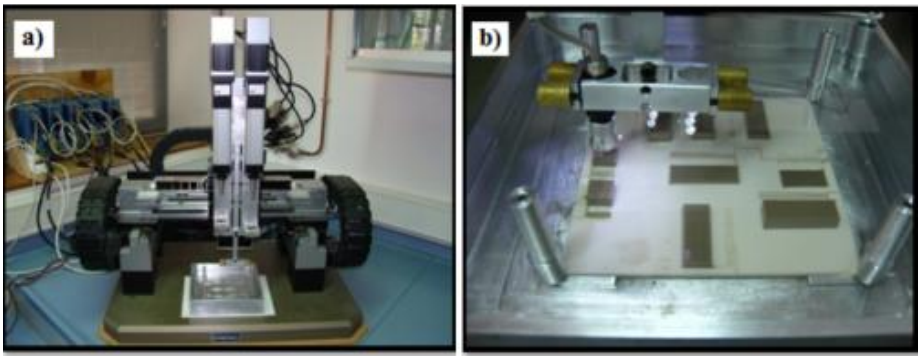

Figure 2.1. Optical images of (a) the robocasting system, (b) 3D structures as-deposited within an oil bath.

To prevent a non-uniform drying of the structure during assembly, the deposition process was carried out within a paraffin oil reservoir at room temperature. After deposition, the samples were removed from the oil bath and dried in ambient conditions for at least one day before thermal treatment.

2.2.4 Thermal processing of assembled structures (Sintering)

Thermal de-binding kinetics of robocast bioglass constructs was evaluated using thermo gravimetric analysis, TGA, and differential thermal analysis, DTA, (Setsys Evolution-16 Setaram). Samples of as-received 45S5 bioactive glass powder and of robocast inks prepared from 45S5 glass milled powders, after drying for 1 day at 100 °C, were heated in air at 5 °C min^{-1} up to 1200 °C. Based on these kinetic data, the following thermal treatments were selected for the removal of the polymeric additive and sintering of the as-printed structures.

Thermal burn-out of CMC was performed in air at 400 °C for 1h, with a heating rate of 1 °C min^{-1}. After this dwell time, heating continued at a rate of 2 °C min^{-1} up to the sintering temperature, which was soaked for 1 h. In order to tailor the microstructure of the rods, several sintering temperatures from 550 °C up to 1000 °C were used. The sintered samples were cooled in the furnace at a rate of approximately 10 °C min^{-1}.

2.3 Deposition of polymer coating on 45S5 bioglass-based robocast scaffolds

Natural biodegradable polymers, including alginate, chitosan and gelatin, and biodegradable synthetic polymers, including PCL and PLA, were chosen to coat 3D 45S5 bioglass scaffolds. Infiltration of natural and synthetic polymers was done by dip coating (Fig. 1.13), i.e. by immersion of the bioglass-derived scaffolds in the polymer dissolved in an organic solvent (for PCL and PLA), water (for alginate and gelatin) and 2 vol.% acetic acid aqueous solution (for chitosan).

Polymer solutions were prepared by gradually dissolving pre-weighed powders/pellets in the solvent under constant stirring until completely dissolved. Dip coating was carried out in air by placing the bioglass scaffold in the polymeric solution under mild stirring for 30 min. Coated 45S5 bioglass scaffolds were then retrieved and kept in an oven during 48 h at 37 °C, for the evaporation of the solvent.

The mechanical and biological properties of the coated scaffold depend on many factors, such as the in-rod microporosity, the selected polymer, variables of the coating process etc. In particular, in this work, the effect of the following factors on the mechanical properties, biodegradability and bioactivity of the coated scaffold were studied.

1. **In-rod microporosity**. In this case, 45S5 bioglass scaffolds sintered in the range 550–1000 °C, and so with different levels of microporosity, were coated with either PCL or PLA. The coating solutions were prepared as follows: PCL and PLA were dissolved in toluene at 60 °C with a concentration of 25 % w/v and 15 % w/v respectively, by magnetically stirring for 1 h. Higher concentrations caused the polymers to partially fill also the pre-designed macropores decreasing their interconnectivity.

2. **Solvent**. 45S5 bioglass robocast scaffolds sintered at 550 °C were used for this task, and the coating process was done with 10 % w/v PCL solution at room temperature. Three different solvents as toluene, xylene and acetone were considered in order to determine the best solvent for dissolving the

PCL. The polymer content and soaking temperature were selected based on the simplicity and speed of coating process.

3. **Solution temperature**. 45S5 bioglass robocast scaffolds sintered at 550 °C were used for this task. The coating was performed in 10 % w/v PCL dissolved in toluene at three different temperatures: RT, 60 °C and 80 °C.

4. **Polymer content**. Solutions of PCL and PLA in toluene, alginate and gelatin in distilled water, and chitosan in a 2 vol.% acetic acid aqueous solution, were tested for scaffold infiltration in order to determine the optimal concentration for each polymer for getting a homogeneous coating at both the micro- and macroscale. 45S5 bioglass scaffolds sintered at 550 °C used for this approach. The soaking temperature was fixed at 60 °C. Polymer concentration was increased in steps of 5 % w/v and the optimal value for each polymer was chosen as the maximum concentration enabling preservation of the pre-designed macropores.

5. **Polymer composition**. For this approach, 45S5 bioglass scaffolds sintered at 550 °C were used and a fixed amount of 5 % w/v of both synthetic and natural polymers was dissolved in the appropriate solvent at 60 °C. For synthetic polymers (PCL and PLA), toluene was selected as solvent, and for natural polymers, distilled water (alginate and gelatin), or acetic acid aqueous solution (chitosan) were used. The pH of natural polymer solutions before and after coating was measured to better analyze the bonding mechanisms of such polymers to the bioglass surface.

2.4 Characterization of bare and polymer coated 45S5 bioglass-based scaffolds

In this section, the techniques used for microstructural and mechanical characterization and also for the evaluation of the *in vitro* biological performance of bare and coated scaffolds are described.

2.4.1 Microstructural characterization

The experimental procedures used in the microstructural characterization of the samples are described in detail in the followings sections.

2.4.1.1 X-ray diffraction

For identification of the phases present, X-ray diffractometry (D8 Advance, Bruker, Germany) using CuKα radiation was performed on 45S5 bioglass grounded samples after sintering at selected temperatures. The XRD data were collected in step-scanning mode (step width 0.03° 2θ, angular intervals 10–65° 2θ and count time 4 s per step).

2.4.1.2 Microscopy and geometrical analysis

The microstructure of bare and coated scaffolds was examined using a scanning electron microscopy (SEM, S-3600N, Hitachi, Japan), after metallization in a sputter-coater. As-cut and as-fractured cross-sections were used when required. In the case of coated scaffolds, these observations allowed to assess the quality of the coating.

Internal dimensions, such as rod diameter, *d*, and in-plane and out-of-plane gaps, *x* and z, respectively (Figure 2.2), of green and sintered scaffolds were determined as the average of a minimum of 100 direct measurements performed on SEM images.

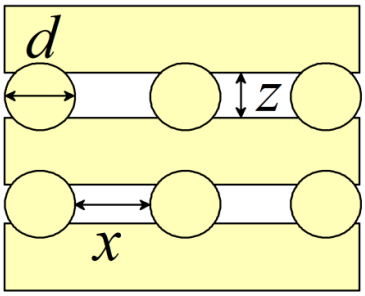

Figure 2.2. Schematic of scaffold's internal dimensions evaluated from SEM micrographs: rod diameter, d, and in-plane and out-of-plane gaps, x and z.

The linear shrinkage, ΔL, of the samples was calculated at specific temperatures from the variation of their external dimensions as:

$$\Delta L = (L_i - L_f)/ L_i \qquad (2.1)$$

where L_i is the initial dimension of the specimen at room temperature and L_f is the dimension after sintering at the selected temperature. Shrinkage was evaluated as the average of measurements performed on four different specimens, with standard deviations as error.

2.4.1.3 Density and porosity evaluation

The density of the green and sintered scaffolds, ρ_s, was determined from the mass and external dimensions of the structures. These values were obtained as the average of measurements performed on four different specimens per condition. The total porosity, p, was then calculated as:

$$p = 1 - \rho_s / \rho_{th} \qquad (2.2)$$

where ρ_{th} = 2.7 g.cm^{-3} is the theoretical density of bulk 45S5 bioglass, as provided by the supplier. The open total porosity was determined using the

apparent density, ρ_a, measured at each sintering temperature by He-pycnometry (SPY-D160-E Quantachrome) instead of ρ_{th} in equation 2.2.

The macroscopic, pre-designed porosity was estimated from geometrical considerations assuming an ideal network of interpenetrating cylinders. For this purpose, the values of the scaffold's internal dimensions evaluated from SEM micrographs were used (Fig. 2.2). The open microporosity on the 45S5 bioglass scaffolds' struts at each sintering temperature was subsequently evaluated from the open total porosity of the scaffold and the macroporosity.

2.4.2 Mechanical characterization

The mechanical response of the materials was evaluated under compression and in some cases also under bending stresses. All tests were performed in air using a universal testing machine (AG-IS 10KN, Shimadzu Corp., Kyoto, Japan), and a constant crosshead speed of 0.6 mm min^{-1}. The force was applied in a direction perpendicular to the printing plane (i.e. orthogonal to the scaffold rods). Prior to mechanical testing, the contact surfaces of each sample were ground to produce smooth parallel surfaces.

For the uniaxial compression tests, nine identical specimens with external dimensions of 3 × 3 × 6 mm were cut from the green, as-sintered and polymer-coated ceramic structures. Engineering stress-strain curves were calculated through normalization of captured load vs. displacement data using the initial external dimensions of each sample. The compressive strength of the structure was evaluated as the maximum applied stress and the toughness was estimated as the strain energy density, G_C, from the integral of the nominal stress–strain curves at 20 % strain.

Four-point bending tests were performed on green, as-sintered and some of the polymer-coated ceramic structures. For each group, nine samples were cut to final dimensions around 25 × 4 × 2 mm with roods aligned parallel to the length and width of the sample. Maximum applied load, F_{max}, was determined from the captured load vs. displacement data and used to estimate the bending strength, σ_f, using the following equation:

$$\sigma_f = 3\,(L_2 - L_1)\,F_{max}\,/2wh^2 \qquad (2.3)$$

where L_1 = 10 mm and L_2 = 20 mm are the distances between the two upper and two lower support cylinders, respectively, w the width of the specimen and h its thickness (Figure 2.3).

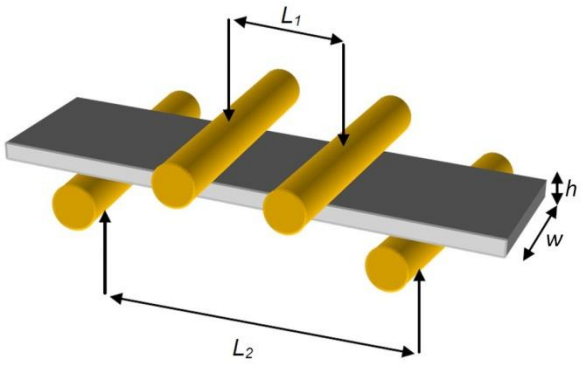

Figure 2.3. Schematic diagram of a 4-point bending test.

Toughness of tested specimens was estimated as the strain energy density, G_f, from the integral of the load-displacement curve (normalized by the effective volume of the sample) at 0.5 mm stroke. The flexural modulus was also measured with the aid of an extensometer.

2.4.3 *In vitro* bioactivity and degradation study

The *in vitro* bioactivity, degradation and mechanical properties evolution of bare and polymer-coated 45S5 scaffolds sintered at 550 °C (amorphous) and 1000 °C (highly crystalline glass-ceramic) were investigated by soaking them in simulated body fluid (SBF). The SBF solution was prepared according to the procedure described by Kokubo.[163] Scaffolds, with dimensions of 3 × 3 × 6 mm, were immersed in polyethylene bottles containing SBF solution at a liquid/solid ratio of 100 ml/g, and kept for up to 8 weeks, without shaking, in an incubator at 37 °C. The SBF solution was not refreshed during the experiment.

Weight loss, HA deposition, pH and mechanical properties evolution with immersion time were evaluated for each type of sample. Different samples were used for each immersion time and type of measurement.

The weight loss was calculated as $\Delta W/W_0$, where $\Delta W=W_0-W_t$, W_0 is the initial mass of the scaffold, and W_t is the mass at time t. To determine W_t, the samples were removed from the SBF solution, rinsed with distilled water and dried at 37 °C for 24 h and the their final weight carefully measured. For each time point, three scaffolds of each material were used to measure the weight loss and results were expressed by as mean ± standard deviation. The morphology of scaffolds after immersion in SBF was observed by SEM to analyze the progress of HA layer deposition.

Evolution of pH was measured on separate samples (2 samples per material and time point). After retrieving these scaffolds from SBF solution, the solution was cooled to room temperature, and its pH was measured.

Separate samples were also used to evaluate the evolution of their mechanical properties with immersion time by compressive tests. A minimum of 9 samples per material and time point were tested.

.

Chapter 3

Results and Discussion

In this chapter the experimental results obtained from this study are presented. First, the results corresponding to the optimization of the robocasting inks and subsequent sintering step used for the fabrication of 45S5 bioglass scaffolds, as well as the microstructural and mechanical characterization of the bare scaffolds are shown and analyzed. Second, the mechanical properties of 45S5 scaffolds coated with synthetic and natural polymers focused on PCL, PLA, chitosan, alginate and gelatin by a dip-coating process are discussed in detail: the effect of various processing parameters on the mechanical properties of the coated scaffolds are discussed. Third, the results of the *in vitro* characterization performed on bare and coated scaffolds are presented; the bioactivity and biodegradation behavior, and subsequent mechanical evolution are discussed in detail. Finally, a comparison of the mechanical properties of the novel biomaterials developed in this work and natural bone is performed and some implications of this study are discussed.

3.1 Fabrication and characterization of 45S5 bioglass-derived scaffolds

In this section the results regarding the fabrication of 45S5 bioglass-derived scaffolds by robocasting, including ink preparation and sintering, are discussed. The microstructural characterization and the mechanical performance of 45S5 scaffolds are also analyzed.

3.1.1 Optimization of 45S5 bioglass robocasting ink

As described in section 2.2.2, the fabrication of the bioglass robocast scaffolds involves, as a critical step, the preparation of a concentrated colloidal suspension (ink) with a very specific rheological behavior, which enables it to be extruded through a narrow nozzle and then retain shape immediately after deposition. Indeed, the main challenge in the robocasting of 45S5 bioglass is ink preparation. This section analyzes the suitable robocasting ink from 45S5 bioglass powders in aqueous medium.

The particle size distribution of the as-milled 45S5 bioglass powder used in preparing the inks for robocasting is shown in Figure 3.1. The particles had a wide distribution of sizes, with a median diameter of 4.3 μm.

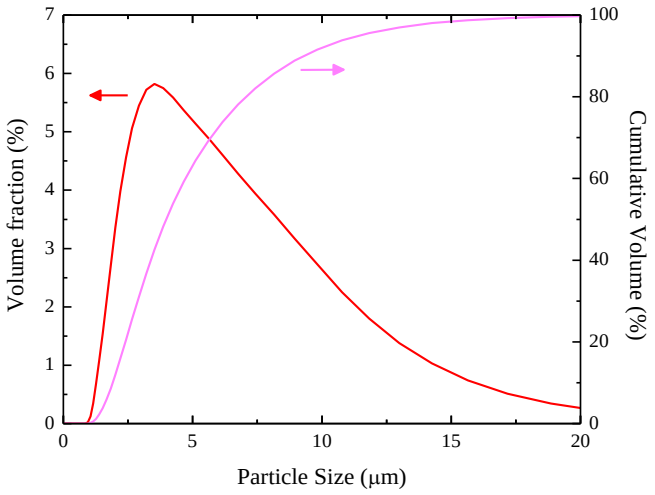

Figure 3.1. Particle size distribution of the as-milled 45S5 bioglass powder.

According to our own preliminary tests, traditional approach—where anionic/cationic interactions of species added to the system in different successive steps are used to promote the rheological transition from a fluid-like behaviour (starting suspension) to a paste-like character (robocasting ink)—could not offer successful prospects for robocasting processing of 45S5

bioglass. Based on all the above considerations, a completely different and simplified approach has been adopted: searching for a single additive that could act as both dispersant and binder for robocasting. In this pursue a single additive named carboxymethyl cellulose (CMC) was used. The less polar character of the CMC chains in comparison to the anionic polyelectrolyte molecules facilitates surface adsorption. Such adsorption is likely to occur, however, through small chain segments, with laces and tails extending to the solution; since it is not electrostatically driven (both CMC molecules and the surface of the particles have the same negative polarity). The predicted configuration of the CMC molecules adsorbed at the surface of the 45S5 Bioglass® particles is likely to play a steric effect which enabled reaching significantly higher solid loadings, up to 45 vol.%, compared to anionic polyelectrolytes.[104] In particular, high molecular weight CMC (Mw = 250 000, Lamberti Iberia s.a.u., Castellón, Spain, with a viscosity η= 1–3 Pa·s for a 2 wt.% aqueous solution) was found more appropriate for the preparation of inks for robocasting since longer chains induced a stronger thickening effect, which was attributed to a bridging flocculation mechanism.

The evolution of the estimated yield stress, τ_y, and the average elastic (storage) modulus, G′, at low shear stress of suspensions with added CMC as the sole binding agent is shown in Figure 3.2 These parameters reflect, respectively, the strength and stiffness of the attractive network structure resulting from interactions between 45S5 bioglass particles, CMC and water. In fact, in the absence of CMC, both the yield stress and the modulus of the suspension are very low. Upon addition of CMC, the yield stress increases linearly with the amount of binder up to a concentration of 1 wt.%, and then decreases at 2 wt.%. This thickening effect promoted by CMC might be attributed to chain entanglement of the molecules adsorbed on the surface of the particles and/or to an increased viscosity of the dispersing medium. On the other hand, the elastic modulus increases first very slowly, then dramatically (by 2 orders of magnitude) at 1 wt.% CMC additions, and finally decreases at 2 wt.% CMC concentrations. The dramatic change in modulus observed for 1 wt.% CMC indicates a fluid-to-gel transition attributed to the occurrence of bridging-flocculation, in which the longer polymeric chains might adsorb at the surface of different neighbouring particles. Further increase of the amount of CMC leads to a higher degree of surface coverage and a denser adsorbed layer, which decreases the probability of one polymeric chain to adsorb in more than one

particle, thus hindering bridging-flocculation and reducing both the modulus and the yield stress.

Since high values of τ_y and G′ are desired features for robocasting inks, 1 wt.% was considered as the optimal CMC amount. This concentration yielded maximum network stiffness (> 100 kPa), and yield stress (> 1 kPa) at a relatively low viscosity, which facilitates flow ability through the deposition nozzle. Indeed, such suspensions exhibited both very good flow ability (unlike suspension with higher CMC concentrations) and excellent shape retention capacity upon deposition, which made them ideal inks for robocasting.

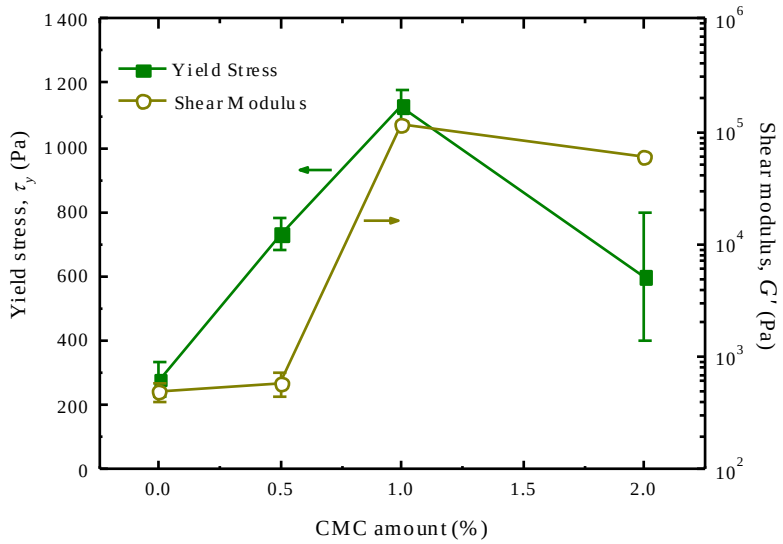

Figure 3.2. The effect of the amounts of CMC on the yield stress, τ_y, and the average shear elastic modulus, G', of 45 vol.% 45S5 bioglass suspensions.

Figure 3.3 shows 45S5 three dimensional porous scaffolds made of multiple layers produced by robocasting using this ink. These results demonstrate that it is possible to create well shaped, uniform lattices having rod sizes in the range of 250-410 μm using 45S5 gels with 1 wt.% CMC-250 as a single additive.

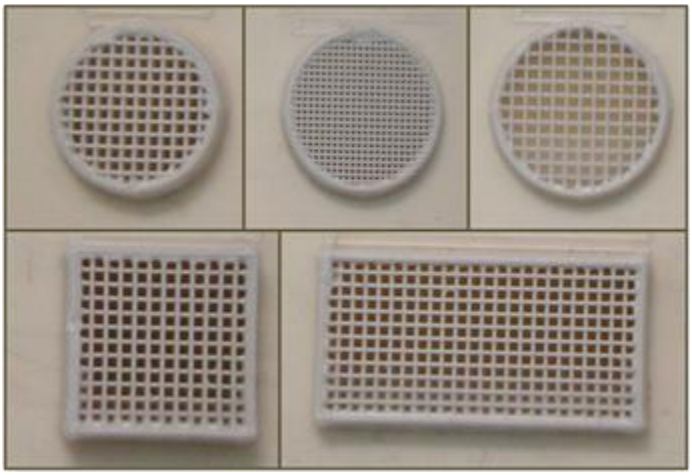

Figure 3.3. 3D porous scaffolds produced by robocasting from a 45S5 bioglass ink with 1 wt.% CMC-250 additive optical image showing different scaffolds geometries with up to 60 layers.

3.1.2 Sintering of 45S5 bioglass robocast scaffolds

In this section, the results of the sintering study performed on 45S5 scaffolds fabricated by robocasting within the temperature range 500-1050 ºC are discussed. The scaffolds used for the study consisted of a tetragonal mesh of cylindrical rods, created using the optimized ink recipe.

TGA and DTA results of 45S5 bioglass as-received powder and of the as-dried ink are shown in Figure 3.4. The as-received powder undergoes a marked weight loss in the range of 200-400 ºC (Fig. 3.4a), which is associated to the evaporation of free water and the release of surface –OH groups, a phenomenon reflected as an endothermic effect, especially observed between room temperature and 200 ºC in the DTA plot (Fig. 3.4b). A second endothermic dip centered at ~ 560 ºC is observed, which is attributed to the first transition temperature of the glass (T_{g1}). This is followed by an exothermic effect starting around ~ 600 ºC and with a maximum at about 685 ºC (T_{p1}), which is attributed to crystallization. A second exothermic peak centered at ~ 850 °C (T_{p2}), attributed to the formation of a secondary crystalline phase, is followed by a new endothermic valley associated to a second glass transition (T_{g2} ~ 910 °C) of

the remaining glass matrix. Melting clearly occurred above 1100 °C, as deduced from the associated endothermic valley.

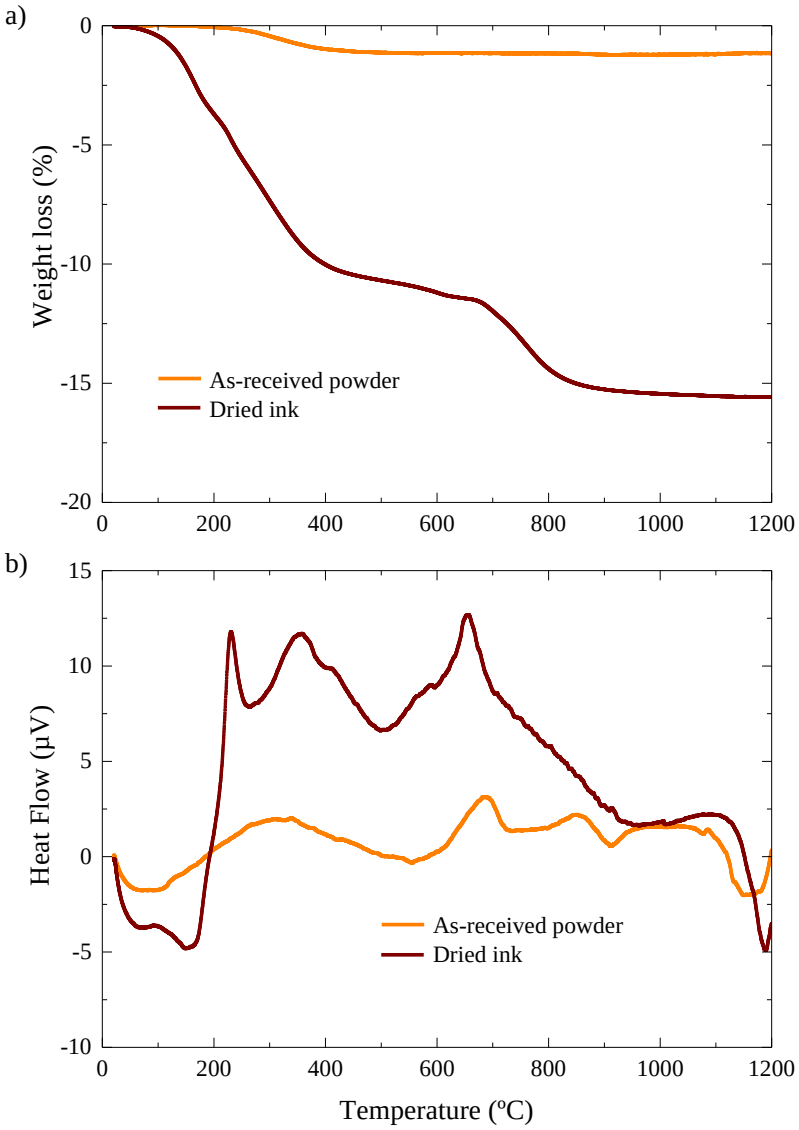

Figure 3.4. *Results of the simultaneous (a) thermal gravimetric analysis (TGA, weight loss) and (b) differential thermal analysis (DTA, heat flow) of 45S5 bioglass as-received powder and as-dried robocasting inks.*[164]

The weight changes (Fig. 3.4a) and the corresponding thermal effects (Fig. 3.4b) were greatly enhanced in the dried ink, probably as a result of a more extended surface hydration of the powder undergone while in contact with dispersion media (ball milling and ink preparation), and of the burnout of CMC additive. Indeed, the weight loss centered in the range of 700–800 °C, but extending beyond these limits, is attributed to the burnout of carbonaceous remnants from CMC degradation. This degradation occurred in two successive steps, originating two exothermic peaks at ~ 225 °C and ~ 350 °C (Fig. 3.4b), as confirmed by a TG/DTA test performed on pure CMC (results are shown in Figure 3.5). This suggested the use of a debinding treatment at 400 ºC for 1 h prior to sintering.

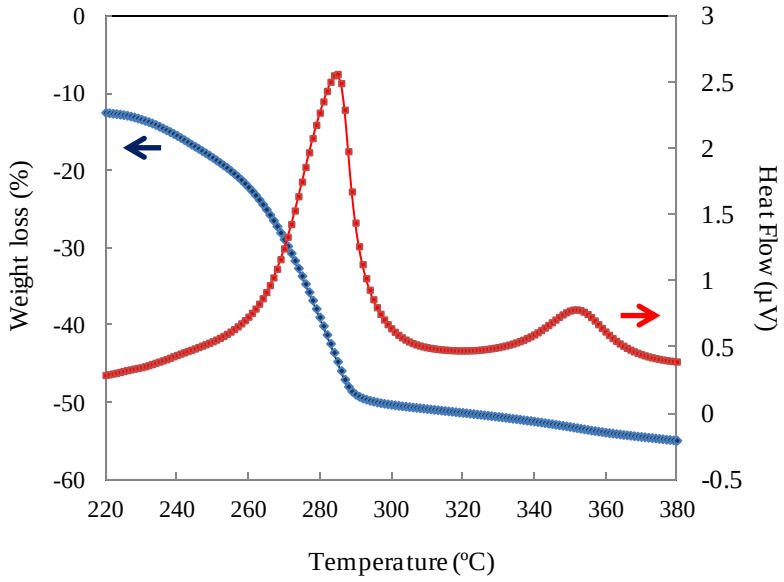

Figure 3.5. Result of TGA/ DTA for CMC-250 powder.

Interestingly, the thermal events T_{g1} and T_{p1} occurred in the ink, respectively, at about 60 °C and 30 °C below the corresponding temperatures in the as-received 45S5 bioglass powder, implying a concomitant shift of the intermediate exothermic effect associated to the nucleation step. This shift is attributed to a change in the composition at/near the particles' surface as a result

of leaching of modifier cations (Na^+, Ca^{2+}) during wet-milling, and also to the reduction in the particle size.[165,166] Besides, T_{p2} and T_{g2} cannot be distinguished for the dried ink, possibly because they are also shifted to lower values and became overlapped with the peak for first crystallization. The apparent increase of melting temperature of the ink is also consistent with the leaching of modifier cations into the milling media.

3.1.3 Microstructural characterization

In this section, the results from the microstructural characterization of the robocast structures are presented.

3.1.3.1 XRD analysis

These results obtained from thermal analysis are in good agreement with the XRD results shown in Figure 3.6. The 45S5 bioglass remained amorphous up to above 550 °C but there is evidence of crystallization already at 600 °C. The angular location and intensity of the new peaks appearing upon crystallization of 45S5 bioglass closely match the standard JCPDF database 77-2189, confirming that the major crystalline phase is $Na_2CaSi_2O_6$. Minor peaks of a secondary phase, attributed to $Na_2Ca_4(PO_4)_2Si_2O_4$ (JCPDF database 32-1053), were also identified on samples sintered at 1000 °C, all in good accordance with previous reports.[167–169]

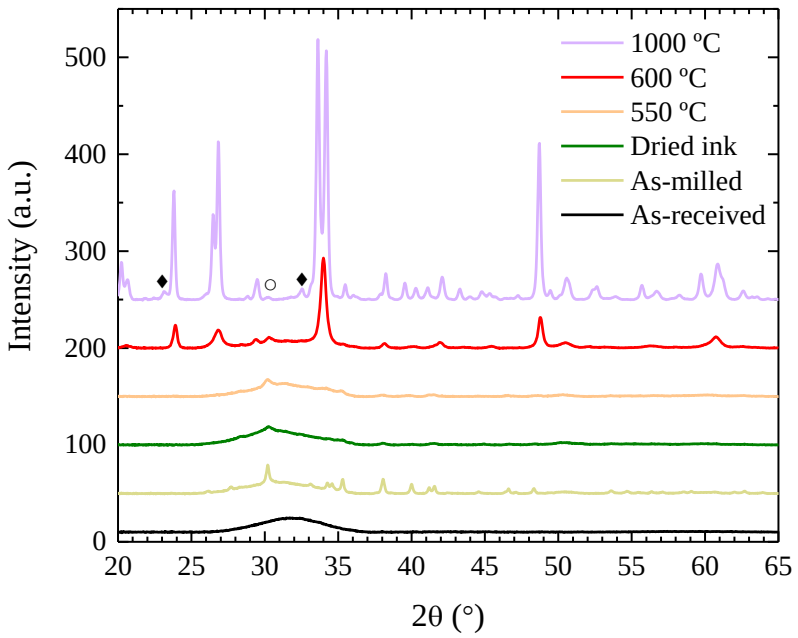

Figure 3.6. X-Ray diffractograms of 45S5 bioglass as-received and as-milled powders, and ground scaffolds sintered at the indicated temperatures. Sodium carbonate (Na_2CO_3, JCPDF database 19-1130) peaks are clearly visible on the as-milled powders, and barely on the sample sintered at 550 °C. Peaks at 600 °C, correspond to $Na_2CaSi_2O_6$ (JCPDF database 77-2189) crystallized from the glass. At 1000 °C, $Na_2CaSi_2O_6$ remains the main crystalline phase with some additional peaks, noted by ♦ and ○, corresponding to $Na_2Ca_4(PO_4)_2Si_2O_4$ (JCPDF database 32-1053) and tetragonal zirconia (ZrO_2, JCPDF database 72-7115), respectively.

There are, however, some peaks already observable at 550 °C and below, which correspond to sodium carbonate (Na_2CO_3, JCPDF database 19-1130) formed during the milling process in ethanol, with some small contribution of tetragonal zirconia from the milling media and container. The sodium carbonate, deposited onto the surface of the particles during milling, partially dissolves in water during ink preparation, which produces a substantial decrease in the intensities of the peaks corresponding to this extraneous phase. Actually, the peaks more clearly observable in the dried ink or in samples sintered at 550 °C, located at

30.2° and 35.3° 2θ, can also be appreciated even at 1000 °C, and are therefore attributed to the overlapping tetragonal zirconia phase rather than the sodium carbonate. Nonetheless, the presence of even small amounts of sodium carbonate in the XRD results support the explanation for the systematic down-shift of thermal events (except melting) in Fig 3.4b based on a changed composition, rich in Na^+ cations, at/near the particles' surface.

3.1.3.2 Geometrical analysis

Figure 3.7 shows the evolution of 45S5 bioglass-derived scaffolds' macroscopic linear shrinkage and internal dimensions with the sintering temperature, with standard deviations as error bars. The data at room temperature correspond to as-dried green structures. The structure shrinkage during sintering was essentially isotropic, and the scaffolds kept the designed parallelepipedical shape upon sintering for 1 h up to 1050 °C. Above 1050 °C or for longer sintering times at this temperature, indications of melting/softening of the material became evident to the naked eye: the scaffold specimen deformed under its own weight and the shape was distorted, with some material accumulation at the bottom. For instance, when treated at 1200 °C for 1 h the samples completely melted and collapsed with almost no remaining macroporosity. Due to the severe distortions they presented, samples sintered above 1050 °C were not characterized.

According to Fig. 3.7, the shrinkage, obtained from measurements of the scaffolds' external dimensions, increases steadily with the sintering temperature, although at a somewhat faster rate around the two glass transition temperatures (500-550 ºC, T_{g1}, and 800-850 ºC, T_{g2}). This result is in good agreement with previous reports.[168,170,171] The internal dimensions of the scaffolds (rod diameter, d, in-plane gap, x, and out-of-plane gap, z) show the same trend as the external dimensions, decreasing

steadily with sintering temperature, but at a faster rate around the glass transitions.

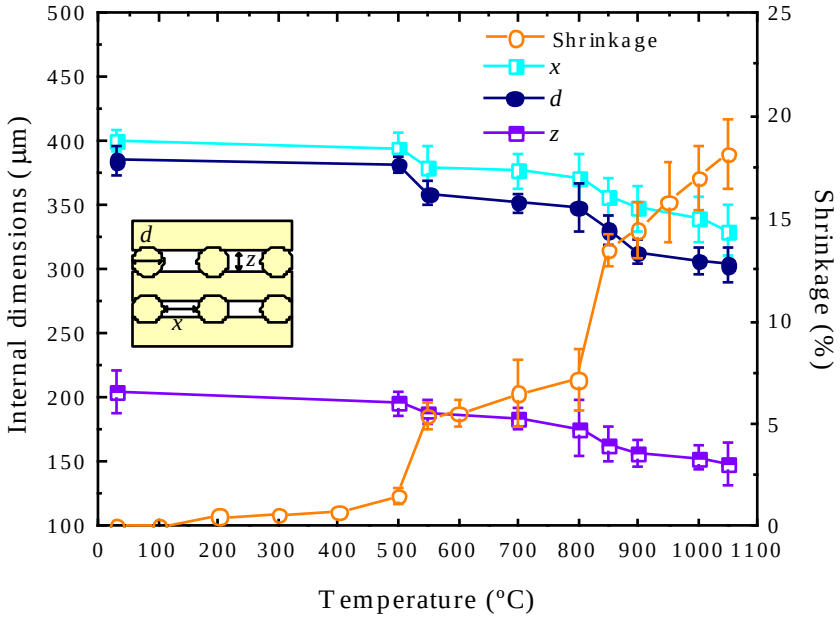

Figure 3.7. The evolution of macroscopic shrinkage and scaffold's internal dimension (indicated) as a function of sintering temperatures. Data represent mean values with standard deviations as error bars.

Figure 3.8 shows the evolution of total, macro- and micro-porosity with sintering temperature. The total open porosity of the scaffolds is reduced upon increasing the sintering temperature and the structure shrinks. This reduction results from densification of the scaffold struts, since the total level of macroporosity remains constant—at 50 % for the scaffold design used here—regardless of the sintering temperature.

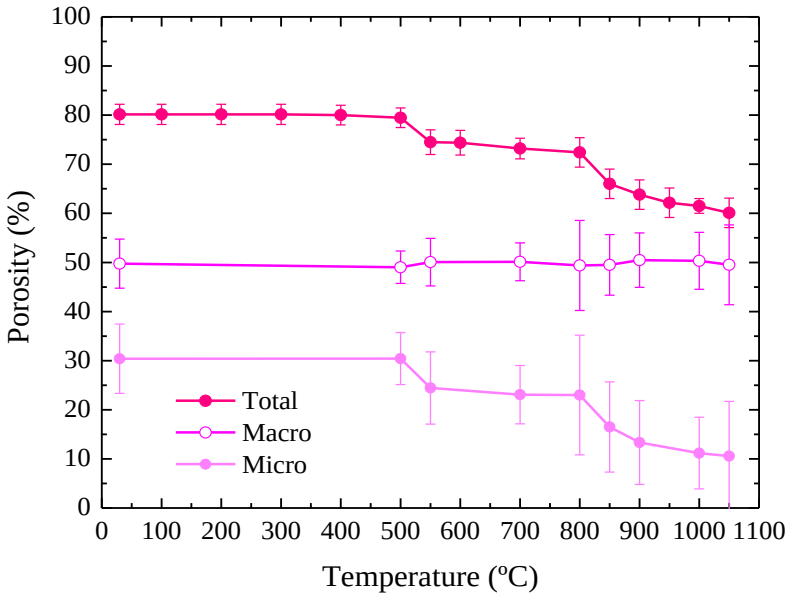

Figure 3.8. The evolution of scaffold porosities as a function of sintering temperatures. Data represents mean values with standard deviations as error bars.

Consequently, all the densification produced during sintering, from an as-dried green body porosity of 80 ± 2 % to a minimum of 60 ± 2 % after sintering at 1050 °C, was associated to a reduction of the microporosity within the glass-ceramic rods. Meaning that the rods reduced their initial ~ 60 % porosity (which roughly agrees with the 45 % solid loading of the inks) to around a final 20 % porosity at the highest sintering temperature. Failure to achieve a high densification of the rods even at temperatures so close to the melting point is not an unexpected result, given the poor sintering ability of 45S5 bioglass even under pressure-assisted sintering.[172,173] Again, as discussed for shrinkage (Fig. 3.7): there is a steady densification of the scaffolds with increasing sintering temperature, but densification is significantly enhanced around the two glass transition temperatures, and sluggish in-between.

3.1.3.3 SEM microstructural analysis

Figure 3.9 shows SEM micrographs of the rod surfaces of scaffold sintered at the indicated temperatures. No sintering occurred up to the glass transition temperature at 550 °C, when the glass softened enough to allow some viscous flow, and even at that temperature the microstructure does not differ all that much from that of green samples (compare top images in Fig.3.9), except for the evidences of inter-particle neck formation (see inset in top-right image of Fig. 3.9). At around 600 °C, just after the glass transition, the glass started to crystallize (Fig. 3.6), which severely slows down the densification process by reducing the species diffusivity and increasing the system viscosity. At this point, it is worth mentioning that the maximum percentage of crystallinity achievable in 45S5 bioglass is about 80 %,[174] so that even at the highest sintering temperatures the material remains a glass–ceramic. Densification regains pace at around 850 °C, when the residual phosphate-rich glassy phase softens and progresses appreciably with further increasing sintering temperature. Indeed, porosity at the rod surfaces is almost gone at 1000 °C (bottom-left image in Fig. 3.9), although there remains a significant level of internal (closed) porosity. Up to this sintering temperature, the rod surface microstructure evidences the presence of crystalline grains homogenously embedded in a glass matrix. However, the intergranular glassy phase seemingly disappeared from the surface of the rods upon increasing the sintering temperature to 1050 °C, or the holding time at 1000 °C to $\geq$ 2 h and the naked grains became apparent (bottom-right image in Fig. 3.9). This inhomogeneous microstructure which consists of bared crystalline particles with virtually no glass matrix reveals an over-sintering process. This over-sintering was accompanied by an apparent increase in surface porosity, while the material's microporosity continued diminishing steadily with the chronothermic increments, as shown in Fig. 3.8. This suggests that the glassy phase—with a very low viscosity so close to the melting temperature—might be draining from the surface towards the interior of the rods and aiding in the reduction of the aforementioned closed porosity.

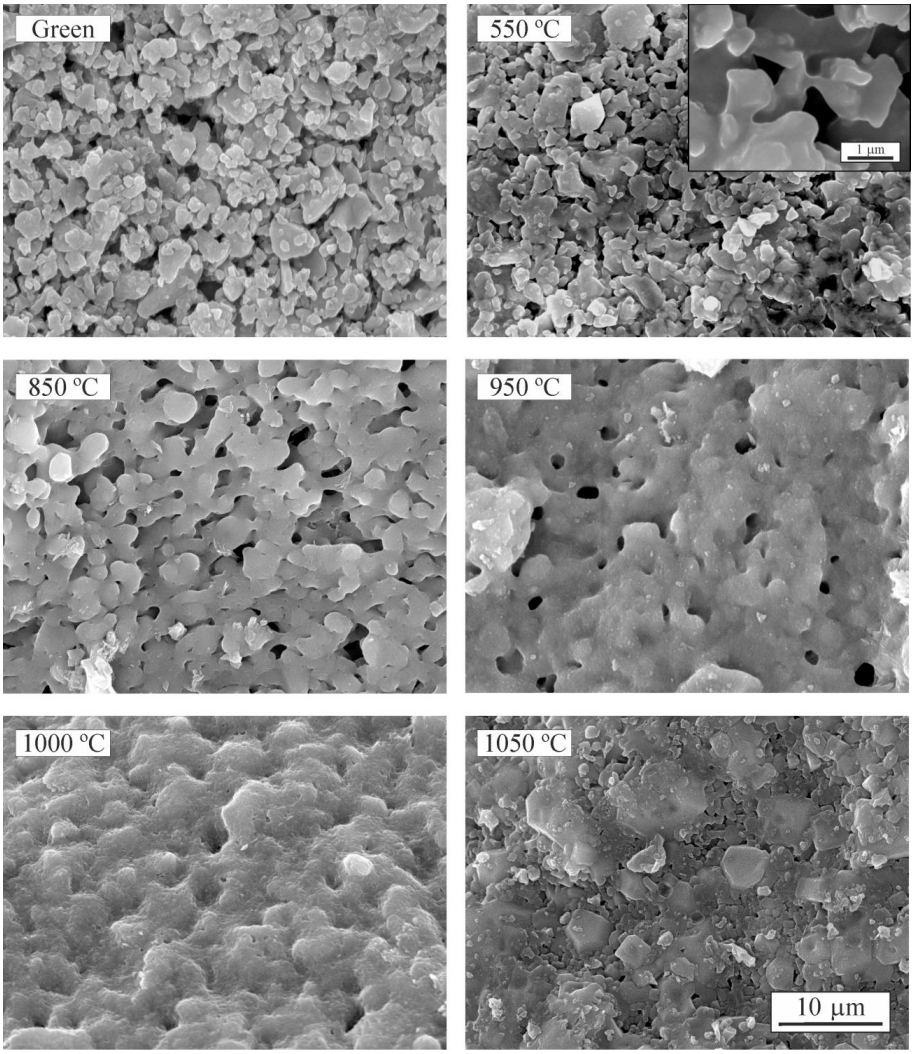

Figure 3.9. SEM micrographs of the rod surfaces of 45S5 bioglass-derived scaffold before and after sintering at the indicated temperatures.

The SEM micrographs of rod surfaces sintered at 550 °C and 1000 °C (Figure 3.10a,b) show that not only the rod size decreases at 1000 °C because of shrinkage but also the rod surface becomes much smoother showing a glassy feature with notably less microporosity.

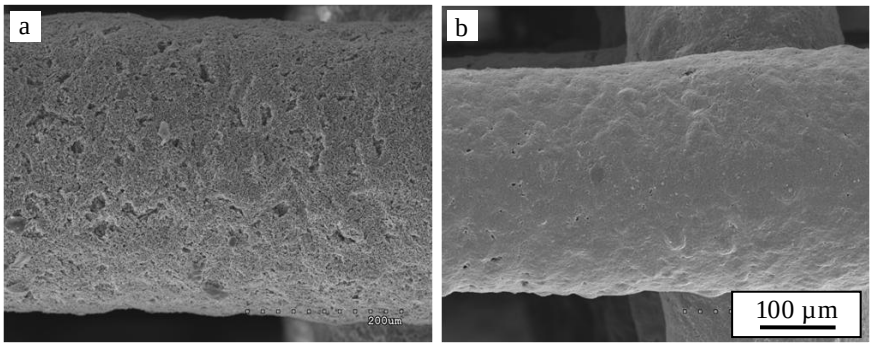

Figure 3.10. SEM micrographs of the 3D 45S5 scaffolds sintered at: (a) 550 °C and (b) 1000 °C.

3.1.4 Mechanical characterization

Figure 3.11 shows representative stress-strain curves of scaffolds both in green state and sintered at 550 °C, 800 °C and 1000 °C for 1 h. These samples were tested under uniaxial compression in the direction perpendicular to the deposition plane. The scaffolds show an elastic response almost until the compressive strength of the structure (i.e. the maximum stress) is reached. At this point, the first longitudinal cracks pops-in, breaking the unsupported rod segments close to the joints with adjacent layers, where maximum tensile stresses are located,[175,176] and the applied stress drops. As cracking multiplies and propagates all over the scaffold, the stress continues decreasing progressively down to zero with some eventual temporary increases associated to a certain densification of the fractured structure under the applied compression, which is typical on cellular structures.[177]

The evolution of the compressive strength of robocast 45S5 bioglass-derived scaffolds with the sintering temperature is shown in Figure 3.12. It is evident that strength increases steadily and strongly with sintering temperature, but there is no clear correlation of strength data with rod density or rod diameter, and the different stages observed in the data for the latter (Figs. 3.7 and 3.8) are not so clearly observed in Fig. 3.12.

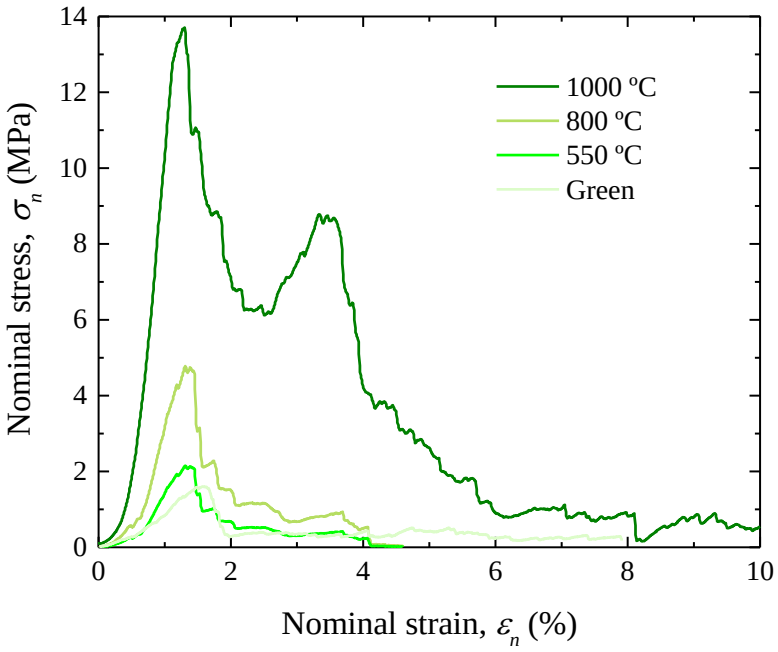

Figure 3.11. Representative compressive stress-strain curves of 45S5 bioglass-derived scaffolds sintered at the indicated temperatures for 1 h.

Especially indicative of this lack of complete correlation is the fact that while densification was improved in scaffolds sintered at 1050 °C, there is a statistically significant ($p < 0.05$) reduction in strength compared to structures sintered at 1000 °C (from 13 ± 1 MPa to 11 ± 1 MPa). This reduction is attributed to the deleterious change in the starting flaw population at the rod surfaces, where cracking initiates,[175,176] upon the aforementioned disappearance of the glass matrix (bottom-right image Fig. 3.9). This result emphasizes that surface defects are to be minimized whenever possible since their negative influence on scaffold strength can counteract and even supersede the positive effect of a reduction in the total porosity of the structure. Thus, surface flaw population effects, and maybe some toughness variations associated to the different microstructural and phase-compositional changes occurring in the material at different sintering temperatures, might be responsible for blurring the correlation between strength data and porosity/shrinkage results.

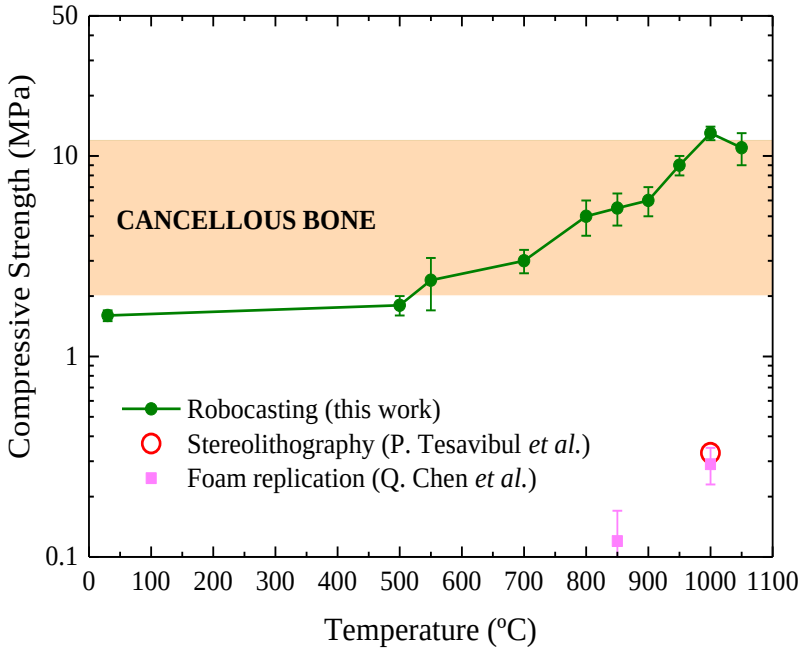

Figure 3.12. Evolution of the compressive strength of 45S5 bioglass-derived scaffolds with sintering temperature. Data represent mean values with standard deviations as error bars. Cancellous bone strength (shaded band)[20] *and results for scaffolds from other authors*[100,178] *are included for comparison.*

In any case, it is evident from these results that, at least in terms of mechanical performance, the optimal condition for sintering 45S5 bioglass-derived scaffolds fabricated by robocasting is 1000 °C for 1 h.

On the other hand, as shown in Fig. 3.12, when comparing these strength results with existing literature reports[100,178,179] and cancellous bone properties, it becomes evident that scaffolds produced by robocasting exhibit strength values far superior to anything previously reported for 45S5 bioglass-derived scaffolds —under the same sintering conditions, the enhancement is well over one order of magnitude (~ 4000 %). The reason for the enhancement of mechanical resistance over conventional scaffolds fabricated by foam replication[179] should be found on the improved pore architecture and thicker struts provided by robocasting. More surprising is the fact that other solid freeform fabrication methods such as stereolithography (STL),[100] which in principle provide the

same advantages, have not been able to duplicate these strength results. Nonetheless, as the authors of the latter report point out, the reason for this may lay in a less-than-optimal selection of the sintering process. 45S5 bioglass is difficult to sinter, especially into complex scaffold geometries, and great care needs to be taken in selecting the thermal treatment parameters to avoid deleterious cracking during sintering. This must be especially critical in the case of STL, were larger amounts of organic binders (compared to robocasting) have to be burnt out in the process. In any case, all robocast 45S5 bioglass-derived scaffolds sintered between 550 °C and 1000 °C fall within or even surpass the range 2-12 MPa frequently quoted for cancellous bone.[180,181] Consequently, robocasting provides, for the first time, a means to produce mechanically competent 45S5 bioglass (not just bioglass-derived) scaffolds. Indeed, the robocast scaffolds sintered at 550 °C remain completely amorphous and exhibit a compressive strength that, while barely improved over that of as-dried green structures, lies at the lower end of cancellous bone range and is enough for safe handling during implantation. This could help overcome one of the hurdles for the successful application of 45S5 bioglass as a broad-use bone substitute material: the difficulty to produce scaffold with sufficient mechanical integrity without reducing the outstanding bioactivity of amorphous 45S5 particles.[8]

At this point it is worth discussing some issues regarding porosity. Although the total porosities reported here (~ 60 % and ~ 80 % for scaffolds sintered at 1000 °C and 550 °C, respectively) are lower than typical values of conventional 45S5 bioglass-derived scaffolds (90-95 %),[178] conventional (foam replication) scaffolds with similar porosities as those reported here will still fall well short of robocast scaffolds in term of strength (as can be easily estimated by extrapolating reported data).[178] Moreover, there is ample evidence that, while such extremely high porosities might be required to attain significant bone in-growth in the tortuous architectures of conventional scaffolds, porosities such as those reported here are enough to allow bone regeneration in the case of calcium-phosphate robocast structures.[182–184] In any case, robocast scaffold porosities could be easily increased to match reported values by modifying the initial design, for example by increasing rod-spacing within each deposition layer.

3.2 Mechanical enhancement of 45S5 bioglass robocast scaffolds by polymeric coatings

In this section, the results from the microstructural and mechanical characterization of 45S5 bioglass structures infiltrated with biodegradable synthetic and natural polymers are presented. The effect of a number of processing parameters affecting the dip-coating process on the mechanical properties of the coated scaffolds is analyzed. The results from this analysis are used to determine the optimal infiltration conditions for each polymer. The mechanical properties of 45S5 scaffolds coated with the different polymers under optimal conditions are compared.

3.2.1 Role of scaffold microporosity

In the dip-coating process, the micropores on scaffold surface play a vital role as channels for polymer infiltration into struts interior. In this section, the effect of in-rod microporosities in the mechanical enhancement provided by polymeric –coatings on 45S5 scaffolds is analyzed. This study was carried out, as described in Section 2.3, using 45S5 bioglass-derived scaffolds sintered at different temperatures, which show different percentages of microporosity (Fig. 3.8), coated two different synthetic polymers, PCL and PLA.

SEM micrographs of representative as-fractured specimens of robocast 45S5 bioglass scaffolds sintered at 550 °C before and after coating with PCL and PLA are shown in Figure 3.13. The images corresponding to the bare structure show the combination of pre-designed macropores (Fig. 3.13a) and in-rod microporosity (Fig. 3.13b) that can be produced by robocasting, which has been shown to be beneficial for bone in-growth.[183] After dip-coating in polymer solutions, the scaffolds' highly interconnected macroporosity was preserved (Fig. 3.13c,e), but at least partial impregnation of the struts' microporosity was achieved (Fig. 3.13d,f). This is clearly evidenced by the PCL fibers visible in the fracture surfaces of the coated rods (Fig. 3.13d, inset); and although on PLA-infiltrated structures no microfibrils are apparent, a reduction of the number of pores is evident (cf. insets in Figs. 3.13b and f).

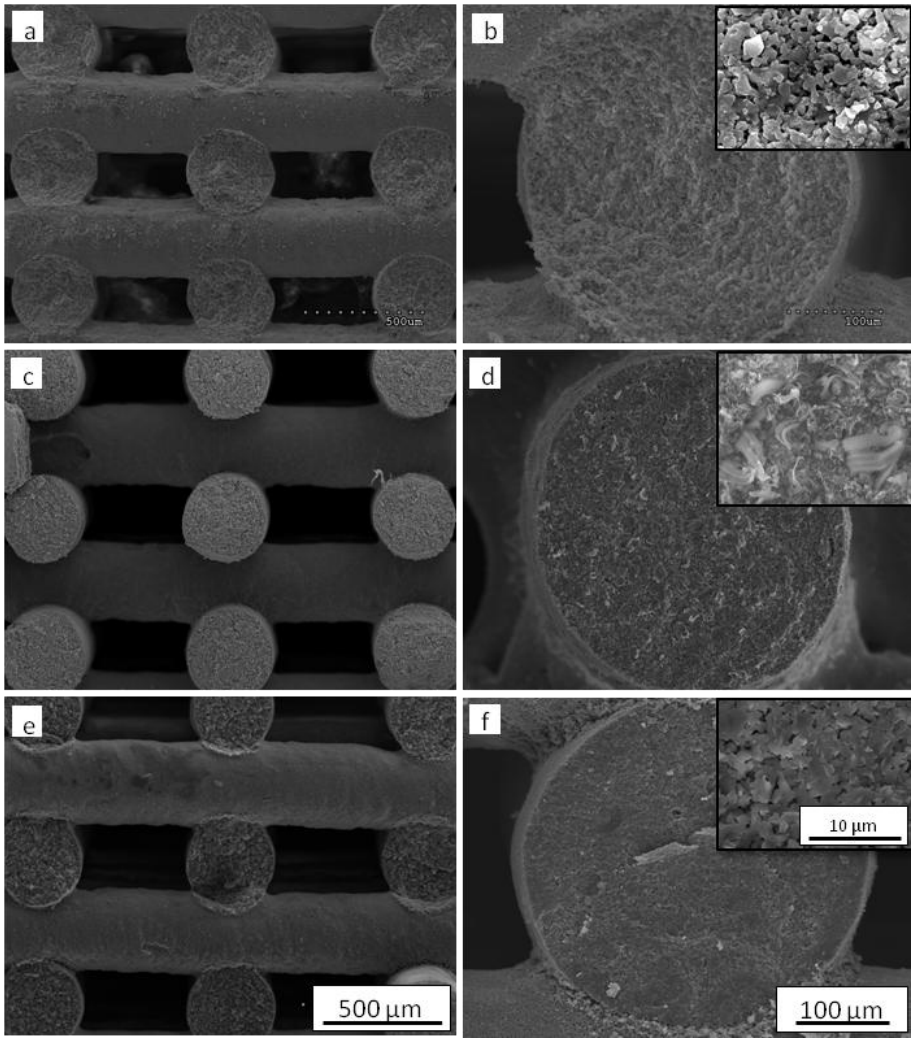

Figure 3.13. SEM micrographs of representative as-fractured specimens of 45S5 bioglass robocast scaffolds sintered at 550 °C: (a, b) bare, (c, d) PCL-coated and (e, f) PLA-coated structures.

The relation between the defect population and the mechanical improvement associated to polymer infiltration was evaluated both in compressive and four point-bending tests, and the results obtained are presented in the following sections:

3.2.1.1 Compression tests

Figure 3.14 shows representative uniaxial compressive stress–strain curves for the 45S5 scaffolds sintered at 550 °C and 1000 °C, before and after coating with PCL or PLA. The bare scaffolds show the typical response of cellular structures under compression, with an elastic response until fracture occurs. Some fracture events may occur even before the maximum stress, i.e. the compressive strength of the material, is reached. The compressive strength increases significantly, as expected, with the sintering temperature. After the maximum, the stress falls to zero progressively; sometimes exhibiting temporary stress increases (especially in the samples sintered at the higher temperatures) associated to as yet unfractured regions of the scaffolds or to densification of the structure fragments.

Polymer infiltration of the bioglass scaffold changes the stress-strain curves significantly (Fig. 3.14). The linear elastic region is extended, but the slope of the curve remains unaltered since the stiff glass skeleton still controls the elastic strain of the material. After failure, which occurs now at an increased stress, the applied stress still declines, but more slowly. It is clearly evident that regardless of the sintering temperature, the addition of the polymeric phase to the structure produces a notable increment in the strength and toughness, measured as area under the curve, of the bioglass structures, despite the fact that this process preserves the pre-designed macropores of the scaffold. However, both the maximum stress and the final asymptotic stress in these curves depend on the sintering temperature of the initial scaffold.

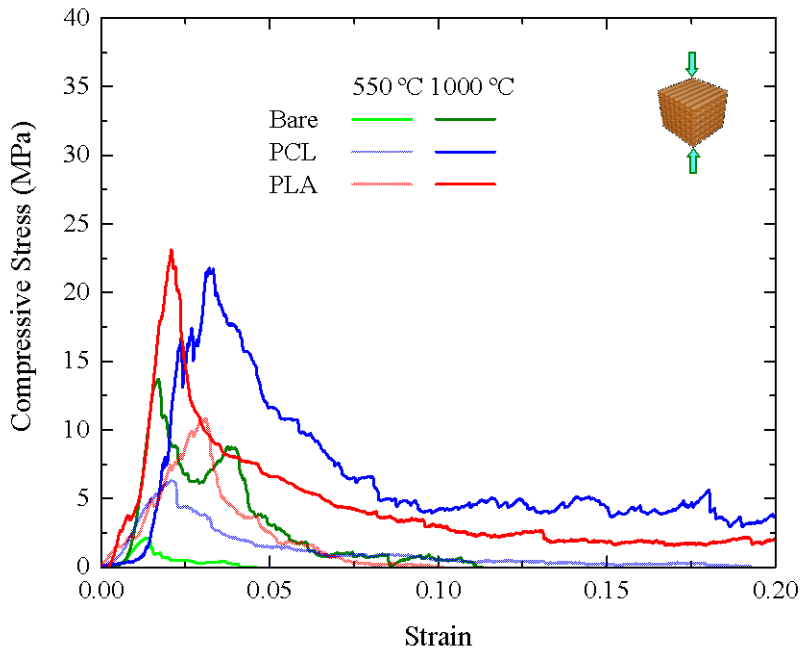

Figure 3.14. Representative uniaxial compressive stress–strain curves for 45S5 bioglass scaffolds sintered at 550 °C and 1000 °C before and after coating with PCL and PLA, as indicated.

To better analyze the strengthening effect of polymer infiltration, Figure 3.15a shows the evolution of the compressive strength versus sintering temperature for the bare robocast 45S5 scaffolds, and for the same structures after coating with PCL and PLA. The results in Fig. 3.15a confirm that polymer coating, either by PCL or PLA, is a valid strengthening procedure for 45S5 porous structures, with PLA providing a slightly greater enhancement. Nonetheless, it is evident that the compressive strength increase steadily and strongly with sintering temperature for the three groups. This highlights the importance of having a scaffold with strong, defect-free struts if mechanical resistance is a major concern for the intended application. Even when polymer infiltration is used for further mechanical enhancement of the structure, maximization of the intrinsic resistance of the struts through an optimal sintering treatment should be sought. Nonetheless, infiltration of the ceramic structure with a polymer is a good alternative to an appropriate sintering treatment. For example, the results of Fig. 3.15a show that a simple PCL

coating can provide a 45S5 scaffold sintered at 550 °C greater strength than sintering at 900 °C; or in the case of PLA, coated-scaffolds sintered above 700 °C already surpass the strength of optimal (i.e. sintered at 1000 ºC) bare scaffolds and cancellous bone performance

The strengthening factor provided by the infiltration method—obtained by normalizing the corresponding results by the strength of the bare structures at each sintering temperature—is shown in Fig. 3.15b versus the in-rod open porosity (from Fig. 3.8). As mentioned in section 1.6.2 the strengthening of polymer-impregnated robocast scaffolds occur by the mechanism of defect healing.[119].

The results of Fig. 3.15b demonstrate that the effectiveness of the defect healing mechanism depends not only on the polymer used for sealing the defects but also on the characteristics of the flaw population in the ceramic struts. The defect-healing strengthening factor increases monotonically with the open porosity of the scaffold struts. Thus, this factor will approach unity for scaffolds with fully dense, pristine struts, which is in good accordance with recent results obtained in 13-93 bioactive glass scaffolds.[81] It is reasonable to assume that the actual dependence of the strengthening factor for healing is with the effective critical flaw size[185,186] rather than the in-rod open porosity, but since both will decrease during strut densification the results of Fig.3.15b are logical. In any case, it is worth highlighting yet again that even if the defect healing mechanism becomes less effective as the flaw population decreases, eliminating strut defects (by improving sintering/densification) is the best strategy for maximizing the strength even in hybrid ceramic/polymer structures (see Fig. 3.15a).

Regarding the toughening effect of polymer infiltration, Figure 3.16a shows the evolution with sintering temperature of the strain energy density, G_C, calculated from the area under experimental stress strain curves, such as the ones presented in Fig. 3.14, at 20 % strain.

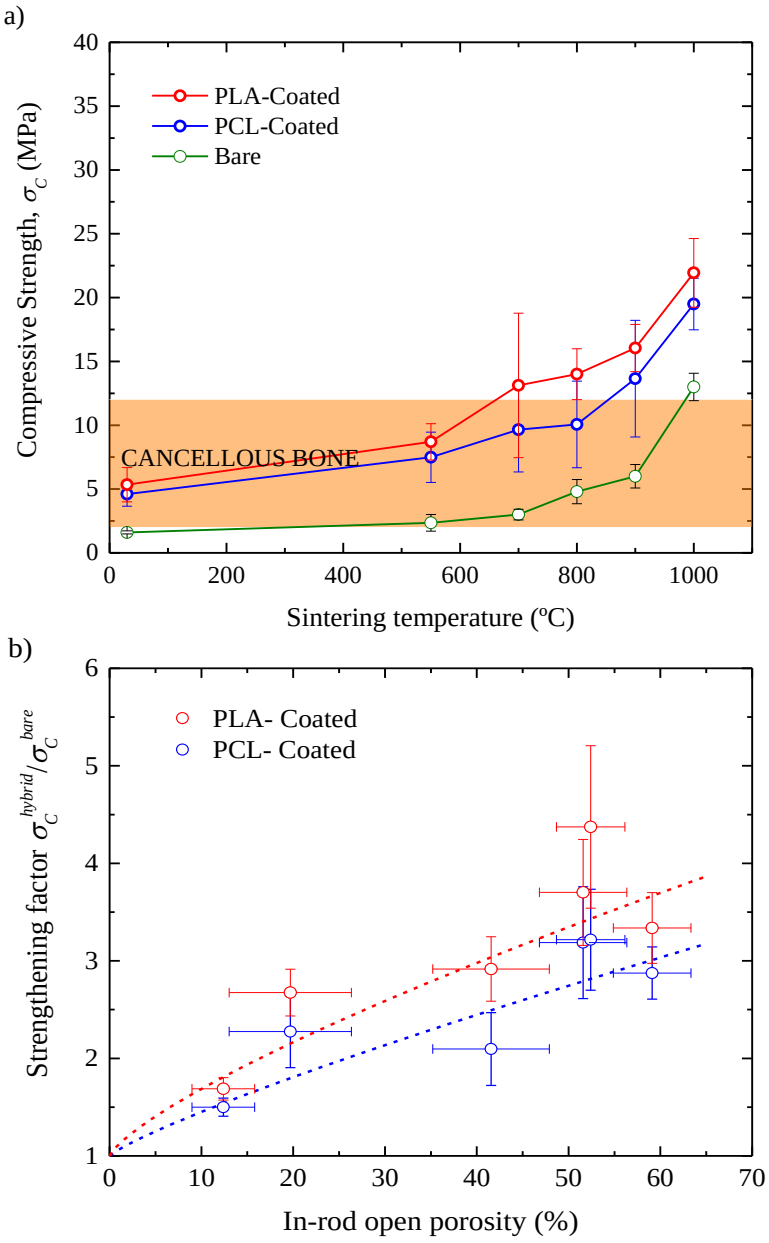

Figure 3.15. (a) The evolution of compressive strength versus sintering temperature of 45S5 scaffolds before and after coating with PCL and PLA. Typical values for human cancellous bone are shown as shaded bands for comparison.[187] *(b) Strengthening factor for PCL and PLA coated structures as a function of the in-rod open porosity (Fig. 3.8). Error bars represent standard deviations, save for the strengthening factors where standard error of the mean are used.*

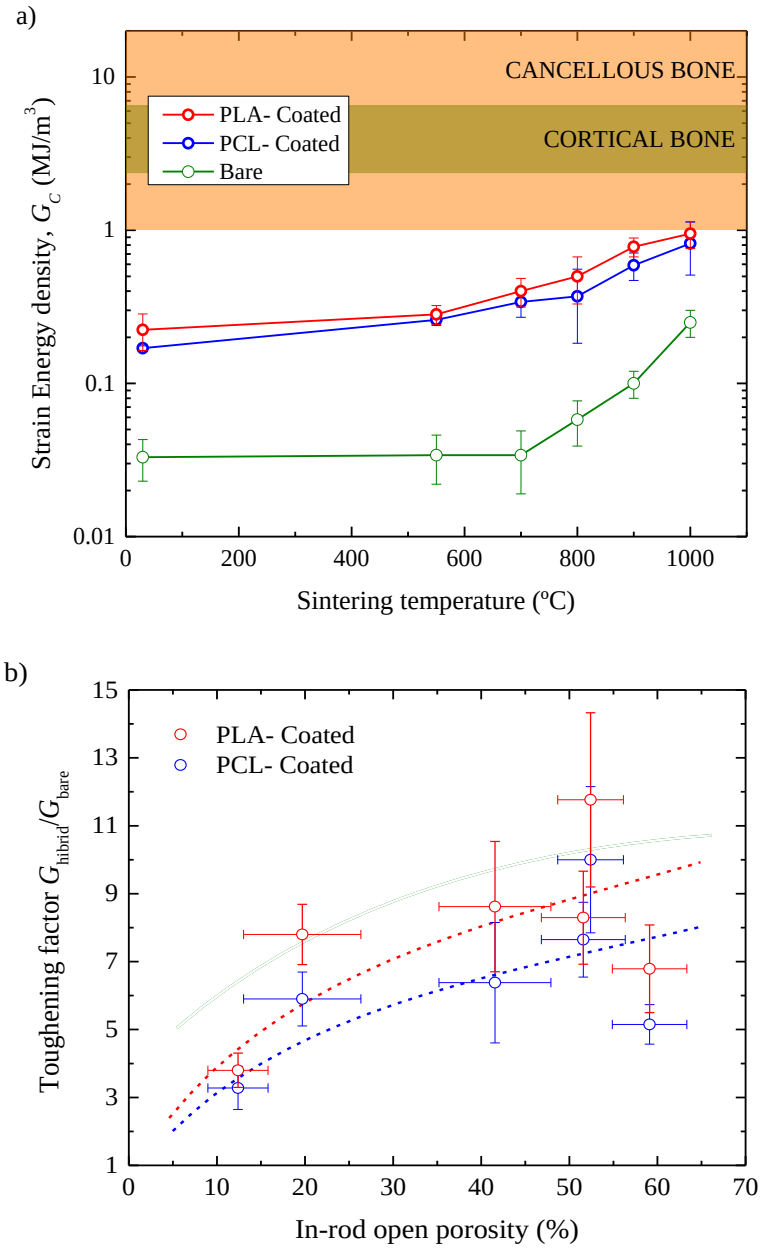

Figure 3.16. Evolution with the sintering temperature of the strain energy density at 20 % strain, G_C, of 45S5 bioglass scaffolds before and after coating with PCL and PLA. Typical G_C values for human bone are shown as shaded bands for comparison.[20,21] *(b) Toughening factor for PCL and PLA coated structures as a function of the in-rod open porosity (Fig. 3.8). Error bars represent standard deviations, save for the toughening factors where standard error of the mean are used.*

A major improvement in the toughness (note the semi-logarithmic scale in Fig. 3.16a) of the bioglass scaffolds is apparent upon coating with PCL or PLA. However, toughness of coated scaffolds barely reaches the level of cancelous bone values.

Fig. 3.16b, shows the toughening factor provided by each polymer—obtained by normalizing the corresponding results by the strain energy density of the bare structures at each sintering temperature—versus the in-rod open porosity (Fig. 3.8). It is obvious that the toughening factor decreases with the microporosity on the scaffold struts both as a consequence of the decreasing strengthening factor and the reduction in the number of polymer microfibrils bridging the crack tip as it propagates. This is clearly shown in Figure 3.17 where a reduction in the number of polymer microfibrils generated upon fracture of PCL-coated struts with increasing sintering temperature (i.e. with decreasing microporosity) is evident. The toughening factor oscillates from a minimum of 3 up to 10 for PCL-coated and from 4 up to 12 for PLA-coated structures. Therefore, PLA-coating shows higher toughening factor compared to PCL-coating structures in spite of PCL's superior ductility. PLA can be a more effective infiltrate than PCL for increasing the strain energy density in compression, because its superior strength, and associated strengthening factor (Fig.3.15b), compensates its inferior ductility and subsequent fibril generation capacity.[188]

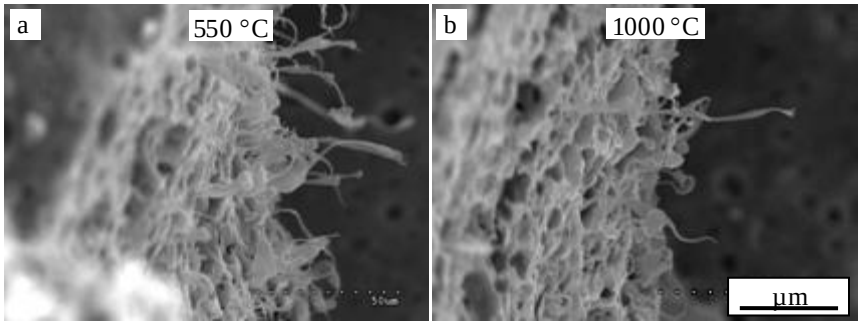

Figure 3.17. SEM images of fractured rods of PCL-coated scaffolds sintered at (a) 550 °C and (b) 1000 °C.

3.2.1.2 Bending tests

The result obtained from four-point bending tests for bare and PCL- or PLA-coated scaffolds are now discussed. In this case only two sintering temperatures were considered 550 °C, which yields a fully amorphous 45S5 bioglass scaffold, and 1000 °C that provides the strongest scaffold. To begin with, the results on Figure 3.18 confirmed that the stiffness of the structure was not significantly ($p > 0.05$) changed by the applied coatings. This simply reflects the fact that the modulus of PCL and PLA are much lower than that of the bioglass skeleton, even for the highly porous structures sintered at 550 °C.

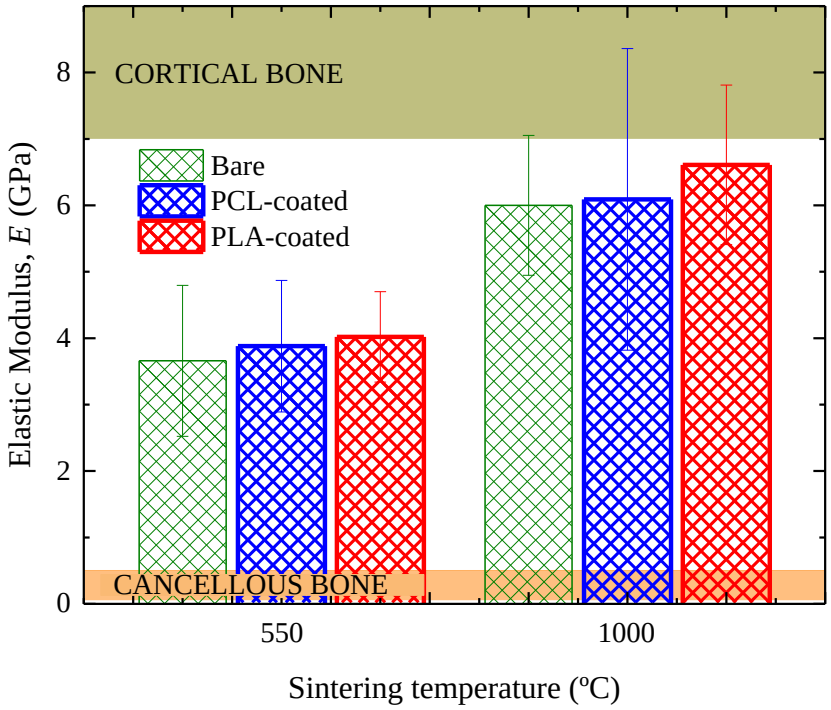

Figure 3.18. Elastic modulus, with standard deviations as error bars, for 45S5 bioglass scaffolds sintered at 550 ºC and 1000 ºC before and after coating with PCL and PLA. Typical values for human bone are also shown for comparison (shaded bands).[189]

The representative force-displacement curves from 4-point bending tests of the bare and infiltrated scaffolds are shown in Figure 3.19. The loads in the curves have been normalized by the effective volume (i.e. that within the external contacts in the 4-point bending jig) of each sample. The bending curves of all presented materials showed significant differences compared to the same curves in compression (Fig. 3.14). A typical brittle, linear elastic behavior could be seen for bare scaffolds, and even in coated samples up to the initial crack pop-in event, which determines the bending strength of the structure. However, it is clearly evident that the addition of the polymeric phase to the structure not only produces a notable increment in the flexural strength but also of and the toughness, measured as area under the curve, of the bioglass scaffolds. While bare structures fail catastrophically after this initial fracture event, coated scaffolds retain a certain mechanical integrity even after large displacements.

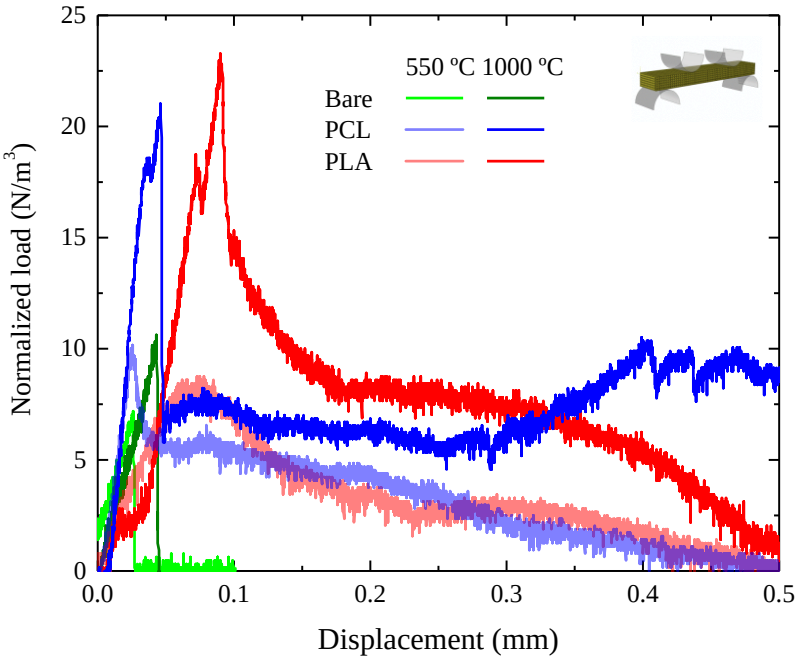

Figure 3.19. Typical bending load–displacement curves for the indicated materials. Loads have been normalized by the effective volume of each sample.

As shown in Figure 3.20, the flexural strength of the structure increases upon the incorporation of both PCL and PLA due to defect healing, and as in compression, the strengthening factor is higher in the amorphous samples (550 ºC) than in the glass-ceramic scaffolds (1000 ºC). Indeed, the factors of strengthening are similar to those in compression (Fig.3.15b). These results confirm that when the mechanical effect of the polymer infiltration is essentially limited to a defect healing, the strengthening achieved is independent of the loading condition. Indeed, since the elastic modulus of the structure does not significantly change with polymer infiltration (Fig. 3.18), the stresses on the ceramic struts are not going to be affected significantly by the presence of the polymer and fracture will occur when the maximum stresses in the structure reach a certain critical value. That value, the intrinsic strength of the ceramic struts, is what is changed by polymer infiltration through the sealing of precursor flaws in the struts surfaces. So, as already discussed, the level of strengthening achieved will depend on the flaw population, but not on the loading configuration. Consequently, as in compression, the strengthening achieved after polymer infiltration is slightly higher (not statistically significant) in the case of PLA, and PLA-coated structures exhibit a superior bending strength.

Figure 3.21 shows the fracture energy, G_F, of bare and polymer-infiltrated 45S5 scaffolds as evaluated from the area under the force-stroke curves from four-point bending tests. Fracture energy in bending is significantly lower than the strain energy densities evaluated in compression for all analyzed structures, as expected for this most deleterious loading condition. Nevertheless, for both polymers, the fracture energy of infiltrated scaffolds was substantially higher than for the bare scaffolds regardless the sintering temperature.

As in compression, PLA-coated scaffolds, showed slightly higher toughness (not statistically significant) than PCL-infiltrated structures due to its superior strength which compensates its inferior ductility. Indeed, the contribution of PLA to fracture energy is basically through the strengthening it provides, while the toughening provided by PCL is contributed both by the strengthening and by the generation of micro-fibrils (see Fig. 3.17) that bridge the crack opening during its propagation.

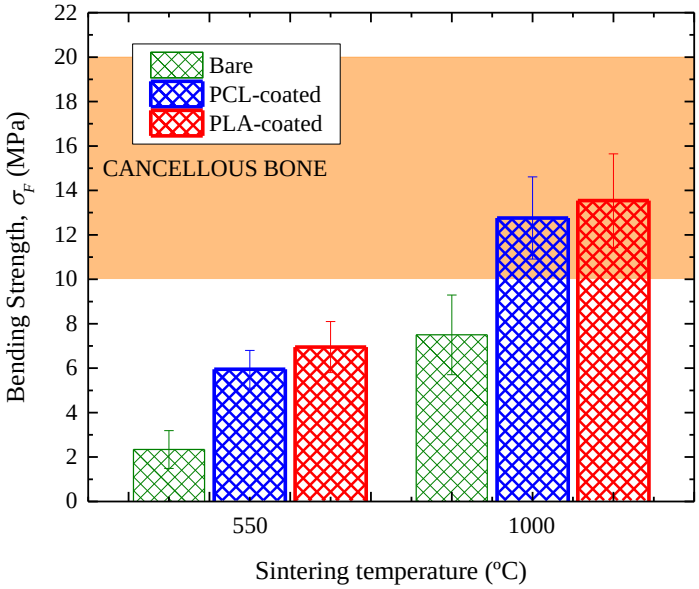

Figure 3.20. Flexural strength, with standard deviations as error bars, for 45S5 bioglass scaffolds sintered at 550 ºC and 1000 ºC before and after coating with PCL and PLA. Typical values for human bone are also shown for comparison (shaded band).[17,189]

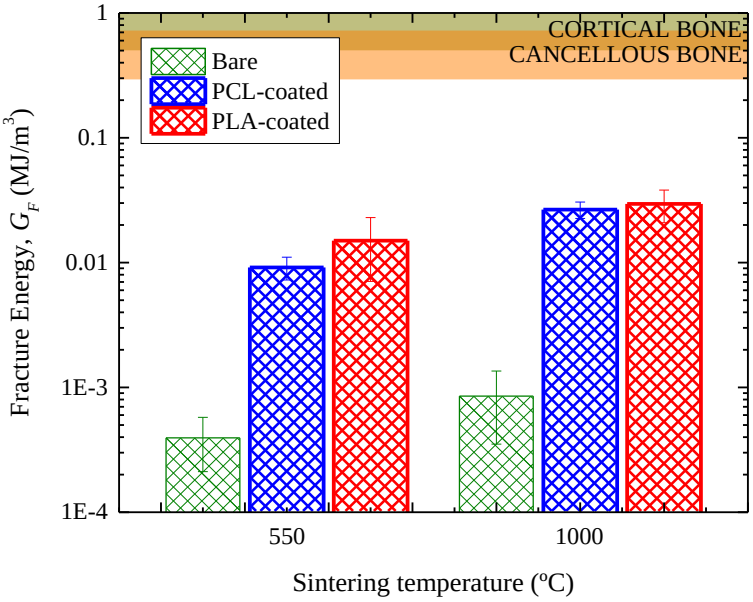

Figure 3.21. The strain energy, G_F, calculated from the area under the load-displacement curves from bending test at the point of 0.5 mm of total deflection. Typical values for human bone are also shown for comparison (shaded bands).[20,21]

All the results from mechanical characterization analyzed in the preceding paragraphs, both regarding compression and bending tests, are summarized in Table 3.1 to facilitate access to the readership.

Table 3.1. Summary of mechanical characterization results for 45S5 bioglass-based scaffolds.

Material	Compression / Bending	**E (GPa)**	σ_0 **(MPa)**	G **(MJ m^{-3})**	$\sigma_0^{hybrid}/\sigma_0^{bare}$
550		-	2.4 ± 0.7	0.034 ± 0.012	-
		3.7 ± 1.1	2.3 ± 0.8	0.0004 ± 0.0002	-
550/PCL		-	7.5 ± 2.0	0.26 ± 0.02	3.1 ± 1.3
		3.9 ± 1.0	6.0 ± 0.9	0.0091 ± 0.0019	2.6 ± 1.0
550/PLA		-	8.7 ± 1.4	0.28 ± 0.04	3.6 ± 1.2
		4.0 ± 0.7	7.0 ± 1.1	0.015 ± 0.0079	3 ± 1
1000		-	13± 1	0.25 ± 0.05	-
		6.0 ± 1.0	7.5± 1.8	0.0008 ± 0.0005	-
1000/PCL			19.5 ± 2.0	0.82 ± 0.31	1.5 ± 0.2
		6.1 ± 2.2	12.8 ± 1.9	0.0266 ± 0.0040	1.7 ± 0.5
1000/PLA		-	21.9 ± 2.7	0.95 ± 0.19	1.7 ± 0.3
		6.6 ± 1.2	13.5 ± 2.1	0.0295 ± 0.0086	1.8 ± 0.5

All these data confirm the that mechanical enhancement, both in therms of strength and toughness, provided by polymer infiltration increases with the microporosity of the bioceramic substrate — although the final strength and toughness values are ultimately higher in scaffolds with denser struts even after coating. As a consequence for the purpose of this study 550°C-sintered 45S5 bioglass scaffolds were deemed more appropriate to evaluate the effect of process variables (solvent composition, solution temperature, polymer content and composition) on the mechanical enhancement produced by coating. Also, since no major differences were observed in the mechanical behavior of coated structure in bending and compression, and for the sake of simplicity, only the latter loading condition was used in the rest of the study.

3.2.2 Role of solvent

The possible effect of solvent on the quality of coating layer deposited was analyzed by dip-coating 45S5 bioglass scaffolds sintered at 550 °C at room temperature in three 10 % w/v PCL solutions with different solvents: xylene, toluene and acetone. At this concentration and temperature, PCL was easily soluble in toluene and xylene resulting in a clear solution. However, it was significantly more difficult in acetone, a more polar solvent, were it was only partially dissolved yielding a cloudy solution with higher viscosity. As shown in Figure 3.22, there are no significant ($p > 0.05$) differences between the three different solvent on the strength of PCL-coated bioglass scaffolds. Therefore, in principle, the role of the solvent ends with its ability to dissolve the appropriate amount of the selected polymer at the deposition temperature, yielding a solution with appropriate viscosity. Acetone was a poorer choice here, which can explain its slightly lower mean value in Fig. 3.22, while toluene provided the fastest dissolution and, therefore, was deemed the optimal solvent for PCL (and also for PLA).

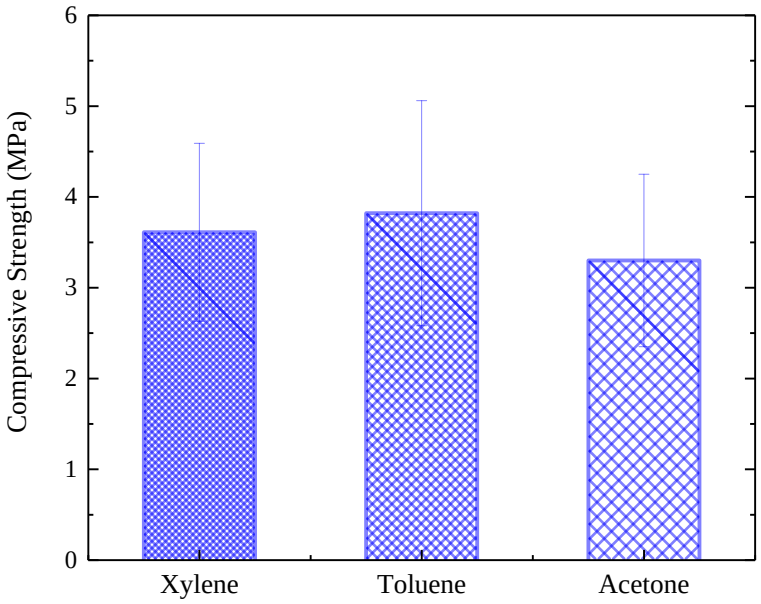

Figure 3.22. Effect of solvent on the compressive strength of 45S5 scaffolds sintered at 550 ºC coated in 10 % (w/v) PCL solutions. Solvents are ordered by increasing polarity.

Nevertheless, this negative result on the effect of solvent cannot rule out the possibility of certain solvents altering the nature of the surface of specific substrates, thereby affecting the bonding strength at the polymer/ceramic interface and, subsequently, the mechanical performance of the resulting hybrid scaffold. At any rate, the issue of the solvent is not so critical in the case of coatings made from natural polymers since they are mostly water-soluble and no other solvent can be considered better than water, especially in terms of its biological compatibility and non-toxicity.

3.2.3 Effect of dip-coating temperature

Figure 3.23 shows the compressive strength of PCL-coated 45S5 bioglass scaffolds sintered at 550 °C as a function of solution (10 % w/v concentration in toluene) temperature during deposition. There is some evidence of a slight increase (~ 25 % in the most favorable case) in the strength with dip-coating temperature, although these differences are not statistically significant ($p > 0.05$). This slight improvement might be attributed to an enhancement of polymer's chain attachment to the bioglass surface, i.e. of the polymer wetting on the scaffold surface, with temperature. In any case, it is clear that at least for the system (PCL/45S5 bioglass) under study such effect, if it really exists, is a minor one.

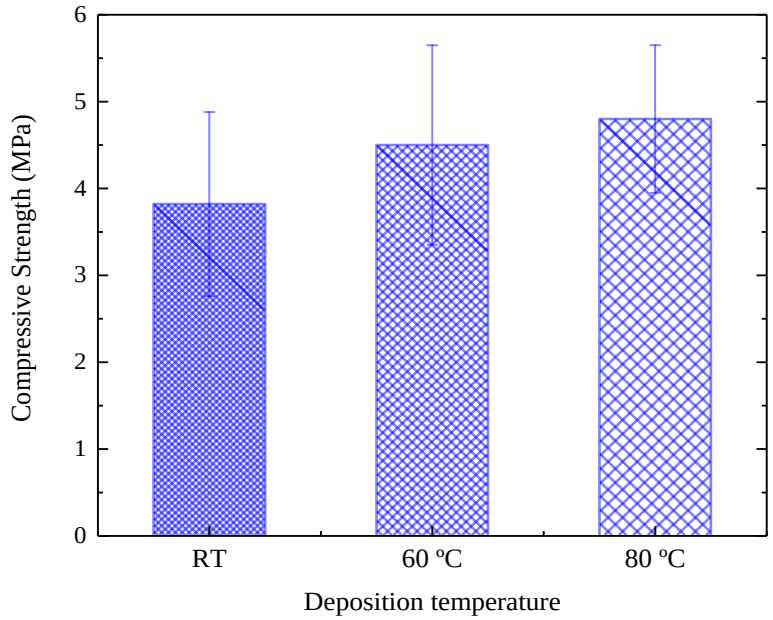

Figure 3.23. Compressive strength of 45S5 scaffolds sintered at 550 ºC coated in 10 % (w/v) PCL solution in toluene at the indicated temperatures.

On the other hand, it is worth mentioning that increasing the working temperature augments the evaporation rate of the solvent which may be affecting the actual polymer concentration. As we will discuss in the following section, concentration is a key parameter for determining the mechanical enhancement produced by the polymeric coating, which might be affecting the results in Fig. 3.23. For both toluene and water, evaporation was quite evident at 80 ºC. This, together with the fact that the mechanical properties were not enhanced significantly anyway (Fig. 3.23) at this temperature, explains why 60 °C was selected as the most appropriate dip-coating temperature for the investigated polymers.

3.2.4 Effect of polymer concentration

Figure 3.24 shows the compressive strength and strain energy density results of 45S5 porous scaffolds sintered at 550 °C dip-coated in PCL solutions (in toluene at 60 °C) with different concentrations. It is clear that the compressive strength (Fig. 3.24a) of the composite scaffolds increased substantially with PCL concentration—from 3.0 ± 0.9 up to 12.1 ± 2.4 MPa for 5 % and 30 % (w/v) concentrations, respectively. The same occurs for toughness (Fig. 3.24b), but even more pronounced, especially at 30 % concentration which exhibit a nearly four-fold increase over the value at 25 % concentration. These results indicates that, unlike dipping temperature or type of solvent, polymer concentration is a most important parameter in determining the ultimate mechanical properties of polymer-coated scaffolds. This implies, however, that both the type of solvent and the solution temperature are indirectly important inasmuch they affect the maximum polymer concentration suitable for the dip-coating process, and thereby the maximum achievable compressive strength and toughness in the hybrid scaffold.

The reason for the monotonic increase in the compressive strength and toughness of PCL/45S5 bioglass composite with the concentration of the PCL solution can be explained by an increased polymeric content deposited within the scaffold struts, filling/sealing existing micropores/microdefects and creating the fibrils responsible for crack microbridging.[190] This becomes evident in the SEM micrographs of PCL/45S5 composite rod fracture surfaces (Figure 3.25) which show an increase in the diameter of PCL microfibers generated with PCL concentration.

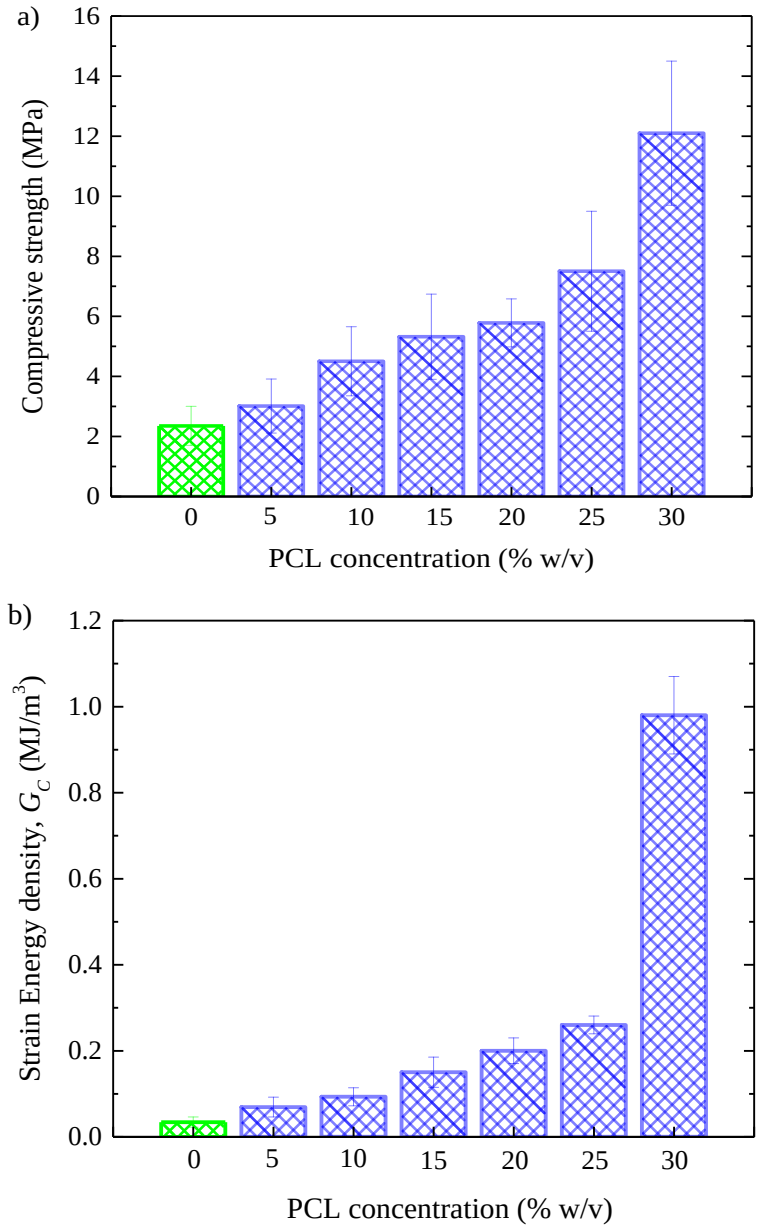

Figure 3.24. Compressive strength (a) and strain energy density at 20 % strain (b) of 45S5 scaffolds sintered at 550 ºC before and after dip-coating in PCL solutions in toluene at 60 ℃ with the indicated concentrations.

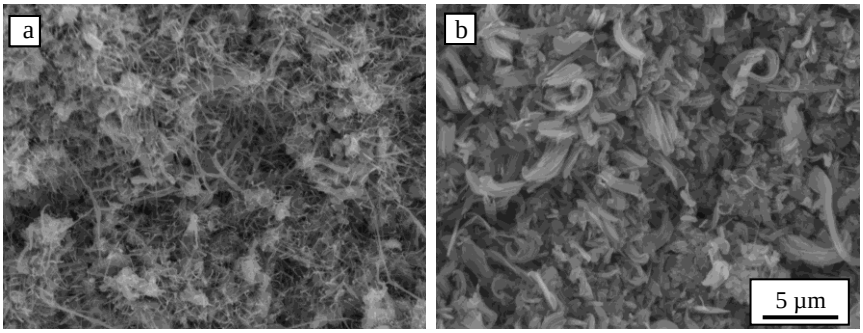

Figure 3.25. Fracture surface of 45S5 scaffolds sintered at 550 ºC coated with PCL solutions at (a) 20 % (b) 25 % concentrations.

Unfortunately, the polymer concentration in the solution cannot be increased indefinitely. On the one hand, as already mentioned, solvent and process temperature will determine the maximum solubility of the polymer. On the other, an increased concentration means also a greater viscosity which may hamper the infiltration process. Indeed, it was found that concentrated PCL solutions with 30 % w/v or higher formed viscous liquids that led to an inhomogeneous thickness of the coating from the top to the bottom of the sample, and also to the macropores of the structure being clogged with the polymer, as shown in Figure 3.26, which explains the extraordinary toughening appreciated in Fig. 3.24b at this concentration.

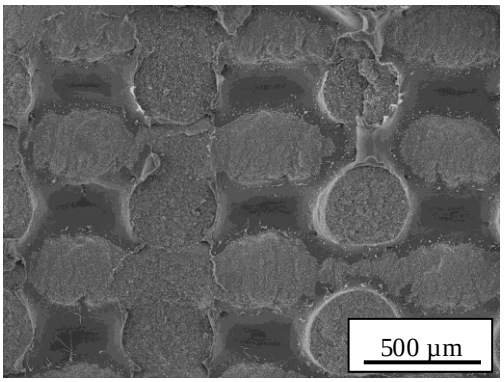

Figure 3.26. Fracture surface of 45S5 scaffolds sintered at 550 ºC coated with PCL solutions at 30 % concentration.

Therefore, an optimal concentration exists for a given set of process variables (substrate, polymer, solvent, temperature) that leads to the formation of a homogeneous coating with maximal thickness but still preserving predesigned scaffold macroporosity. For the PCL/45S5 system using toluene at 60 ºC as solvent, 25 % (w/v) concentration was deemed the optimal condition among all those tested.

When proceeding similarly with PLA solutions (in toluene at 60 °C) the optimal polymer concentration to maximize strength while preserving pore interconnectivity was 15 % (w/v), since in scaffolds coated at 20 % PLA concentrations some macropores were already partially closed. For all the natural polymers tested (alginate, chitosan and gelatin) the maximum workable concentrations of the aqueous solutions at 60 °C was found to be 5 % (w/v). At all optimal concentrations tested, the polymers formed a coating homogeneous layer on the bioglass struts, as proven by SEM observations.

3.2.5 Effect of polymer composition

The effect of different polymer compositions, including natural and synthetic ones deposited using solutions with the same concentration (5 % w/v) and temperature (60 °C), on compressive strength and strain energy density of infiltrated 45S5 bioglass scaffolds sintered at 550 °C is shown in Figure 3.27. It is clear that scaffolds coated with natural polymers exhibited greater strength (Fig. 3.27a) and toughness (Fig. 3.27b) than those coated with the two synthetic polymers, despite the significantly superior intrinsic mechanical properties of the latter. In particular, chitosan-coated scaffolds showed the highest mechanical strengthening and toughening, with close to a six-fold and 25-fold increase, respectively, over the bare structures.

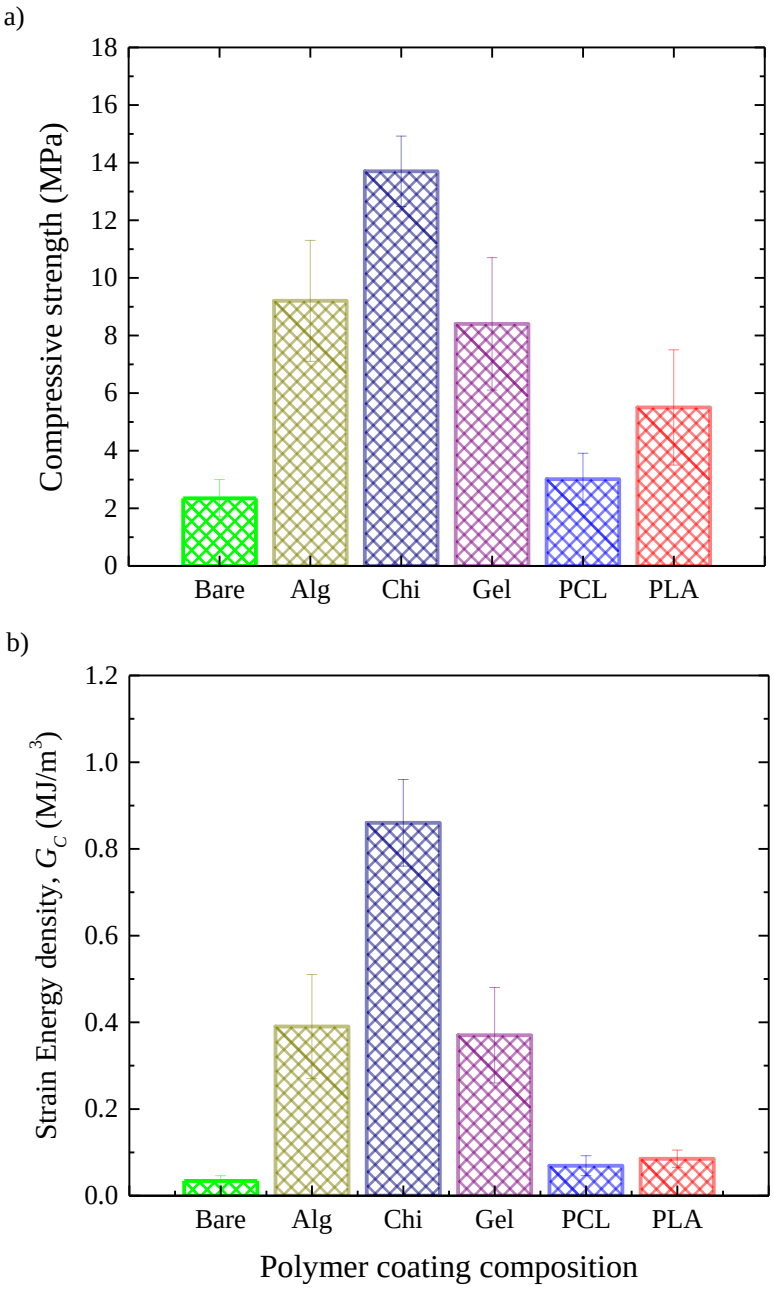

Figure 3.27. Compressive strength (a) and strain energy density at 20 % strain (b) of 45S5 scaffolds sintered at 550 ºC before and after coating with different polymers at 60 ºC using polymeric solutions at 5 % (w/v) concentration. Solvent was water for alginate (Alg), chitosan (Chi) and gelatin (Gel), and toluene for PCL and PLA.

This result is attributed to differences in the bonding strength between each polymeric coating and the 45S5 bioglass surface. Indeed, the interfacial adhesion achieved between the hydrophilic bioglass struts and the hydrophilic natural polymers (i.e. alginate, chitosan or gelatin) is likely to be stronger than that obtained with the more hydrophobic synthetic polymers (e.g., PCL or PLA).[191] Individual differences should be explained in terms of the specific chemical interactions between the involve species.

Generally, the mechanisms controlling the polysaccharide–silicate interactions depend on the nature of both components and involve ionic interactions, van der Waals forces, hydrogen bonds and water bridges. Polysaccharide chains, like those of alginate and chitosan, can then be easily adsorbed on the external surface of silicates.[192] The main interactions of the silica phase with the polysaccharide are due to hydrogen bonds between the silanol groups and groups of the biopolymer chains.[193,194]

In the case of chitosan polymer, hydrogen bonding can be formed between silanol groups of bioglass and C=O and N–H groups of the chitosan as well as by electrostatic interactions.[195] Indeed, in positively charged polymers such as chitosan, electrostatic interactions can take place between chitosan amino groups and silanol groups, and even covalent bonds could be established from transesterification of chitosan hydroxy-groups by silanol.[195–197] Under the acidic conditions employed (pH 5.5), the amine group of chitosan which has a pKa value of ~ 6.5,[198] is protonated and forms an NH_3^+ ion which, in turn, is an even better hydrogen-bonding partner than an uncharged NH_2 group.[199] On the other hand, the pH of the solution didn't change during the coating process, and this acidic condition results in an enhanced dissolution of bioglass surface, which facilitates ion exchange and leads to stronger ionic bondings with the amino groups. Thanks to these strong interactions, it is expected that 45S5 bioglass–chitosan hybrids exhibited an increased interfacial adhesion, and thereby improved mechanical properties (Fig. 3.26).[197] According to Fig. 3.26, alginate-coated 45S5 scaffolds showed higher compressive strength after chitosan-coated ones, closely followed by gelatin-coated scaffolds. Hydrogen bondings can be easily created between silanol groups on the surface of bioglass and the hydroxyl or carboxyl groups (COO^-) of alginate,[200–202] The pH of alginate aqueous solution was ~ 6-6.5 before the coating process. However 45S5 bioglass caused a typical dramatic pH rise up to ~ 9 during the coating procedure due to the ion exchange between modifier ions (Na^+ and Ca^{2+}) in the glass and protons (H^+) in the dissolution medium.[203] Therefore, the electrical

charge of alginate, which was already negative at the initial pH (since the isoelectric point, *iep*, of alginate is around pH 3-4),[204] increased in magnitude due to highly charged anionic carboxylic ($–COO^-$) groups.[205] Hence, strong interactions of the carboxylic group present in alginate with multivalent cations such as Ca^{2+} in the bioglass can take place[191] and could form intermolecular cross-linking leading to enhanced mechanical properties of the alginate.[200,201]

In the case of gelatin, a complex reaction between Ca^{2+} ions of bioglass and gelatin molecules may happen. Also, the –COOH and $–NH_2$ groups in the gelatin molecule can form strong (ionic) chemical bonds with silanol groups of bioglass depending on the pH of the solution. However in this work, since the gelatin type A has *iep* ~ 8-9,[58] while the amino groups in the gelatin solution at initial pH ~ 5.5 become protonated, after immersion of the 45S5 scaffolds in the gelatin solution, the pH of the solution gradually increases until it reaches the gelatin iep range. At this point, the positively charged amino groups become equal to negatively charged carboxyle groups, which may cause the maximum chain folding and contraction, leading to rigid and stiff matrix,[206] and can hinder more chemical reactions between gelatin and bioglass surface. This phenomenon could be also observed by an increase in turbidity of gelatin solution.

The level of interfacial bonding to bioglass is significantly lower for the synthetic polymers. The ester carbonyl groups (C=O) of PCL and PLA are capable of forming hydrogen bonds with the silanol groups (Si-OH) on the surface of the inorganic network.[207] However, stronger ionic bonds are not possible in a non-polar media such as the toluene used as solvent for these polymers. Moreover, in the case of PCL, the chain ratio between the methylene non-polar groups ($-CH_2-$) and the ester polar groups (C=O), is of 5:1, while in PLA this ratio is 1:1. This explains why PLA exhibit significantly greater interfacial adhesion, and thereby increased strengthening effect than PCL. The differences in toughening are not so marked between both synthetic polymers since the higher ductility of PCL make the crack microbridging mechanism more effective in its case.

Although the results in Fig. 3.27 prove without doubt that the natural polymers are more effective as reinforcing agents for 45S5 bioglass scaffolds than PCL and PLA, it might be argued that —according to the results of the preceding section—the selected 5 % (w/v) concentration is optimal for the natural polymers but not for PCL or PLA. Consequently, Figure 3.28 shows the compressive strength of 45S5 bioglass scaffolds coated with all investigated

polymers at optimal concentrations. Even after increasing the concentrations on PCL and PLA to 25 % and 15 %, respectively, the relative positions of the different polymeric coatings as reinforcing agents remains unaltered. Chitosan continues to be the optimal choice and PCL-coated scaffolds the weakest structures despite having used the greatest by far polymeric concentration in the dip-coating process.

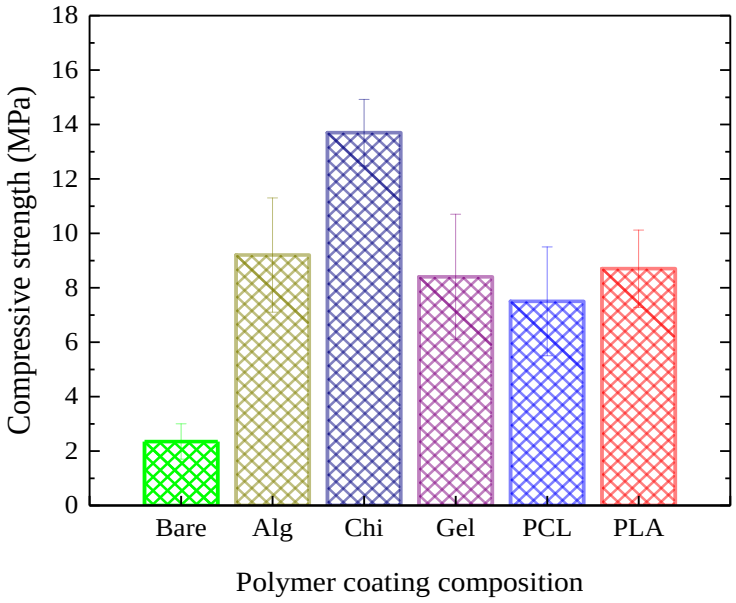

Figure 3.28. Compressive strength of 45S5 scaffolds sintered at 550 ºC coated with polymers at optimal concentrations: 5 % w/v for alginate (Alg), chitosan (Chi) and gelatin (Gel); 25 % w/v for PCL and 15 % w/v for PLA.

The same results are obtained when analyzing the toughening provided by the polymeric coatings. Figure 3.29 shows the compressive strain energy density G_C of 45S5 bioglass scaffolds coated with all investigated polymers at optimal concentrations. Although the enhancement in term of toughness over the bare structures is far greater than the strengthening produced, the relative position of the different polymeric coatings remains the same. Chitosan coatings increase the toughness of the 45S5 bioglass structures nearly 25-fold, and even

the weakest PCL-coatings improve the toughness by nearly an order of magnitude (toughening factor of ~ 7.6).

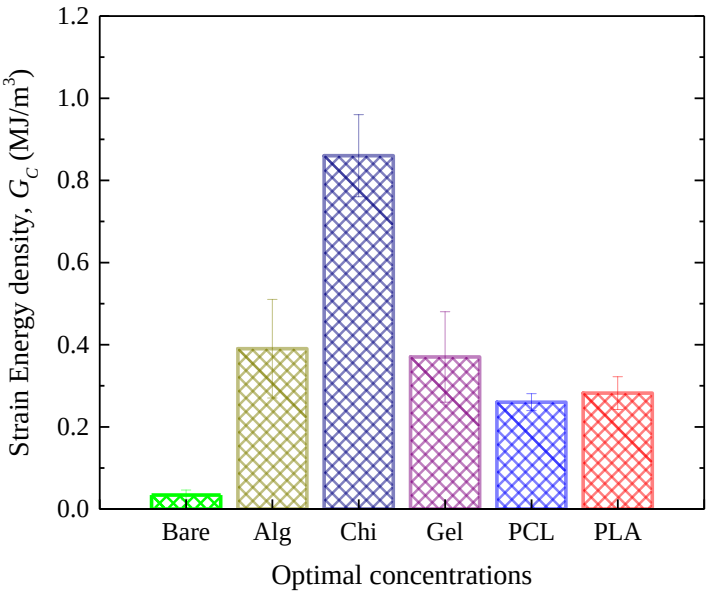

Figure 3.29. The strain energy density at 20% compressive strain, G_C, of 45S5 bioglass scaffolds sintered at 550 ºC coated with polymers at optimal concentrations: 5 % w/v for alginate (Alg), chitosan (Chi) and gelatin (Gel); 25 % w/v for PCL and 15 % w/v for PLA.

All in all, the results in this section highlight the important role of polymer composition on the mechanical enhancement produced by the deposited coating. The strengthening and toughening effects obtained are likely to be determined by the wettability of polymer solution on the scaffold struts and the interfacial adhesion between the polymeric coating and the scaffold material. Although the results presented cannot completely rule out the effect of the intrinsic mechanical properties (strength, stiffness, toughness) of the polymer, they suggest that such polymeric properties play only a minor or secondary role. Indeed, if such properties played a major role, synthetic polymers such as PCL and PLA, with mechanical properties orders of magnitude higher than those of

the natural polymers tested in this study, should have provided a significantly better performance as reinforcing infiltrates. On the other hand, since the interfacial adhesion plays such a major role in the mechanical enhancement provided by the polymeric coating, one suitable strategy to enhance the performance of coated structures would be to graft the corresponding polymer's functional group onto the bioglass surface to produce chain entanglements that will drastically improve the mechanical properties.[208–210] This type of direct strong bonding between the polymeric coating and the bioceramic material of the scaffold could also be achieved by performing the polymerization *in situ* with the scaffold immersed in a monomeric solution.[119]

3.3 *In vitro* bioactivity and degradation of bare and coated 45S5 bioglass robocast scaffolds

In this section, the *in vitro* bioactivity and degradation behavior of 45S5 bioglass scaffolds before and after coating with polymers are investigated. The degradation behavior is evaluated from measurements of the weight loss and pH variation upon immersion in simulated body fluid (SBF). Also the concurrent formation of hydroxyapatite on the scaffold surface during immersion in SBF and the effect of the degradation on the scaffolds compressive strength are analyzed.

3.3.1 Bare 45S5 bioglass robocast scaffolds

The *in vitro* study in bare structures has been done both in amorphous (sintered at 550 °C) and (semi)crystalline (sintered at 1000 °C) samples, to analyze the effect of crystallinity and densification on the bioactivity and degradation behavior of 45S5 bioglass robocast scaffolds.

3.3.1.1 *In vitro* degradation and bioactivity assessment

Figure 3.30 shows the evolution of the SBF solution's pH and the weight loss of the bare robocast scaffolds (both amorphous and crystalline 45S5 bioglass) during the soaking experiment. The same reactions that lead to scaffold weight loss also control the variation of pH in the solution.[211,212] The pH changes are attributed to the ionic exchange between the ions such as Ca^{2+} and Na^{+} from 45S5 bioglass network and H^{+}, H_3O^{+} and OH^{-} from the SBF solution. As a result silanol group (Si–OH) is formed on the bioglass surface due to reaction of Si with OH^{-} ions that act as nucleation sites for HAp formation. Initially, alkali ion leaching from bioglass to the solution leads to increase the pH and weight loss. For both kinds of structures, a fast raise in pH was seen in the initial times of immersion (the first 1 week) and then a pH stabilization was achieved which remained fairly constant until the end of soaking period (Fig. 3.30a). The amorphous 45S5 tends to leach alkali ions faster to the solution, and pushes the equilibrium to a higher pH value in comparison to crystalline 45S5. Such equilibrium plateaus appearing in pH curves are due to formation of a hydroxyapatite layer on the surface of the samples that consequently makes the surface of 45S5 bioglass more passive.

The weight loss of bare scaffolds increased monotonously with culturing time but at a continuously decreasing rate (Fig. 3.30b). For example, up to the first 1 week of immersion the scaffolds lost up to 14 % of their weight in amorphous bioglass and 12 % in crystalline samples, and then the weight loss from 1 to 8 weeks was reduced to around an additional 8 %. The degradation of both materials is, nonetheless, fast and data can be fitted properly by a three-dimensional diffusion model (3DM) function:[213,214]

$$\Delta W/W_0 = \Delta W_{max}/W_0\{1-[1-(kt)^{1/2}]^3\} \qquad (3.1)$$

where, the maximum weight loss $\Delta W_{max}/W_0$ and the kinetic constant k are adjustable parameters and t is the immersion time. 3DM diffusion model assumes that volumetric diffusion to the reaction interface is what controls the degradation rate, rather than the interfacial reaction. For both materials the maximum weight loss is similar (~ 21 %) but the kinetic constant is around 40 % higher for vitreous scaffolds ($4.6 \pm 0.3 \cdot 10^{-6}$ h^{-1} *vs.* $3.2 \pm 0.5 \cdot 10^{-6}$ h^{-1}). The validity of the 3DM model implies that it is the intrinsically faster ionic

diffusion of the amorphous structure rather than its higher microporosity and surface area that is responsible for the faster degradation observed in the samples sintered at 550 °C.

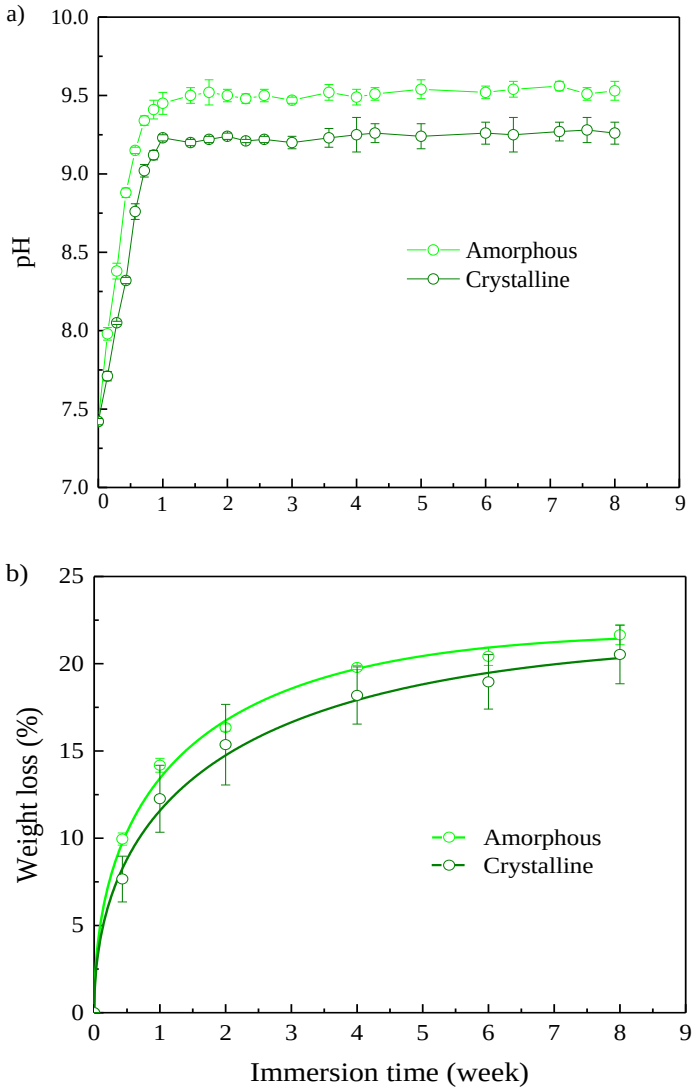

Figure 3.30. Evolution of (a) pH of SBF solution and (b) scaffolds' weight loss as a function of immersion time for amorphous and crystalline 45S5 bioglass samples. Error bars represent standard deviations. Curves in (b) are best fits of 3DM model, Eq. (3.1), to data.

The evolution of HAp formation with immersion time in SBF in amorphous and crystalline bare 45S5 scaffolds is shown, respectively, in Figures 3.31 and 3.32. It is obvious that in both cases the amount of the HAp increases with the soaking time. However, nucleation of HAp in crystalline structures occurred slightly later than in amorphous structures. In the amorphous scaffolds the HAp nuclei are observable already after 1 day of soaking in SBF (see inset in Fig. 3.31a), but they are absent in crystalline 45S5 (Fig. 3.32a). In fact, it has been proven that presence of crystalline phase decreases the kinetics of apatite formation but does not inhibit the growth of an apatite layer on the surface of the material.[168,174,215] After 3 days of immersion in SBF, the HAp particles are already numerous in both structures. The high-resolution SEM image of the crystalline surface after 3 days (inset in Fig. 3.32b) shows that the HAp particles consist of a porous network of nanometer-sized, needle-like crystals, characteristic of HAp deposited by precipitation from solution.[212] The growth of HAp continued at a fast rate up to 1 week of immersion where a uniform HAp layer was observed, which is in agreement with the results obtained from pH measurements (Fig. 3.30a). The appearance of the HAp layer on both structures (amorphous and crystalline) after 1 week of immersion is basically not distinguishable. From then on, the growth of the HAp layer proceeded alternating the formation of excrescences of HAp crystals and their coalescence to form more uniform layers (this is especially evident in the denser crystalline samples, Fig.e 3.32).

All in all, the results of this section demonstrate that a similar degradation behavior occurs in amorphous and crystalline 45S5 bioglass robocast scaffolds, with the amorphous structures exhibiting around 40 % faster degradation kinetics. This means that while bioactivity of 45S5 glass is maintained it is somewhat delayed, if not dramatically, by crystallization. Therefore, a faster and, possibly, stronger bonding to surrounding bone tissue are to be expected if scaffolds made from the glassy phase were used instead of the glass-ceramic derivatives traditionally reported in the literature. Such a possibility has been enabled by the use of robocasting, which has permitted for the first time to produce amorphous 45S5 scaffolds with sufficient mechanical integrity (see Fig. 3.12).

.

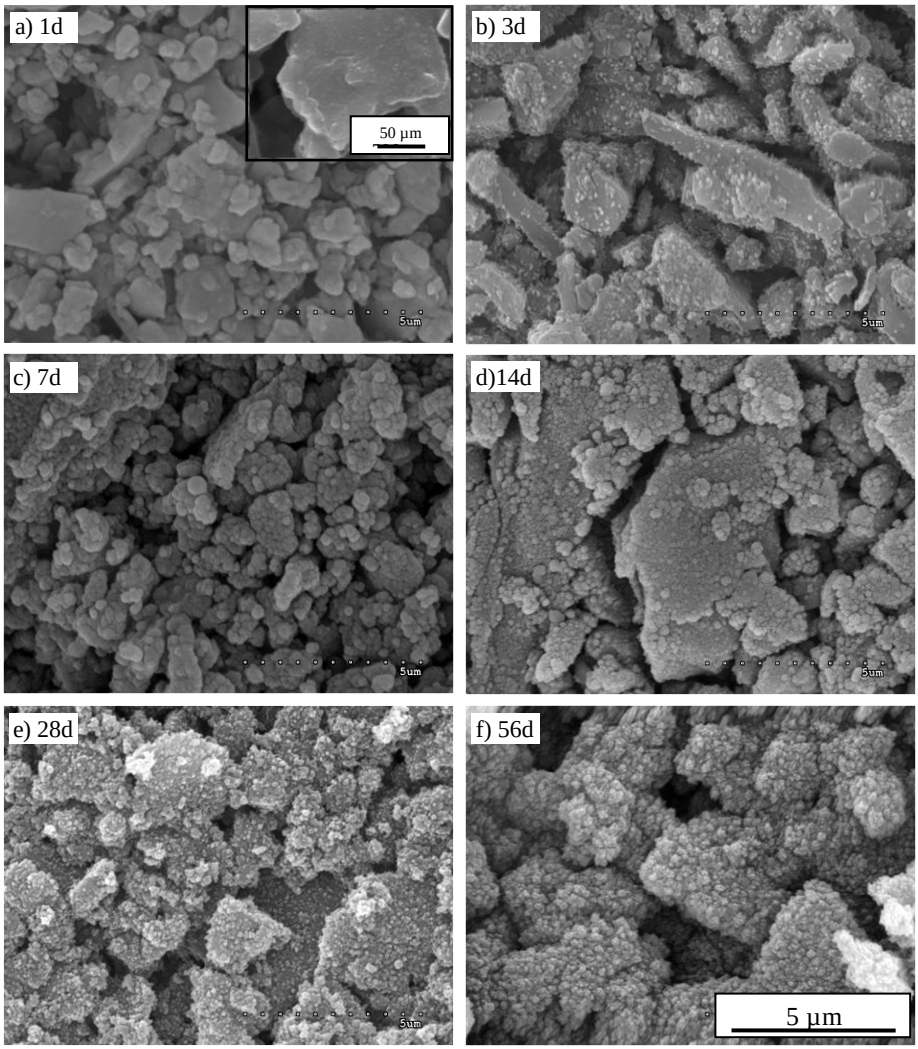

Figure 3.31. SEM micrographs of the rod surfaces on amorphous 45S5 bioglass robocast scaffolds soaked in SBF for the indicated times.

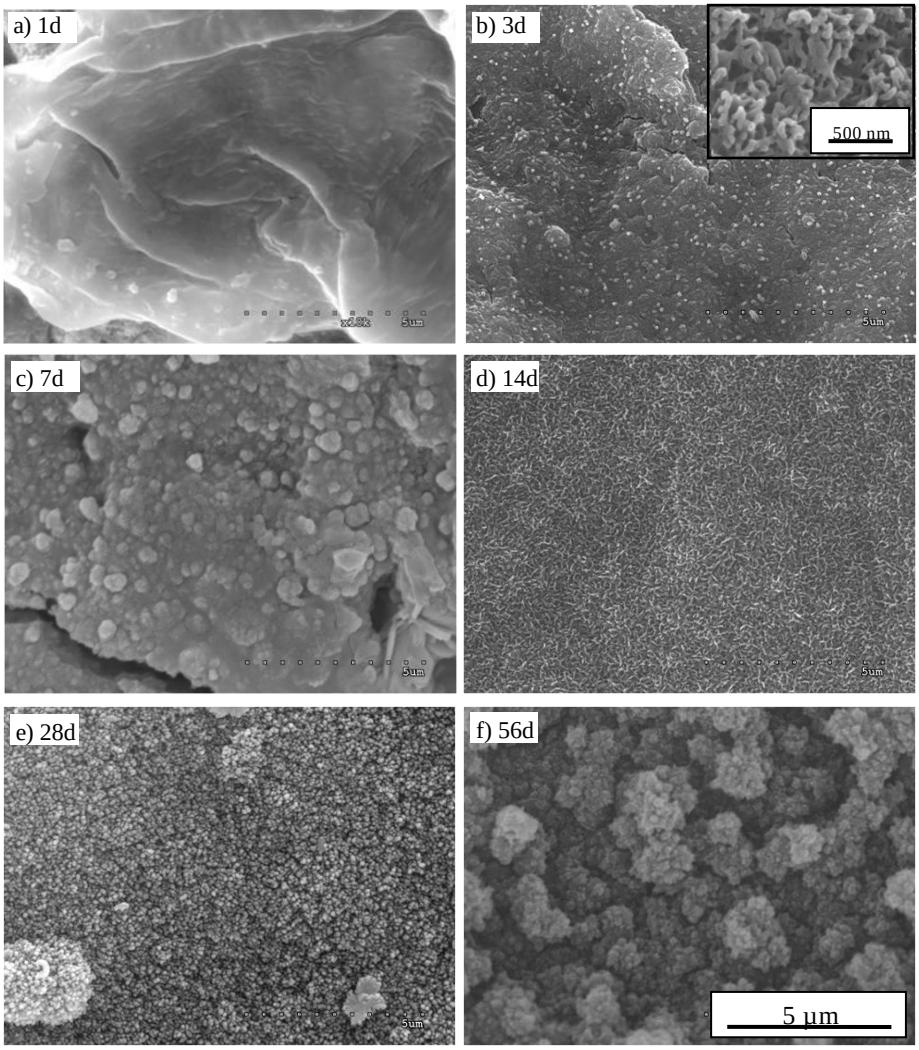

Figure 3.32. SEM micrographs of the rod surfaces on crystalline 45S5 bioglass scaffolds soaked in SBF for the indicated times.

3.3.1.2 Compressive strength degradation

The evolution of compressive strength of amorphous and crystalline 45S5 scaffolds as a function of immersion time in the SBF is shown in Figure 3.33.

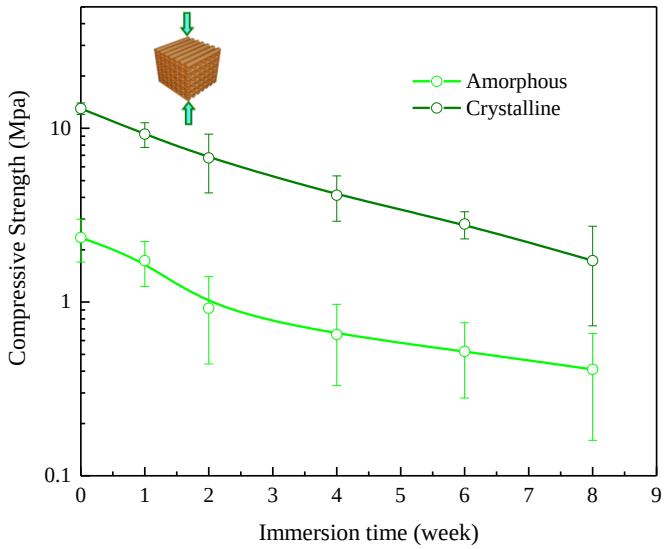

Figure 3.33. Compressive strength of amorphous and crystalline 45S5 scaffolds as a function of immersion time in the SBF with standard deviation as error bars.

In both cases, the dissolution of the bioactive glass/glass-ceramic and its conversion to a porous HAp-like product resulted in a reduction of compressive strength. Due to the faster dissolution of the amorphous scaffolds during immersion in SBF (see Fig. 3.30), the amorphous structures also showed initially a slightly faster strength loss comparing to crystalline ones. However, in the case of amorphous scaffolds, the rate of this reduction decreases significantly after two weeks of immersion in SBF, while such a reduction is not so clear in the crystalline material.

This results in the overall reduction of strength after 8 weeks being slightly smaller in amorphous structures (~ 83 %, vs. ~ 87 % for the crystalline scaffolds). The reason for this could be related to the generation of cracks in the converted HAp layer on crystalline scaffolds. Figure 3.34 shows SEM micrographs of a rod surface of amorphous and crystalline samples soaked for 3 days and 8 weeks in SBF. In the case of crystalline samples (Fig. 3.34b,d), it is evident that the HAp layer formed on the rod surfaces has cracked, probably due to the up growth of residual stresses as the thickness of the continuous HAp layer increases. This has been reported earlier for partially crystallized 45S5 samples after immersion in PBS.[216] According to Fig. 3.34b, the surface of the

crystalline sample after 3days of immersion already shows clearly crack paths uniformly distributed all around the rod. These cracks became bigger and more prone to produce detachment from the substrate by increasing the immersion time to 8 weeks (Fig. 3.34d). On the contrary, there is no evidence of peeling or cracking in amorphous samples neither at 3 days nor even after 8 weeks of immersion (Fig. 3.34a,c). This could be simply a consequence of the higher level of microporosity in the amorphous structures which helps relieve residual stresses. However, other authors have suggested that the mineralized layer is bonded more loosely to the crystalline phase than to the amorphous bioactive glass, which facilitates peeling off the layer to release strain energy.

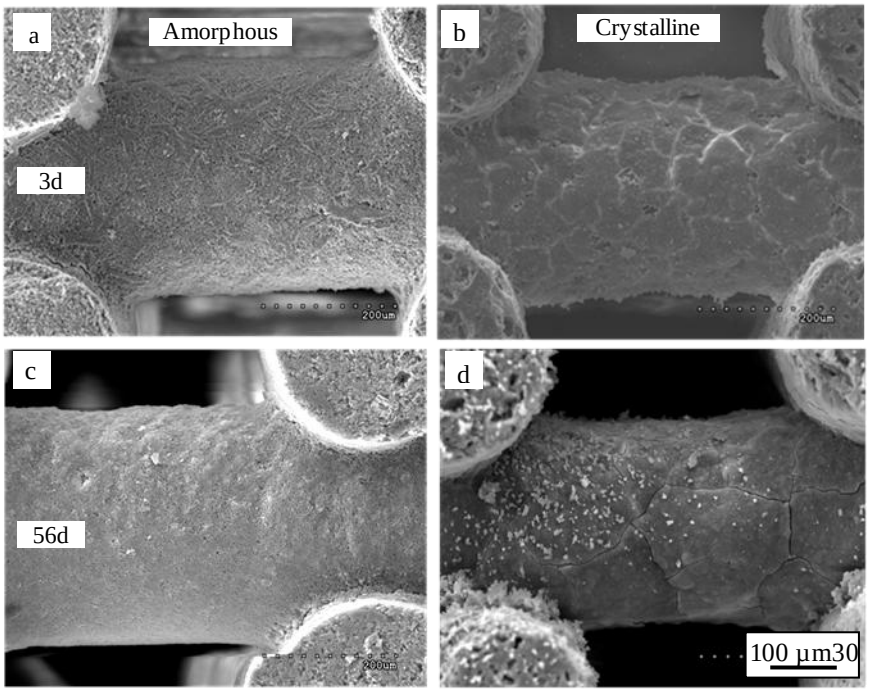

Figure 3.34. SEM micrographs of the rod surface on amorphous (a, c) and crystalline (b, d) 45S5 bioglass scaffolds after soaking in SBF for 3 and 56 days, as indicated.

Nonetheless, despite this apparent resistance to HAp layer detachment—and the mechanical enhancement provided by the fabrication by robocasting which

has permitted for the first time to produce amorphous 45S5 scaffolds with sufficient mechanical integrity—the mechanical performance of such amorphous materials is still far from what can be achieved by improving densification. Indeed, crystalline structures after 8 weeks of degradation are still almost as strong as the non-degraded glassy scaffolds (Fig. 3.32).

3.3.2 Polymer-coated 45S5 bioglass scaffolds

In this section, the results of *in vitro* bioactivity and degradation behavior is analyzed on 45S5 bioglass scaffolds coated with the different polymers under optimal deposition conditions: solutions at 60 °C, with a concentration (w/v) of 25 % for PCL, 15 % for PLA (with toluene solvent in both cases), and 5 % for all the natural polymers (alginate and gelatin in distilled water and chitosan in 2 vol.% acetic acid aqueous solution). Since no basic differences (only different rates) exist in the *in vitro* behavior of amorphous and crystalline 45S5 bioglass scaffolds (Section 3.4.1), the study is performed only using the amorphous structures, sintered at 550 °C.

3.3.2.1 *In vitro* degradation and bioactivity assessment

The variation of the pH in the SBF solution with the immersion time of polymer-coated 45S5 bioglass scaffolds is shown in Figure 3.35. For comparison, the data for bare scaffolds sintered at 550 ºC (from Fig. 3.30a) have been included in Fig. 3.35. In these hybrid structures, the pH of the SBF solution was simultaneously influenced by the dissolution of the bioglass and the degradation of the polymer coating. Indeed, besides constituting a barrier for the degradation of the bioglass substrate, the different polymers exhibit diverse degradation rates and release different degradation products to the solution that can affect the pH. Consequently, the differences shown in Figure 3.36 between the various polymer-coated 45S5 scaffolds are not surprising.

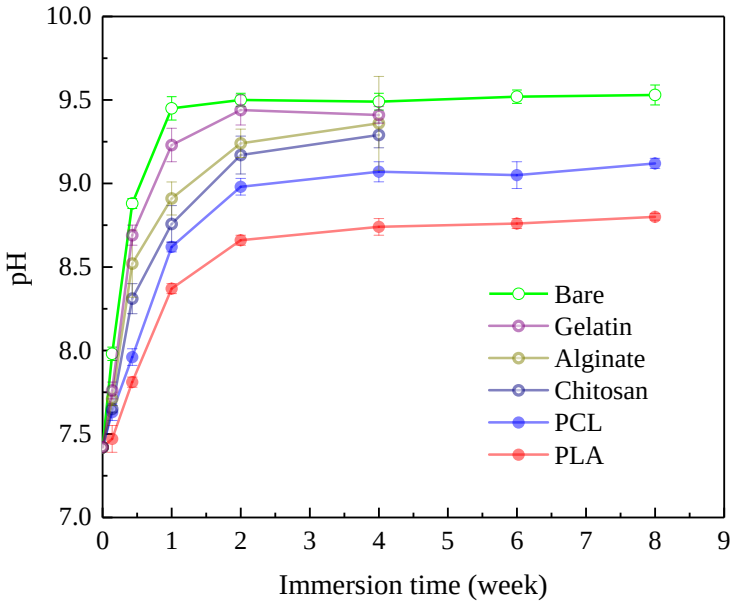

Figure 3.35. Evolution of the pH of the SBF solution as a function of immersion time for amorphous 45S5 bioglass scaffolds before and after coating with the indicated polymers, with standard deviations as error bars.

All coatings, with the possible exception of gelatin, seemed to increase the time needed to balance the solution pH (from 1-2 week to 2-4 weeks) and tended to reduce the final equilibrium value. This confirms, on the one hand, that polymeric coatings are delaying the bioglass scaffold degradation, reducing the ion exchange rate in comparison to bare scaffolds. On the other hand, it implies that the biodegradation products of all polymers are mildly acidic, with the natural polymer coatings (open symbols in Fig. 3.35) leading to the highest pH values and synthetic ones (full symbols), especially the poly-lactic acid, producing the more acidic degradation products.

Fig. 3.36 shows the weight loss curves for coated scaffolds as a function of SBF immersion time with data for bare scaffolds (from Fig. 3.30b) included for comparison. Now a more clear distinction can be made between polymers with a slow hydrolysis rate, such as PCL and PLA,[217,218] and water soluble natural polymers (alginate, chitosan and gelatin). The bioglass scaffolds coated with synthetic polymers showed significantly lower degradation rate compared to the bare structures. The biodegradation behavior of PLA and PCL coated scaffolds

exhibits the same trend indicating that both aliphatic polyesters provide similar degradation profile. However, the PCL degradation takes place more slowly than for PLA.[219]

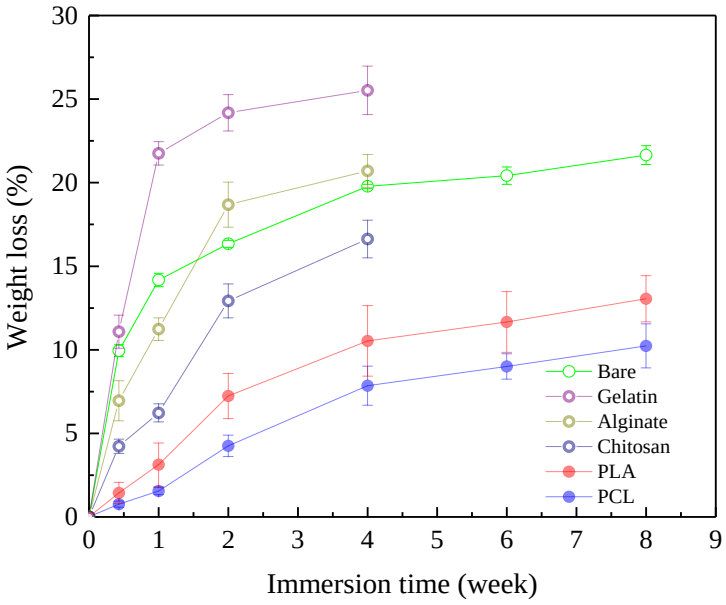

Figure 3.36. Evolution of weight loss with immersion time for amorphous 45S5 bioglass scaffolds before and after coating with the indicated polymers. Error bars represent standard deviations.

In contrast, natural polymers have a higher degradation rate than bioceramics,[220] and although the presence of this coating can delay the degradation of the bioglass substrate, their own degradation contributes significantly to the overall weight loss of the structure. Indeed, scaffolds coated with natural polymers not only showed faster degradation rate compared to PCL- or PLA-coated scaffolds because of their higher resorption rate, but in some cases exhibited faster weight loss than the bare structures.

This is for example the case of gelatin-coated scaffolds which exhibited a faster degradation than the bare 45S5 bioglass scaffolds at least up to 1-2 weeks, and then eventually the weight loss rate became similar to that of the bare scaffolds. This is likely caused by the high dissolution rater of this highly hydrophilic polymer, especially at the incubation temperature (37 °C).[221]

Indeed, SEM observations showed a detectable gelatin coating, at least in part of the strut surfaces up to 1 week immersion in SBF and disappeared afterwards, which is in good agreement with the literature.[36]

For alginate-coated scaffolds, during the first week of immersion the degradation rate was initially slower than in the bare scaffolds. However, it declined more slowly during the second week of immersion and eventually, the weight loss of the hybrid structure exceeded that of the bare structures, which is attributed to the loss of the alginate layer adding to the bioglass dissolution. Between 2 and 4 weeks of immersion, the rate of weight loss did not change significantly which was likely due to cross-linking effect between alginate and Ca^{2+} ions in the SBF solution which improves the alginate network stability and slows down the alginate coating degradation during immersion in the SBF.[222]

Finally, the biodegradation rate of chitosan-coated samples was the slowest among the hybrid structures made from natural polymers and was lower than that of the bare structures during the whole tests. It closely related to the trends exhibited by the synthetic polymers although still degrading significantly faster than them. The reason for this intermediate behavior might be related to the which stronger interfacial adhesion of the chitosan layer, and the lower water absorption ability of chitosan,[223] which retards both the dissolution of bioglass and its own biodegradation.

Regarding bioactivity, the apatite forming ability of polymer-coated scaffolds depended strongly on the nature of the polymer. On the one hand, synthetic polymers tended to delay apatite formation. Figures 3.37 and 3.38 show the SEM micrographs portraying the evolution with immersion times in SBF of the microstructure on the struts surfaces of, respectively, PCL- and PLA-coated scaffolds. By comparing these images with those of bare amorphous 45S5 bioglass scaffolds (Fig. 3.31), it can be concluded that the HAp layer required more time to nucleate and grow during the immersion on the surface of coated samples, since no evidence of HAp nucleation was found after one day of immersion (Figs. 3.37a and 3.38a). Nucleation of HAp on both PCL-and PLA-coated surfaces was observed after 3 days immersion in SBF as illustrated in Figs. 3.37b and 3.38b. Most HAp crystallites are embedded in the polymer layer, implying that the HAp formed on the bioglass surface (or bioglass/polymer interface) upon diffusion of the appropriate species through the coating. As HAp growth progresses (e.g. after 1 week of immersion), more HAp becomes apparent on the surface of the rods and microcracks start to develop in the polymeric coating (Figs. 3.36c and 3.37c). The partial disruption of the polymer layer facilitates SBF penetration into the interface increasing the

degradation rate, in good agreement with the results in Fig. 3.36, and the growth of apatite deposits. After 8 weeks of incubation HA particles densely covered the entire surface of the rods (Figs. 3.36d and 3.37d). At all soaking times HAp formation was greater on the PLA-coated structures compared to PCL hybrids, in good accordance with the faster degradation rate exhibited by PLA-coated scaffolds (Fig. 3.36). This enhanced degradation of PLA-coated structures is attributed to the faster hydrolysis of PLA in the SBF and the more acidic degradation products it generates, which enhance dissolution of the bioglass producing a local supersaturation of calcium and phosphate ions that facilitates the nucleation of apatite.[224]

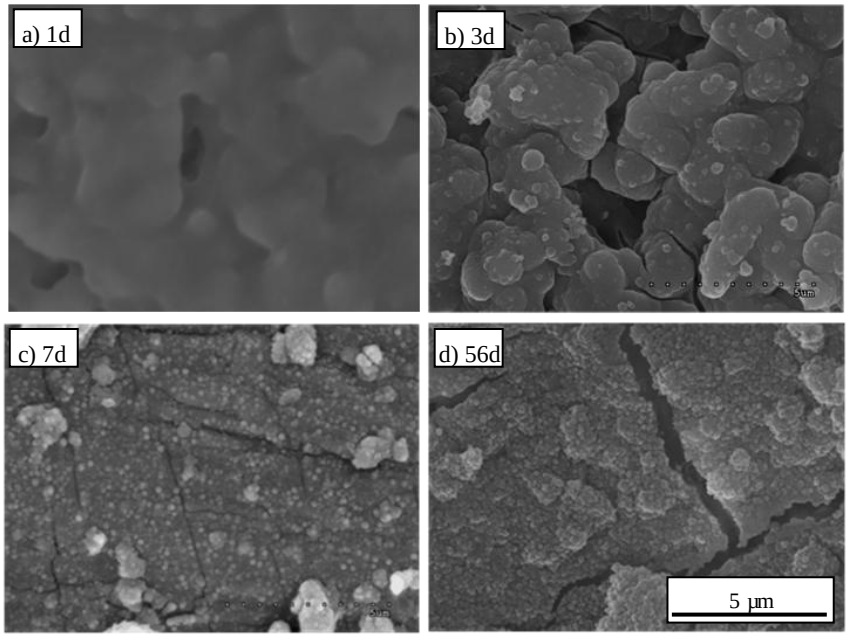

Figure 3.37. SEM micrographs of the sturt surfaces of PCL-coated amorphous 45S5 bioglass scaffolds soaked in SBF for the indicated times.

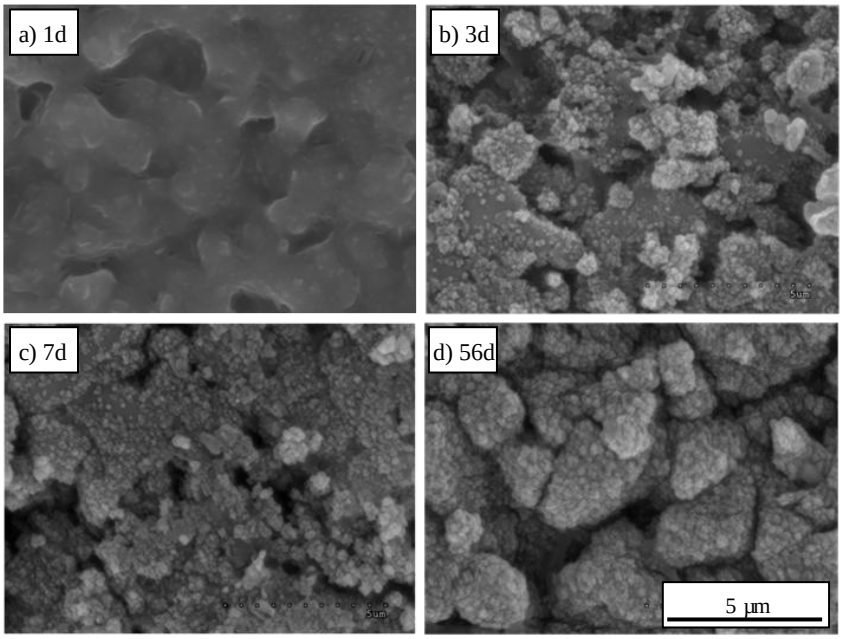

Figure 3.38. SEM micrographs of the strut surfaces of PLA-coated amorphous 45S5 bioglass scaffolds soaked in SBF for the indicated times.

On the other hand, as shown in Figures 3.39-3.41, 45S5 bioglass scaffolds coated with natural polymers exhibited enhanced bioactivity (HAp formation ability) compared not only to synthetic polymer-coated scaffolds but also over the bare bioglass structures. All scaffolds coated with natural polymers showed a significant amount of apatite on their surface after 1 day immersion in SBF as shown in Figs 3.39a-3.41a. Apatitic clusters were larger and more numerous than on the bare bioglass surface after the same immersion period (Fig. 3.31a). This is attributed to the hydrophilicity and high resorption rate of natural polymers in the physiological fluid, and the mildly acidic nature of the degradation byproducts, which can facilitate the interfacial reactions between bioglass and the physiological solution, accelerating HAp nucleation. This faster HAp nucleation may explain why the weight loss was slightly slower in the scaffolds coated by natural polymers (with the exception of gelatin) than in the bare structures despite the polymer contributing to it with their own biodegradation. Growth of this clusters progressed at longer soaking times and the struts were fully covered by HAp crystals after 4 weeks, although evidences

of residual alginate and chitosan are still found at this time (Figs 3.40d and 3.41d). The survival of these polymers for such a long time—unlike gelatin which has already disappeared at 4 weeks (Fig. 3.39d) — is probably caused by the cross-linking of alginate by Ca^{2+} ions in the SBF solution that retards alginate dissolution,[222] and the fact that chitosan becomes insoluble when pH increases above 6.[225]

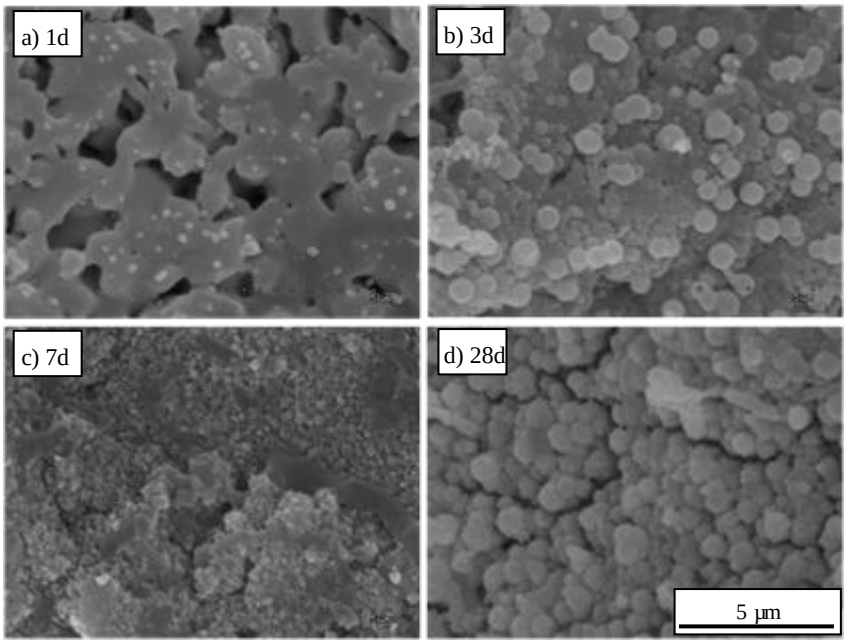

Figure 3.39. SEM micrographs of the struts surfaces of gelatin-coated amorphous 45S5bioglass scaffolds soaked in SBF for the indicated times.

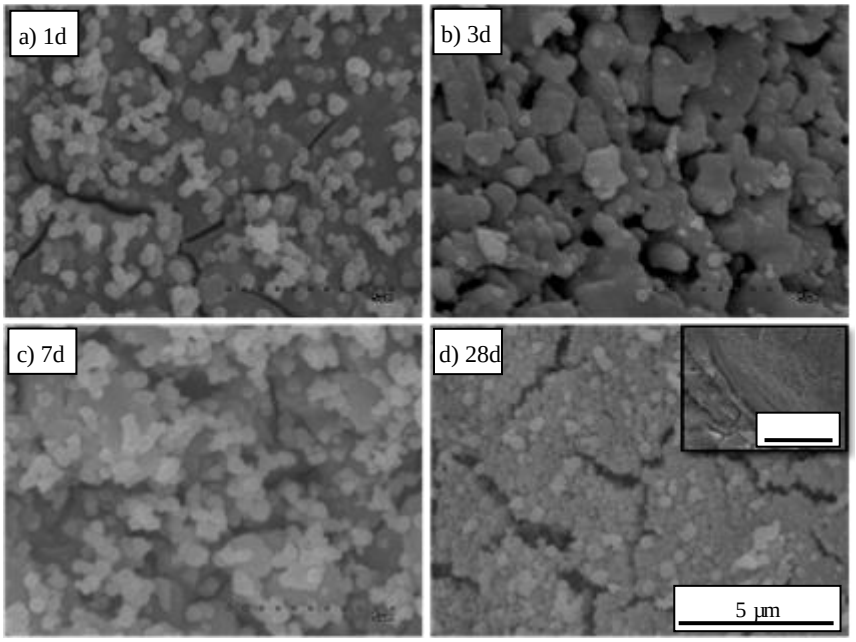

Figure 3.40. SEM images of the struts surfaces of alginate-coated amorphous 45S5 bioglass scaffolds soaked in SBF for the indicated periods.

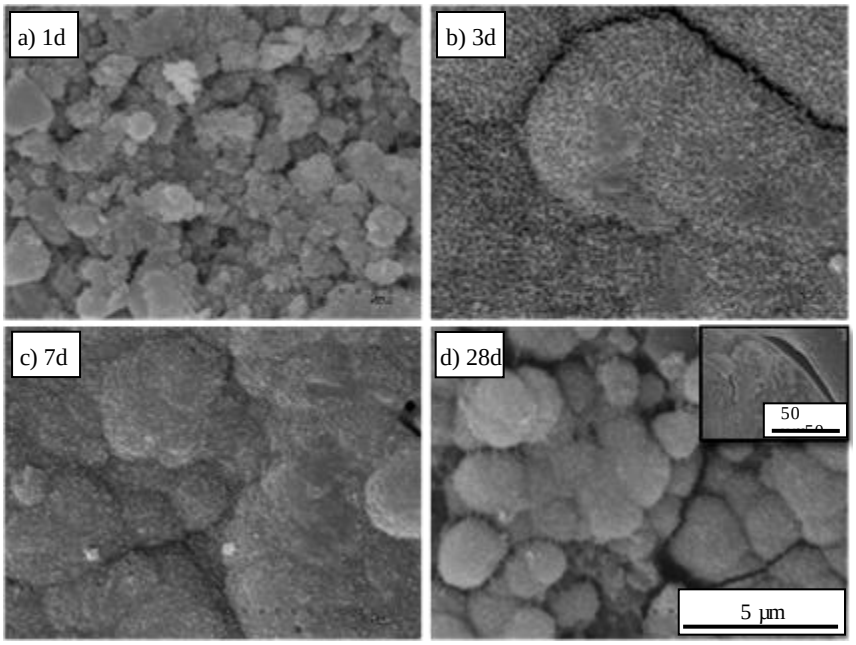

Figure 3.41. SEM images of the struts surfaces of chitosan-coated amorphous 45S5 bioglass scaffolds soaked in SBF for the indicated periods.

Consequently, unlike for synthetic compositions, the application of natural polymers as coatings have a positive effect on the bioactivity of 45S5 glass, accelerating the formation of a HAp layer. And most interestingly, they can do so while simultaneously reducing (except in the case of gelatin) its degradation (weight loss) rate (Fig. 3.37), which has a positive impact on the evolution of their mechanical properties, as shown in the following section. Of course, the results of this *in vitro* study should be complemented in future works with cell culture experiments and *in vivo* test to completely assess if such polymeric coatings can be indeed beneficial for the enhancement of the biological performance of 45S5 scaffolds.

3.3.2.2 Compressive strength degradation

The evolution of the compressive strength of polymer-infiltrated 45S5 bioglass scaffolds as a function of immersion time in the SBF solution is shown in Figure 3.42. For comparison, the data for bare scaffolds sintered at 550 ºC (from Fig. 3.32) have been included in Fig. 3.42.

It is clear from the absolute values shown in Fig. 3.42a that the compressive strengths of coated scaffolds are significantly higher than that of the bare 45S5 bioglass scaffolds at all times points tested. A monotonous decrease of compressive strength was observed in all samples over the whole degradation period, in which chitosan-coated samples showed the highest compressive strength among all groups.

To better analyze the degradation of the mechanical properties upon immersion in SBF, Fig. 3.42b plots the compressive strength loss, defined as $\Delta\sigma/\sigma_0$; where $\Delta\sigma = \sigma_0 - \sigma_t$, σ_0 is the initial compressive strength of the scaffold, and σ_t is the compressive strength at time t. From this plot, it is evident that the fastest degradation and the highest overall compression loss (~ 82 %) was exhibited by gelatin-coated scaffolds, which was even greater that for the bare scaffolds (72 %), in good accordance with the results of weight loss (Fig. 3.37). Alginate-coated scaffolds exhibited initially also a greater strength loss, but the curve flattened out after 2-weeks immersion. Nonetheless, despite the fast mechanical degradation of both natural polymers, their corresponding hybrid structures remained stronger than than the bare scaffolds over the immersion period analyzed.

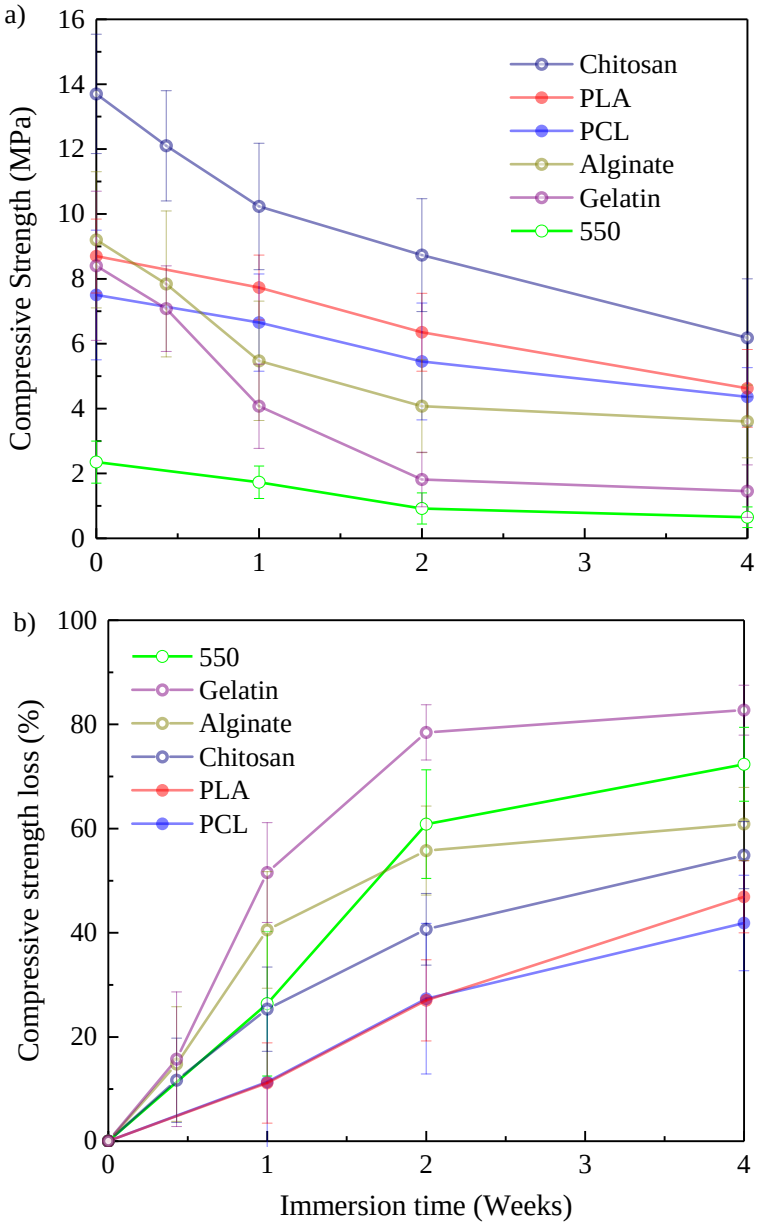

Figure 3.42. (a) Compressive strength and (b) compressive strength loss as a function of immersion time for bare and coated amorphous 45S5 bioglass scaffolds, with standard deviation as error bars.

However, the most significant protective effect against *in vitro* mechanical degradation (as measured by the compression strength loss) was provided by coating the 45S5 bioglass scaffolds with, in this order, PCL, PLA and chitosan, which reduced the overall loss to 42, 47 and 55 % respectively. Especially significant is the result for chitosan, which clearly outstands as the most attractive reinforcing polymer, since it not only provides the greater initial strengthening, but also reduces the mechanical degradation nearly as much as the more inert synthetic polymers. And all that while enhancing the bioactivity of 45S5 glassy scaffolds, as pointed out in the preceding section.

3.4 Comparison to human bone properties

To conclude this chapter, in this section the results of the mechanical characterization of all the bare and polymer coated 45S5 bioglass-derived scaffolds developed in this study are compared to natural human bone. This comparison is pertaining to materials whose intended use is as bone graft substitutes for bone replacement and regeneration.

As already mentioned, the challenge in the development of materials for bone replacement and regeneration lies in obtaining osteoconductive materials with mechanical performance close to that of natural bone tissue. This study has explored several paths leading towards this long sought after goal.

First, this work demonstrates how producing more regular struts and reducing the scaffold's struts microdefects lead to significant improvements in the strength of bioglass-derived—and, by extension, any bioceramic—scaffolds. Indeed, as shown in Figure 3.43, structures with uniform strut dimensions such as those created by robocasting exhibit significantly superior (note logarithmic scale) strength compared to scaffolds fabricated by conventional means with the same porosity (dashed lines are extrapolation of experimental results from the literature[174] according to Gibson and Ashby model.[227]

The enhancement produced by improving densification and, thus, reducing flaw population in the scaffold's struts is also apparent in the 45S5 bioglass data in Fig. 3.43. As the microdefect decreases in number and size, the density increases, and the strength of the 45S5 bioglass-derived scaffolds gets progressively closer to bone values, as predicted by Keller's model.[228]

Consequently, by optimizing the pore architecture and densification of scaffolds struts it seem feasible to produce bioceramic scaffolds with bone-like strengths. But obviously, strength is not the only critical mechanical parameter: modulus and, especially, toughness should also be taken into account. As can be appreciated in the Ashby diagrams of Fig. 3.43, even the best bare bioglass-derived scaffolds are quite far from completely mimicking natural bone mechanical performance.

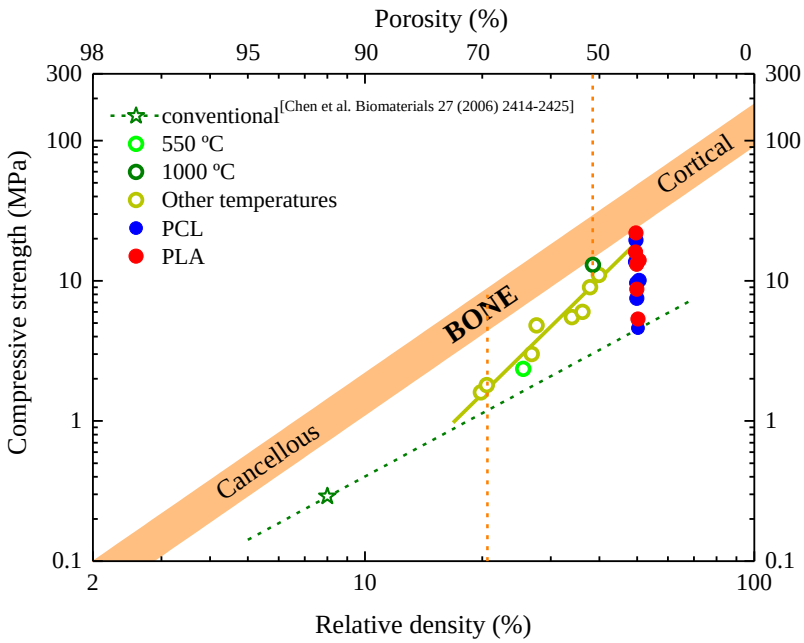

Figure 3.43. Summary of compressive strength results as a function of relative density for bare and coated 45S5 bioglass-derived scaffolds. Data for conventional 45S5[174] *scaffolds and bone properties*[228] *are included for comparison.*

Regarding modulus, the analyzed bare 45S5 bioglass-derived scaffolds, with over 50 % porosity in all cases, exhibited elastic moduli closer to cortical than to cancellous bone (Figure 3.44a). The same is true for coated structures, since their modulus is virtually unaffected by the polymeric coating, as shown in Fig. 3.18. This implies, however, that both the pure bioceramic scaffolds and the polymer-coated structures will have a hard time mimicking the mechanical performance of cancellous bone. Indeed, while an increase in porosity will

provide a reduced modulus, porosity affects more dramatically the strength with comparing values corresponding to 45S5 scaffolds sintered at 550 and 1000 °C. This might not be however a big hurdle in practice since their stiffness is not higher than those of cortical bone, and these materials, unlike bioinert metals, will degrade with time upon implantation.

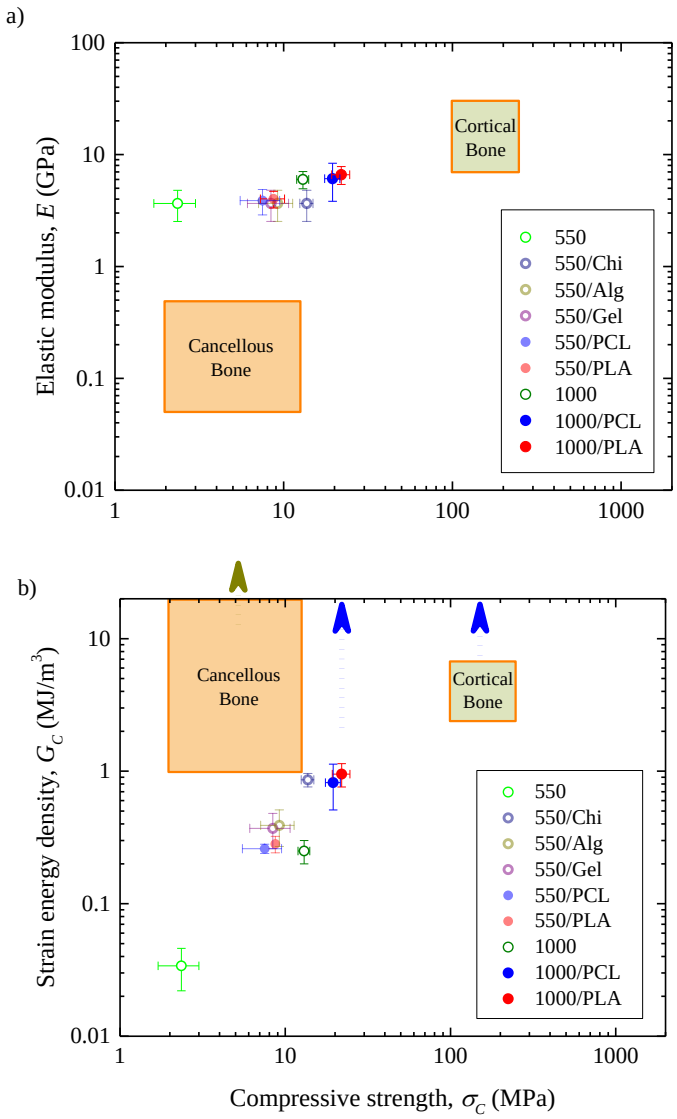

Figure 3.44. Plot of (a) elastic modulus, E, and (b) strain energy density, G_C, versus compressive strength, σ_C, for the materials evaluated in this study. Results are compared to bone properties.[228]

Indeed, the greatest problem of these pure bioceramic structures lies in their brittleness. As can be seen in Fig. 3.44b the strain energy density in compression is much lower than the lower limit of cancellous bone values. The lack of any type of ductility in these materials makes it difficult to overcome this limitation by simply modifying the scaffold's architecture. The results of this study demonstrate, however, that it is possible to substantially improve both the strength and toughness of these structures by coating them with biodegradable polymers. While unfortunately, none of the coated 45S5 bioglass robocast scaffolds closely matches the performance of cortical bone in compression in terms of the three mechanical properties analyzed (stiffness, strength and toughness), the biodegradable polymers coatings have enabled the fabrication of hybrid scaffolds with strengths clearly superior and toughness significantly closer to cancellous bone performance. An all that has been done while preserving the pre-designed interconected macroporosity provided by robocasting. Moreover, not only the initial mechanical performance is improved but the degradation of such properties in physiological environment has also been reduced (Section 3.3.2.2). While all this mechanical enhancement comes at the cost of reducing the bioactivity of the 45S5 bioglass scaffold when synthetic polymers are used, the selection of natural polymers yields hybrid structures with an enhanced bioactivity. In this sense chitosan coatings appear as the most promising alternative since they produce the greatest mechanical improvement among all the polymers tested.

Chapter 4

Conclusions

In this work, fabrication of 45S5 bioglass scaffolds by robocasting was successfully achieved after developing an appropriate ink and optimizing the sintering routine. Besides, biodegradable polymer-coated scaffolds were successfully fabricated in order to improve the mechanical properties of bioglass-derived scaffolds. Different polymer compositions, including natural (alginate, chitosan, gelatin) and synthetic ones (PLC and PLA) were deposited onto the robocast structures by immersion in the corresponding polymeric solutions (i.e. by dip-coating). The effect of a number of parameters in the dip-coating process on the mechanical properties of the coated scaffolds was analyzed. These parameters included in-rod microporosity of 45S5 bioglass-derived struts, solvent, solution temperature, as well as the polymer concentration and composition. The results from this analysis were used to determine the optimal coating conditions for each polymer. The mechanical properties and *in vitro* bioactivity and biodegradation behavior of 45S5 bioglass-derived scaffolds before and after coating with different polymers were compared. Among the most relevant conclusions of this study, it is worth highlighting the following:

Regarding 45S5 bioglass ink preparation and robocasting

1- Robocasting technique provides a means to produce 45S5 bioglass-derived scaffolds with customized external geometry and internal pore architecture with compressive strengths that are far superior to any previously reported values. This is achieved through the use of carboxymethyl cellulose (CMC)

as a single, multifunctional additive that allows one to prepare the concentrated suspensions required by robocasting, overcoming the inherent difficulties associated to the colloidal processing of 45S5 bioglass. The enhancement in mechanical performance associated to the novel pore architectures, with thicker struts and wider interconnections, produced by robocasting is enormous: more than one order of magnitude compared to existing scaffold strength data and well within, or even surpassing, cancellous bone strength range.

2- Robocasting allows one to produce, by sintering at sufficiently low temperature (550 ºC), fully amorphous robocast 45S5 bioglass scaffolds, which preserve intact all the outstanding bioactivity of 45S5 bioglass, with enough mechanical integrity for practical use. Therefore it could be said that robocasting, and perhaps also other solid freeform fabrication techniques, can overcome the main obstacle for the successful application of 45S5 bioglass as a broad use bone substitute material. The simplicity and versatility of the proposed robocasting process will greatly facilitate the development of patient-specific 45S5 bioglass scaffolds and significantly extend the current range of biomedical applications of this excellent bioactive material.

Regarding polymer coating

3- The results of this study demonstrate that dip coating method can be used as a simple, cost-effective process for producing polymer/bioglass composites in a reliable way from both synthetic and natural commercial polymers. The deposited polymers can penetrate into the microporosity on the scaffold struts while preserving intact the pre-designed interconnected macroporosity of robocast structures

4- This study demonstrates the positive effect of polymeric coatings on the mechanical properties of robocast ceramic or glass scaffolds regardless of the type of loading configuration (compression or bending). All polymer coatings studied led to significant improvement of both the compressive strength and toughness of the bare scaffolds, without significantly affecting their Young's modulus.

5- This work's results prove also, for the first time, that existing micro-defects (microporosity) has a major role on the mechanical enhancement produced

by polymer coatings of robocast scaffolds. The strengthening, produced by defect healing, is greatly reduced as the pre-existing flaw population decreases. The same occurs with the toughening since fibrils generated from the polymer within the ceramic microporosity can significantly contribute to enhance fracture energy through a crack microbridging mechanism.

6- Despite the diminishing effectiveness of the polymer infiltrate as a reinforcing agent as the microporosity is reduced, denser ceramic struts yield stronger and tougher hybrid structures after polymer coating. Consequently, optimization of the sintering conditions for the ceramic skeleton should still be a major concern for the maximization of the mechanical performance of ceramic/polymer composites.

7- Among the different parameters of the dip-coating process, the results of this study suggest that polymer concentration is one of the most important in determining the ultimate mechanical properties of polymer-coated scaffolds. While the mechanical performance is improved monotonically with polymer concentration, this concentration cannot be increased indefinitely. An optimal concentration exists for a given set of process variables (substrate, polymer, solvent, temperature) that leads to the maximal polymer infiltration into the strut microporosity while preserving predesigned scaffold macroporosity.

8- Conversely, although they might, in principle, affect wettability of the polymer/ceramic system, the selected solvent and solution temperature play only a minor direct role in the mechanical properties of the composite, at least in the PCL/45S5 bioglass system for the solvents and temperatures analyzed. However, both variables can have a significant impact in determining the maximum suitable concentration of the polymer in the dip-coating solution, and thereby in the maximum achievable mechanical performance of the resulting hybrid scaffold. In this sense temperature should be maximized within the limits imposed by the selected polymer/solvent system, especially since evaporation might become an issue were reproducibility of the process is concerned.

9- Polymer composition has an important role on the mechanical enhancement produced by the deposited coating. This study showed that scaffolds sintered at 550 ºC coated with natural polymers exhibited greater strength and toughness than those coated with the two synthetic polymers, despite the significantly superior intrinsic mechanical properties of the

latter. This result suggests that interfacial adhesion, most likely stronger between the hydrophilic bioglass struts and the hydrophilic natural polymers than with the more hydrophobic synthetic polymers, plays a major role in the mechanical enhancement provided by polymeric coating, while the polymer intrinsic properties (strength, stiffness toughness) play only a secondary role. Among the studied polymer, chitosan seems to be the optimal candidate as reinforcing coating for 45S5 bioglass, since it provided the highest level of strengthening and toughening.

Regarding the in vitro performance of the fabricated scaffolds

10- During immersion of bare 45S5 bioglass-derived scaffolds in SBF, the amorphous glass tends to leach more alkali to the solution, causing a larger weight loss and a higher increase of pH, due to the greater volumetric diffusion of involved species through the amorphous structure. This provides not only faster degradation kinetics but also a means for enhanced overall conversion factor of the bioactive glass to HA. In both cases, the conversion of the material to a weak porous HA-like product resulted in a degradation of compressive strength, which in the case of crystalline scaffolds is accelerated by the formation of cracks in the HA layer. These results suggest that a simple means for controlling the degradation behaviour of bioglass derived robocast materials is by tailoring their degree of crystallinity.

11- The results of the *in vitro* test demonstrate that coating with a polymer provides another means for tailoring the degradation behavior of bioceramic scaffolds. With the sole exception of gelatin, polymeric coatings provide a barrier for the degradation of the bioglass substrate. Synthetic polymers constitute the most effective barriers against degradation; however, they do so by simultaneously reducing the bioactivity (i.e. HAp formation ability) of the material. On the contrary, alginate and, especially, chitosan coatings can reduce the rate of weight loss and degradation of mechanical properties while simultaneously enhancing the *in vitro* bioactivity of the scaffolds—gelatin can also enhance bioactivity but while increasing biodegradation rate.

About the comparison with natural bone properties

12- This work demonstrates that bare 45S5 bioglass-derived scaffolds with uniform strut dimensions created by robocasting, while significantly surpassing the compressive strength of scaffolds fabricated by conventional techniques, still fall short of the values for natural bone with the same porosity. Elastic moduli similar to cortical bone are also easily attainable in bioceramic structures, but their strain energy densities fall far short of the values for natural tissue.

13- The results of this study demonstrate, that by applying biodegradable polymers coatings over 45S5 bioglass-derived structures it is possible to fabricate hybrid scaffolds with strengths clearly superior and toughness significantly closer to cancellous bone performance in compression. And all that was achieved while preserving the pre-designed interconected macroporosity provided by robocasting.

As a final remark it is worth highlighting that among all synthetic and natural polymers analyzed in this study, chitosan outstands as the optimal coating materials for the mechanical and biological enhancement of 45S5 bioglass-derived scaffolds.

Conclusiones

En este trabajo, se han fabricado andamiajes derivados de biovidrio 45S5 mediante moldeo robotizado (robocasting). Ello ha requerido desarrollar una tinta adecuada y optimizar el proceso de sinterización. Además, con el objetivo de mejorar las propiedades mecánicas, los andamiajes de biovidrio se han recubierto con polímeros biodegradables tanto naturales (alginato, quitosano, gelatina) como sintéticos (PLC y PLA), mediante inmersión en las disoluciones poliméricas correspondientes. Se ha analizado el efecto de diferententes parámetros del proceso de recubrimiento en las propiedades mecánicas de los andamiajes recubiertos. Estos parámetros incluyen la microporosidad de las barras de biovidrio 45S5 que constituyen los andamiajes, el disolvente, la temperatura de la disolución, así como la concentración de polímero y su composición. Los resultados de este análisis se han utilizado para determinar las condiciones del proceso de recubrimiento óptimas para cada polímero. También se han determinado las propiedades mecánicas y la bioactividad y la biodegradación *in vitro* de los andamiajes de biovidrio 45S5 y de los andamiajes híbridos biovidrio 45S5/polímero. Entre las conclusiones más relevantes de este estudio, cabe destacar:

En relación a la fabricación de andamiajes de biovidrio 45S5

1- 1- La técnica de moldeo robotizado permite fabricar andamiajes derivados de biovidrio 45S5 con la forma exterior y la arquitectura de poros deseadas y con resistencia a compresión muy superior a cualquier valor publicado anteriormente. La utilización de carboximetilcelulosa como único aditivo ha permitido preparar suspensiones coloidades con la concentración adecuada para moldeo robotizado, superando las dificultades inherentes al procesado coloidal de biovidro 45S5. La mejora en las propiedades mecánicas asociada a la nueva arquitectura de poros obtenida mediante

moldeo robotizado, con barras cerámicas más gruesas y con mayor grado de interconectividad, es enorme: en el caso de la resistencia a fractura se obtienen valores más de un orden de magnitud superior a los obtenidos hasta ahora y dentro, o incluso por encima, del rango de valores del hueso esponjoso.

2- El moldeo robotizado permite, mediante sinterización a temperaturas suficientemente bajas (550 ºC), fabricar andamiajes de 45S5 amorfo—preservando así la bioactividad del biovidrio 45S5— con la integridad mecánica suficiente como para ser utilizado. Por tanto, el moldeo robtizado, y quizás también otras técnicas de conformado libre, permite superar el principal obstáculo para el uso de biovidrio 45S5 como sustituto óseo. La simplicidad y versatilidad del proceso de moldeo robotizado facilitarán permitirá fabricar andamiajes de biovidrio 45S5 con la geometría necesaria para adaptarse a la lesión de cada paciente y extender el ámbito actual de aplicación de este excelente material bioactivo.

En relación al recubrimiento de los andamiajes de biovidrio 45S5 con polímero

3- Los resultados de este estudio demuestran que la inmersión de los andamiajes de biovidrio en una disolución de polímero es una técnica simple y económica que puede ser utilizada para fabricar andamiajes compuestos biovridrio/polímero a partir de polímeros sintéticos y naturales. El polímero puede penetrar en los microporos de las barras de biovidrio que constituyen el andamiaje a la vez que se preserva intacta la macroporosidad interconectada de la estructura fabricada mediante moldeo robotizado.

4- Los resultados de este estudio confirman el efecto positivo del recubrimiento con polímeros en las propiedades mecánicas de andamiajes derivados de biovidrio 45S5, independientemente del modo de carga (compresión o flexión). Todos los polímero utilizados mejoran significativamente tanto la resistencia a compresión como la tenacidad del andamiaje de biovidrio sin prácticamente modificar su módulo de Young.

5- Los resultados de este trabajo prueban, por primera vez, que la existencia de microporosidad en las barras juega un papel importante en el refuerzo mecánico que se obtiene mediante el recubrimiento con polímeros de estructuras fabricadas mediante moldeo robotizado. El aumento de

resistencia que se produce por curación de defectos disminuye considerablemente al disminuir la población de defectos precursores (microporos). Lo mismo ocurre con el aumento de tenacidad debido a que las fibras del polímero que está dentro de los microporos contribuye al mecanismo de refuerzo por puenteo de fisuras

6- Aunque el poder reforzante del polímero disminuye al reducir la microporosidad, los andamiajes derivados de biovidrio 45S5 recubiertos con polímero más resistentes y tenaces son aquellos en los que la estructura cerámica está constituido por barras densas. Por tanto, la optimización del proceso de sinterización del esqueleto cerámico es indispensable para maximizar la respuesta mecánica del andamiaje compuesto cerámicos/polímero.

7- Entre los diferentes parámetros del proceso de recubrimiento por inmersión, los resultados de este estudio sugieren que la concentración de polímero es uno de los más importantes en la determinación de las propiedades mecánicas finales de los andamiajes recubiertos de polímero. Mientras que el comportamiento mecánico se mejora monótonamente con la concentración de polímero, esta concentración no se puede aumentar indefinidamente. Existe una concentración óptima para un conjunto dado de las variables del proceso (sustrato, polímero, disolvente, temperatura) que conduce a la infiltración máxima de polímero en la microporosidad de las barras que constituyen el andamiaje preservando al mismo tiempo la macroporosidad prediseñada.

8- Por el contrario, si bien podrían, en principio, afectar a la mojabilidad del sistema polímero/cerámico, el disolvente y la temperatura de la disolución juegan solo un papel secundario en las propiedades mecánicas, al menos en el sistema compuesto PCL/45S5 biovidrio para los disolventes y las temperaturas analizadas. Sin embargo, ambas variables pueden tener un impacto significativo en la determinación de la concentración máxima del polímero en la disolución, y por lo tanto en el comportamiento mecánico máximo alcanzable por el andamiaje híbrido resultante. En este sentido la temperatura debe ser maximizada dentro de los límites impuestos por el sistema polímero /solvente seleccionado, sobre todo porque la evaporación podría convertirse en un problema en cuanto a la reproducibilidad del proceso se refiere.

9- La composición del polímero juega un papel importante en la mejora mecánica producida por el recubrimiento. Los resultados de este estudio

muestran que los andamiajes sinterizadas a 550 ºC recubiertos con polímeros naturales poseen mayor resistencia y tenacidad que los recubiertos con los dos polímeros sintéticos, a pesar de que las propiedades mecánicas intrínsecas de estos últimos son significativamente superiores. Este resultado sugiere que la adhesión interfacial, probablemente más fuerte entre el hidrófilo biovidrio y los hidrófilos polímeros naturales que en el caso de los hidrófobos polímeros sintéticos, juega un papel importante en la mejora mecánica proporcionada por recubrimiento polimérico, mientras que las propiedades intrínsecas del polímero (resistencia, rigidez, tenacidad) juegan sólo un papel secundario. Entre los polímeros estudiados, el quitosano parece ser el candidato óptimo para recubrir al biovidrio 45S5, ya que proporciona el mayor aumento de resistencia y tenacidad.

En relación al comportamiento in vitro de los andamiajes fabricados

10- Durante la inmersión de andamiajes de biovidrio 45S5 sinterizados a 550 ºC (amorfo) se produce una mayor pérdida de peso y aumento del pH que en el caso de andamiajes sinterizados a 1000 ºC debido a la mayor disolución de especies alcalinas, debido a la mayor difusión en volumen de las especies involucradas en la estructura amorfa. Esto proporciona no solo una mayor velocidad de degradación si no también un medio para mejorar la conversión de biovidrio a HAp. En ambos materiales, la conversión a una capa porosa de HA da lugar a una degradación de la resistencia a compresión, que en el caso del andamiaje cristalino está acelerada por la formación de fisuras en la capa de HAp. Estos resultados sugieren que una forma simple para controlar la degradación de los andamiajes derivados de biovidrio 45S5 es controlar su grado de cristalinidad.

11- Los resultados de los ensayos *in vitro* demuestran que el recubrimiento con un polímero proporciona otra forma para controlar la degradación de los andamiajes biocerámicos. Con la única excepción de la gelatina, los recubrimientos poliméricos proporcionan una barrera para la degradación del sustrato de biovidrio. Los polímeros sintéticos constituyen las barreras más eficaces contra la degradación, sin embargo, lo hacen a la vez que reducen la bioactividad (es decir, la capacidad de formación de HAp) del material. Por el contrario, el alginato y, especialmente, los recubrimientos

de quitosano pueden reducir la tasa de pérdida de peso y la degradación de las propiedades mecánicas a la vez que mejoran simultáneamente la bioactividad *in vitro* de la andamiajes—la gelatina también puede mejorar la bioactividad pero a la vez que aumentan la velocidad de biodegradación.

En relación a la comparación con las propiedades del hueso

12- Este trabajo demuestra que los andamiajes derivados de biovidrio 45S5 constituidos por barras de dimensiones uniformes, fabricados mediante moldeo robotizado, aunque superan significativamente la resistencia a compresión de los andamiajes fabricados mediante técnicas convencionales, aún están lejos de los valores correspondientes al hueso natural con la misma porosidad. Módulos elásticos similares a los del hueso cortical también son fácilmente alcanzables en las estructuras biocerámicos, pero su tenacidad está muy por debajo de los valores correspondientes al tejido óseo natural.

13- Los resultados de este estudio demuestran, que mediante la aplicación de recubrimientos de polímeros biodegradables sobre las estructuras de biovidrio 45S5 es posible fabricar andamiajes híbridos con resistencia claramente superior y tenacidad significativamente más cerca de los valores correspondientes al hueso esponjoso, en compresión. Y ello se logra preservando la macroporosidad interconectada proporcionada por la técnica de moldeo robotizado.

Como observación final, cabe destacar que entre todos los polímeros sintéticos y naturales analizados en este estudio, el quitosano destaca como el material de recubrimiento más adecuado para mejorar el comportamiento mecánico y biológico de los andamiajes derivados de biovidrio 45S5.

List of References

1. Oryan, A., Alidadi, S., Moshiri, A. & Maffulli, N. Bone regenerative medicine: classic options, novel strategies, and future directions. *J. Orthop. Surg. Res.* **9,** 18 (2014).
2. Amini, A. R., Laurencin, C. T. & Nukavarapu, S. P. Bone tissue engineering: recent advances and challenges. *Crit. Rev. Biomed. Eng.* **40,** 363–408 (2012).
3. Mouriño, V. & Boccaccini, A. R. Bone tissue engineering therapeutics: controlled drug delivery in three-dimensional scaffolds. *J. R. Soc. Interface* **7,** 209–227 (2010).
4. Bose, S., Roy, M. & Bandyopadhyay, A. Recent advances in bone tissue engineering scaffolds. *Trends in Biotechnology* **30,** 546–554 (2012).
5. De Aza, P. N., de Aza, A. H., Pena, P. & de Aza, S. Bioactive glasses and glass-ceramics. *Boletin de la Sociedad Espanola de Ceramica y Vidrio* **46,** 45–55 (2007).
6. Gerhardt, L.-C. & Boccaccini, A. R. Bioactive Glass and Glass-Ceramic Scaffolds for Bone Tissue Engineering. *Materials* **3,** 3867–3910 (2010).
7. Hench, L. L. The story of Bioglass?? in *Journal of Materials Science: Materials in Medicine* **17,** 967–978 (2006).
8. Jones, J. R. Review of bioactive glass: From Hench to hybrids. *Acta Biomaterialia* **9,** 4457–4486 (2013).
9. Xynos, I. D., Edgar, A. J., Buttery, L. D. K., Hench, L. L. & Polak, J. M. Gene-expression profiling of human osteoblasts following treatment with the ionic products of Bioglass® 45S5 dissolution. *J. Biomed. Mater. Res.* **55,** 151–157 (2001).
10. Reilly, G. C., Radin, S., Chen, A. T. & Ducheyne, P. Differential alkaline phosphatase responses of rat and human bone marrow derived

mesenchymal stem cells to 45S5 bioactive glass. *Biomaterials* **28,** 4091–4097 (2007).

11. Fu, Q., Saiz, E., Rahaman, M. N. & Tomsia, A. P. Bioactive glass scaffolds for bone tissue engineering: state of the art and future perspectives. *Mater. Sci. Eng. C. Mater. Biol. Appl.* **31,** 1245–1256 (2011).
12. Fu, Q., Saiz, E. & Tomsia, A. P. Direct ink writing of highly porous and strong glass scaffolds for load-bearing bone defects repair and regeneration. *Acta Biomater.* **7,** 3547–3554 (2011).
13. Huang, T. S. *et al.* Porous and strong bioactive glass (13-93) scaffolds fabricated by freeze extrusion technique. *Mater. Sci. Eng. C* **31,** 1482–1489 (2011).
14. Barone, D. T.-J., Raquez, J.-M. & Dubois, P. Bone-guided regeneration: from inert biomaterials to bioactive polymer (nano)composites. *Polym. Adv. Technol.* **22,** 463–475 (2011).
15. Poinern, G. E. J., Brundavanam, R. K. & Fawcett, D. Nanometre scale hydroxyapatite ceramics for bone tissue engineering. *American Journal of Biomedical Engineering* (2013). doi:10.5923/j.ajbe.20130306.04
16. Wegst, U. G. K., Bai, H., Saiz, E., Tomsia, A. P. & Ritchie, R. O. Bioinspired structural materials. *Nat. Mater.* **14,** 23–36 (2015).
17. *Biomaterials, artificial organs and tissue engineering - CRC Press Book*. (CRC Press, 2005).
18. Taylor, D. & Kuiper, J. H. The prediction of stress fractures using a ‘stressed volume’ concept. *J. Orthop. Res.* **19,** 919–26 (2001).
19. Weibull, W. A statistical distribution function of wide applicability. *J. Appl. Mech.* **18,** 293–297 (1951).
20. Carter, D. R., Schwab, G. H. & Spengler, D. M. Tensile fracture of cancellous bone. *Acta Orthop. Scand.* **51,** 733–741 (1980).
21. Keaveny, T. M. & Hayes, W. C. in *Bone* 285–344 (1993).
22. Fröhlich, M. *et al.* Tissue engineered bone grafts: biological requirements, tissue culture and clinical relevance. *Curr. Stem Cell Res. Ther.* **3,** 254–64 (2008).
23. Al-Munajjed, A. A. *et al.* Development of a biomimetic collagen-hydroxyapatite scaffold for bone tissue engineering using a SBF immersion technique. *J. Biomed. Mater. Res. - Part B Appl. Biomater.* **90,** 584–591 (2009).

24. Shao, R. *et al.* Porous hydroxyapatite bioceramics in bone tissue engineering : current uses and perspectives. *J. Ceram. Soc. Japan* **123,** 17–20 (2015).
25. Kim, H. M. Ceramic bioactivity and related biomimetic strategy. *Curr. Opin. Solid State Mater. Sci.* **7,** 289–299 (2003).
26. Vastel, L., Meunier, A., Siney, H., Sedel, L. & Courpied, J.-P. Effect of different sterilization processing methods on the mechanical properties of human cancellous bone allografts. *Biomaterials* **25,** 2105–2110 (2004).
27. Logeart-Avramoglou, D., Anagnostou, F., Bizios, R. & Petite, H. Engineering bone: challenges and obstacles. *J. Cell. Mol. Med.* **9,** 72–84 (2005).
28. Shadjou, N. & Hasanzadeh, M. Bone tissue engineering using silica-based mesoporous nanobiomaterials:Recent progress. *Mater. Sci. Eng. C* **55,** 401–409 (2015).
29. Chen, Q., Roether, J. A. and & Boccaccini, A. R. Tissue Engineering Scaffolds from Bioactive Glass and Composite Materials. *Top. Tissue Eng.* **4,** 1–27 (2008).
30. Arahira, T., Maruta, M., Matsuya, S. & Todo, M. Development and characterization of a novel porous β-TCP scaffold with a three-dimensional PLLA network structure for use in bone tissue engineering. *Mater. Lett.* **152,** 148–150 (2015).
31. Pilia, M., Guda, T. & Appleford, M. Development of composite scaffolds for load-bearing segmental bone defects. *BioMed Research International* **2013,** (2013).
32. Rahaman, M. N. *et al.* Bioactive glass in tissue engineering. *Acta Biomaterialia* **7,** 2355–2373 (2011).
33. Lawrence, B. J. & Madihally, S. V. Cell colonization in degradable 3D porous matrices. *Cell Adh. Migr.* **2,** 9–16
34. Bose, S., Roy, M. & Bandyopadhyay, A. Recent advances in bone tissue engineering scaffolds. *Trends Biotechnol.* **30,** 546–54 (2012).
35. Woodard, J. R. *et al.* The mechanical properties and osteoconductivity of hydroxyapatite bone scaffolds with multi-scale porosity. *Biomaterials* **28,** 45–54 (2007).

36. Nooeaid, P. Multilayered Scaffolds for Osteochondral Tissue Engineering Based on Bioactive Glass and Biodegradable Polymers. (University of Erlangen-Nuremberg, 2014).
37. Mallick, S., Tripathi, S. & Srivastava, P. Advancement in Scaffolds for Bone Tissue Engineering: A Review. *IOSR J. Pharm. Biol. Sci.* **10,** 37–54 (2015).
38. Philippart, A., Boccaccini, A. R., Fleck, C., Schubert, D. W. & Roether, J. a. Toughening and functionalization of bioactive ceramic and glass bone scaffolds by biopolymer coatings and infiltration: a review of the last 5 years. *Expert Rev. Med. Devices* **12,** 93–111 (2015).
39. Amini, A. R., Laurencin, C. T. & Nukavarapu, S. P. Bone tissue engineering: recent advances and challenges. *Crit. Rev. Biomed. Eng.* **40,** 363–408 (2012).
40. Mouthuy, P. A., Crossley, A. & Ye, H. Fabrication of calcium phosphate fibres through electrospinning and sintering of hydroxyapatite nanoparticles. *Mater. Lett.* **106,** 145–150 (2013).
41. Hoppe, A., Güldal, N. S. & Boccaccini, A. R. A review of the biological response to ionic dissolution products from bioactive glasses and glass-ceramics. *Biomaterials* **32,** 2757–2774 (2011).
42. Stevens, M. M. Biomaterials for bone tissue engineering. *Materials Today* **11,** 18–25 (2008).
43. Brauer, D. S. Bioactive Glasses-Structure and Properties. *Angew. Chemie Int. Ed.* **54,** 4160 –4181 (2015).
44. Hench, L. L., Splinter, R. J., Allen, W. C. & Greenlee, T. K. Bonding mechanisms at the interface of ceramic prosthetic materials. *J. Biomed. Mater. Res.* **5,** 117–141 (1971).
45. Polo-Corrales, L., Latorre-Esteves, M. & Ramirez-Vick, J. E. Scaffold Design for Bone Regeneration. *J. Nanosci. Nanotechnol.* **14,** 15–56 (2014).
46. Vroman, I. & Tighzert, L. Biodegradable polymers. *Materials (Basel).* **2,** 307–344 (2009).
47. Sabir, M. I., Xu, X. & Li, L. A review on biodegradable polymeric materials for bone tissue engineering applications. *J. Mater. Sci.* **44,** 5713–5724 (2009).
48. Rong, X. & Keif, M. A Study of PLA Printability with Flexography. *59th TAGA Proceeding* 605–613 (2007).

49. Garlotta, D. A Literature Review of Poly(Lactic Acid). *J. Polym. Environ.* **9,** 63–84 (2001).
50. Razak, S. I. A., Sharif, N. F. A. & Rahman, W. A. A. Biodegradable Polymers and their Bone Applications : A Review. *Int. J. Eng. Sci.* **12,** 31 – 49 (2012).
51. Ndazi, B. S. & Karlsson, S. Characterization of hydrolytic degradation of polylactic acid/rice hulls composites in water at different temperatures. *Express Polym. Lett.* **5,** 119–131 (2011).
52. Ng, C. S., Teoh, S. H., Chung, T. S. & Hutmacher, D. W. Simultaneous biaxial drawing of poly (E-caprolactone) films. *Polymer (Guildf).* **41,** 5855–5864 (2000).
53. Zhao, X. *et al.* Calcium phosphate coated Keratin-PCL scaffolds for potential bone tissue regeneration. *Mater. Sci. Eng. C. Mater. Biol. Appl.* **49,** 746–53 (2015).
54. Venkatesan, J., Bhatnagar, I., Manivasagan, P., Kang, K.-H. & Kim, S.-K. Alginate composites for bone tissue engineering: a review. *Int. J. Biol. Macromol.* **72,** 269–81 (2015).
55. Lee, K. Y. & Mooney, D. J. Alginate: Properties and biomedical applications. *Prog. Polym. Sci.* **37,** 106–126 (2012).
56. Christensen, K. *et al.* Freeform inkjet printing of cellular structures with bifurcations. *Biotechnol. Bioeng.* **112,** 1047–55 (2015).
57. Sun, J. & Tan, H. Alginate-based biomaterials for regenerative medicine applications. *Materials* **6,** 1285–1309 (2013).
58. Gómez-Guillén, M. C., Giménez, B., López-Caballero, M. E. & Montero, M. P. Functional and bioactive properties of collagen and gelatin from alternative sources: A review. *Food Hydrocoll.* **25,** 1813–1827 (2011).
59. Begam, H., Shukla, R. N. & Bajpai, A. K. Preparation and Characterization of Genipin Crosslinked Gelatin Nanoparticles and Study of Their Water Intake Behavior. *Int. J. Nanomater. Biostructures* **5,** 24–31 (2015).
60. Mohamed, K. R. in *Composites and Their Applications* (ed. Hu, N.) 113–143 (InTech, 2012).
61. Torricelli, P. *et al.* Co-electrospun gelatin-poly(L-lactic acid) scaffolds: modulation of mechanical properties and chondrocyte response as a function of composition. *Mater. Sci. Eng. C. Mater. Biol. Appl.* **36,** 130–8 (2014).

62. Kim, M. S. *et al.* The development of genipin-crosslinked poly(caprolactone) (PCL)/gelatin nanofibers for tissue engineering applications. *Macromol. Biosci.* **10,** 91–100 (2010).
63. Ge, L. *et al.* Integration of nondegradable polystyrene and degradable gelatin in a core-sheath nanofibrous patch for pelvic reconstruction. *Int. J. Nanomedicine* **10,** 3193–201 (2015).
64. Azami, M., Rabiee, M. & Moztarzadeh, F. Glutaraldehyde crosslinked gelatin/hydroxyapatite nanocomposite scaffold, engineered via compound techniques. *Polym. Compos.* **31,** 2112–2120 (2010).
65. Farris, S., Song, J. & Huang, Q. Alternative reaction mechanism for the cross-linking of gelatin with glutaraldehyde. *J. Agric. Food Chem.* **58,** 998–1003 (2010).
66. Su, Y. & Mo, X. Genipin crosslinked gelatin nanofibers for tissue engineering. *J. Control. Release* **152 Suppl ,** e230–2 (2011).
67. Sisson, K., Zhang, C., Farach-Carson, M. C., Chase, D. B. & Rabolt, J. F. Evaluation of cross-linking methods for electrospun gelatin on cell growth and viability. *Biomacromolecules* **10,** 1675–80 (2009).
68. Rieux, A., Duhem, N. & Je, C. Chitosan and Chitosan Derivatives in Drug Delivery and Tissue Engineering. *Adv. Polym. Sci.* **244,** 19–44 (2011).
69. Roether, J. a. *et al.* Development and *in vitro* characterisation of novel bioresorbable and bioactive composite materials based on polylactide foams and Bioglass® for tissue engineering applications. *Biomaterials* **23,** 3871–3878 (2002).
70. Giesen, E. B. ., Ding, M., Dalstra, M. & van Eijden, T. M. G. . Mechanical properties of cancellous bone in the human mandibular condyle are anisotropic. *J. Biomech.* **34,** 799–803 (2001).
71. Van Rietbergen, B. *et al.* Assessment of cancellous bone mechanical properties from micro-FE models based on micro-CT, pQCT and MR images. *Technol. Health Care* **6,** 413–420 (1998).
72. Mohamad Yunos, D., Bretcanu, O. & Boccaccini, A. R. Polymer-bioceramic composites for tissue engineering scaffolds. in *Journal of Materials Science* **43,** 4433–4442 (2008).
73. Blaker, J. J., Maquet, V., Jérôme, R., Boccaccini, A. R. & Nazhat, S. N. Mechanical properties of highly porous PDLLA/Bioglass® composite

foams as scaffolds for bone tissue engineering. *Acta Biomater.* **1,** 643–652 (2005).

74. Rezwan, K., Chen, Q. Z., Blaker, J. J. & Boccaccini, A. R. Biodegradable and bioactive porous polymer/inorganic composite scaffolds for bone tissue engineering. *Biomaterials* **27,** 3413–31 (2006).
75. Olalde, B. *et al.* Multifunctional bioactive glass scaffolds coated with layers of poly(d,l-lactide-co-glycolide) and poly(n-isopropylacrylamide-co-acrylic acid) microgels loaded with vancomycin. *Mater. Sci. Eng. C* **33,** 3760–3767 (2013).
76. Kim, H.-W., Knowles, J. C. & Kim, H.-E. Hydroxyapatite/poly(ε-caprolactone) composite coatings on hydroxyapatite porous bone scaffold for drug delivery. *Biomaterials* **25,** 1279–1287 (2004).
77. Murthy, R. in *Controlled and novel drug delivery* (ed. Jain, N.) 27–51 (CBS Publishers & Distributors, 1997).
78. Zhao, J., Duan, K., Zhang, J. W., Lu, X. & Weng, J. The influence of polymer concentrations on the structure and mechanical properties of porous polycaprolactone-coated hydroxyapatite scaffolds. *Appl. Surf. Sci.* **256,** 4586–4590 (2010).
79. Peroglio, M. *et al.* Toughening of bio-ceramics scaffolds by polymer coating. *J. Eur. Ceram. Soc.* **27,** 2679–2685 (2007).
80. Eqtesadi, S., Motealleh, A., Pajares, A., Guiberteau, F. & Miranda, P. Influence of sintering temperature on the mechanical properties of ϵ-PCL-impregnated 45S5 bioglass-derived scaffolds fabricated by robocasting. *J. Eur. Ceram. Soc.* **35,** 3985–3993 (2015).
81. Eqtesadi, S., Motealleh, A., Pajares, A., Guiberteau, F. & Miranda, P. in *Journal of Non-Crystalline Solids* (2015).
82. Mantsos, T. *et al.* Non-crystalline composite tissue engineering scaffolds using boron-containing bioactive glass and poly(D,L-lactic acid) coatings. *Biomed. Mater.* **4,** 055002 (2009).
83. Henriksen, S. S., Ding, M., Juhl, M. V., Theilgaard, N. & Overgaard, S. Mechanical strength of ceramic scaffolds reinforced with biopolymers is comparable to that of human bone. *J. Mater. Sci. Mater. Med.* **22,** 1111–1118 (2011).

84. Liu, W. & Cao, Y. in *Tissue Engineering for the Hand: Research Advances and Clinical Applications* (eds. Chang, J. & Gupta, G.) 271 (World Scientific, 2010).

85. Agrawal, C. M. & Ray, R. B. Biodegradable polymeric scaffolds for musculoskeletal tissue engineering. *J. Biomed. Mater. Res.* **55,** 141–50 (2001).

86. Boccaccini, A. R. & Maquet, V. Bioresorbable and bioactive polymer/Bioglass?? composites with tailored pore structure for tissue engineering applications. *Compos. Sci. Technol.* **63,** 2417–2429 (2003).

87. Kim, K. *et al.* The influence of stereolithographic scaffold architecture and composition on osteogenic signal expression with rat bone marrow stromal cells. *Biomaterials* **32,** 3750–63 (2011).

88. Zadpoor, A. A. Bone tissue regeneration: the role of scaffold geometry. *Biomater. Sci.* **3,** 231–245 (2015).

89. Balasubramanian, P., Roether, J. A., Schubert, D. W., Beier, J. P. & Boccaccini, A. R. Bi-layered porous constructs of PCL-coated 45S5 bioactive glass and electrospun collagen-PCL fibers. *J. Porous Mater.* (2015).

90. Chen, Q. Z., Thompson, I. D. & Boccaccini, A. R. 45S5 Bioglass®-derived glass-ceramic scaffolds for bone tissue engineering. *Biomaterials* **27,** 2414–2425 (2006).

91. Vitale-Brovarone, C., Baino, F. & Verné, E. High strength bioactive glass-ceramic scaffolds for bone regeneration. *J. Mater. Sci. Mater. Med.* **20,** 643–53 (2009).

92. Studart, A. R., Gonzenbach, U. T., Tervoort, E. & Gauckler, L. J. Processing Routes to Macroporous Ceramics: A Review. *J. Am. Ceram. Soc.* **89,** 1771–1789 (2006).

93. Hong, Y., Zhou, J. G. & Yao, D. Porogen Templating Processes: An Overview. *J. Manuf. Sci. Eng.* **136,** 031013 (2014).

94. Studart, A. R., Gonzenbach, U. T., Tervoort, E. & Gauckler, L. J. Processing routes to macroporous ceramics: A review. in *Journal of the American Ceramic Society* **89,** 1771–1789 (2006).

95. Pokhrel, A., Seo, D. N., Lee, S. T. & Kim, I. J. Processing of Porous Ceramics by Direct Foaming. *J. Korean Ceram. Soc.* **50,** 93–102 (2013).

96. Liu, F.-H. Synthesis of bioceramic scaffolds for bone tissue engineering by rapid prototyping technique. *J. Sol-Gel Sci. Technol.* **64,** 704–710 (2012).
97. Abdelaal, O. A. M. & Darwish, S. M. H. in *Characterization and Development of Biosystems and Biomaterials* (eds. Öchsner, A., da Silva, L. F. M. & Altenbach, H.) 33–54 (Springer Berlin Heidelberg, 2013).
98. Yang, S., Leong, K.-F., Du, Z. & Chua, C.-K. The design of scaffolds for use in tissue engineering. Part II. Rapid prototyping techniques. *Tissue Eng.* **8,** 1–11 (2002).
99. Du, D., Asaoka, T., Ushida, T. & Furukawa, S, K. Fabrication and perfusion culture of anatomically shaped artificial bone using stereolithography. *Biofabrication* **6,** 1–11 (2014).
100. Tesavibul, P. *et al.* Processing of 45S5 Bioglass® by lithography-based additive manufacturing. *Mater. Lett.* **74,** 81–84 (2012).
101. Kim, J. Y. *et al.* Development of a bone scaffold using HA nanopowder and micro-stereolithography technology. *Microelectron. Eng.* **84,** 1762–1765 (2007).
102. Liu, J., Hu, H., Li, P., Shuai, C. & Peng, S. Fabrication and Characterization of Porous 45S5 Glass Scaffolds via Direct Selective Laser Sintering. *Mater. Manuf. Process.* (2013).
103. Kolan, K. C. R., Leu, M. C., Hilmas, G. E., Brown, R. F. & Velez, M. Fabrication of 13-93 bioactive glass scaffolds for bone tissue engineering using indirect selective laser sintering. *Biofabrication* **3,** 025004 (2011).
104. Eqtesadi, S. *et al.* A simple recipe for direct writing complex 45S5 Bioglass® 3D scaffolds. *Mater. Lett.* **93,** 68–71 (2013).
105. Fu, Q., Saiz, E. & Tomsia, A. P. Direct ink writing of highly porous and strong glass scaffolds for load-bearing bone defects repair and regeneration. *Acta Biomater.* **7,** 3547–54 (2011).
106. Lewis, J. A. & Gratson, G. M. Direct writing in three dimensions. *Mater. Today* **7,** 32–39 (2004).
107. Chang, C. C., Boland, E. D., Williams, S. K. & Hoying, J. B. Direct-write bioprinting three-dimensional biohybrid systems for future regenerative therapies. *J. Biomed. Mater. Res. B. Appl. Biomater.* **98,** 160–70 (2011).
108. Lewis, J. A., Smay, J. E., Stuecker, J. & Cesarano, J. Direct ink writing of three-dimensional ceramic structures. *J. Am. Ceram. Soc.* **89,** 3599–3609 (2006).

109. Lewis, J. A. Direct ink writing of 3D functional materials. *Adv. Funct. Mater.* **16,** 2193–2204 (2006).

110. Cesarano, J. A Review of Robocasting Technology. *MRS Proc.* **542,** 133 (1998).

111. Cesarano, J., Segalman, R. & Calvert, P. Robocasting provides moldless fabrication from slurry deposition. *Ceram. Ind.* **148,** 94–102 (1998).

112. Dellinger, J. G., Cesarano, J. & Jamison, R. D. Robotic deposition of model hydroxyapatite scaffolds with multiple architectures and multiscale porosity for bone tissue engineering. *J. Biomed. Mater. Res. - Part A* **82,** 383–394 (2007).

113. Gratson, G. M. Colloidal and polyelectrolyte inks for direct-write assembly of 3D periodic structures. *ProQuest Diss. Theses; Thesis (Ph.D.)--University Illinois Urbana-Champaign* (2005).

114. Cai, K. *et al.* Geometrically Complex Silicon Carbide Structures Fabricated by Robocasting. *J. Am. Ceram. Soc.* **95,** 2660–2666 (2012).

115. Dellinger, J. G., Wojtowicz, A. M. & Jamison, R. D. Effects of degradation and porosity on the load bearing properties of model hydroxyapatite bone scaffolds. *J. Biomed. Mater. Res. A* **77,** 563–71 (2006).

116. Deliormanlı, A. M. & Rahaman, M. N. Direct-write assembly of silicate and borate bioactive glass scaffolds for bone repair. *J. Eur. Ceram. Soc.* **32,** 3637–3646 (2012).

117. Gao, C., Rahaman, M. N., Gao, Q., Teramoto, A. & Abe, K. Robotic deposition and *in vitro* characterization of 3D gelatin-bioactive glass hybrid scaffolds for biomedical applications. *J. Biomed. Mater. Res. A* **101,** 2027–37 (2013).

118. Attia, S., Wang, J., Wu, G., Shen, J. & Ma, J. Review on Sol—Gel Derived Coatings: Process, Techniques and Optical Applications. *J. Mater. Sci. Technol.* **18,** 211–218 (2002).

119. Martínez-Vázquez, F. J., Miranda, P., Guiberteau, F. & Pajares, A. Reinforcing bioceramic scaffolds with in situ synthesized ε-polycaprolactone coatings. *J. Biomed. Mater. Res. - Part A* **101,** 3551–3559 (2013).

120. Bretcanu, O. *et al.* Electrospun nanofibrous biodegradable polyester coatings on Bioglass®-based glass-ceramics for tissue engineering. *Mater. Chem. Phys.* **118,** 420–426 (2009).

121. Califano, V. *et al.* Matrix assisted pulsed laser evaporation (MAPLE) of poly(D,L lactide) (PDLLA) on Three Dimensional Bioglass Structures. *Adv. Eng. Mater.* **11,** 685–689 (2009).
122. Peroglio, M. *et al.* Toughening of bio-ceramics scaffolds by polymer coating. *J. Eur. Ceram. Soc.* **27,** 2679–2685 (2007).
123. Martínez-Vázquez, F., Pajares, A., Guiberteau, F. & Miranda, P. Effect of Polymer Infiltration on the Flexural Behavior of β-Tricalcium Phosphate Robocast Scaffolds. *Materials (Basel).* **7,** 4001–4018 (2014).
124. Roohani-Esfahani, S. I., Nouri-Khorasani, S., Lu, Z., Appleyard, R. & Zreiqat, H. The influence hydroxyapatite nanoparticle shape and size on the properties of biphasic calcium phosphate scaffolds coated with hydroxyapatite-PCL composites. *Biomaterials* **31,** 5498–5509 (2010).
125. Roohani-Esfahani, S. I., Nouri-Khorasani, S., Lu, Z. F., Appleyard, R. C. & Zreiqat, H. Effects of bioactive glass nanoparticles on the mechanical and biological behavior of composite coated scaffolds. *Acta Biomater.* **7,** 1307–1318 (2011).
126. Kang, Y. *et al.* Enhanced mechanical performance and biological evaluation of a PLGA coated ??-TCP composite scaffold for load-bearing applications. *Eur. Polym. J.* **47,** 1569–1577 (2011).
127. Martínez-Vázquez, F. J., Perera, F. H., Miranda, P., Pajares, A. & Guiberteau, F. Improving the compressive strength of bioceramic robocast scaffolds by polymer infiltration. *Acta Biomater.* **6,** 4361–4368 (2010).
128. Miao, X., Tan, L. P., Tan, L. S. & Huang, X. Porous calcium phosphate ceramics modified with PLGA-bioactive glass. *Mater. Sci. Eng. C* **27,** 274–279 (2007).
129. Kang, Y. *et al.* Enhanced mechanical performance and biological evaluation of a PLGA coated β-TCP composite scaffold for load-bearing applications. *Eur. Polym. J.* **47,** 1569–1577 (2011).
130. Kim, H.-W., Knowles, J. C. & Kim, H.-E. Development of hydroxyapatite bone scaffold for controlled drug release via poly(epsilon-caprolactone) and hydroxyapatite hybrid coatings. *J. Biomed. Mater. Res. B. Appl. Biomater.* **70,** 240–249 (2004).
131. Peroglio, M. *et al.* Mechanical properties and cytocompatibility of poly(ε-caprolactone)- infiltrated biphasic calcium phosphate scaffolds with bimodal pore distribution. *Acta Biomater.* **6,** 4369–4379 (2010).

132. Bang, L. T., Tsuru, K., Munar, M., Ishikawa, K. & Othman, R. Mechanical behavior and cell response of PCL coated α-TCP foam for cancellous-type bone replacement. *Ceram. Int.* **39,** 5631–5637 (2013).

133. Foroughi, M. R., Karbasi, S. & Ebrahimi-Kahrizsangi, R. Physical and mechanical properties of a poly-3-hydroxybutyrate-coated nanocrystalline hydroxyapatite scaffold for bone tissue engineering. *J. Porous Mater.* **19,** 667–675 (2011).

134. Foroughi, M. R., Karbasi, S. & Ebrahimi-Kahrizsangi, R. Mechanical evaluation of nHAp scaffold coated with poly-3-hydroxybutyrate for bone tissue engineering. *J. Nanosci. Nanotechnol.* **13,** 1555–62 (2013).

135. Chen, Q. Z. & Boccaccini, A. R. Poly(D,L-lactic acid) coated 45S5 Bioglass??-based scaffolds: Processing and characterization. *J. Biomed. Mater. Res. - Part A* **77,** 445–457 (2006).

136. Bretcanu, O. *et al.* Biodegradable polymer coated 45S5 Bioglass-derived glass-ceramic scaffolds for bone tissue engineering. *Glas. Technol. Eur. J. Glas. Sci. Technol. Part A* **48,** 227–234 (2007).

137. Li, W. *et al.* Preparation and characterization of PHBV microsphere/45S5 bioactive glass composite scaffolds with vancomycin releasing function. *Mater. Sci. Eng. C* **41,** 320–328 (2014).

138. Li, J. J. *et al.* Multiple silk coatings on biphasic calcium phosphate scaffolds: Effect on physical and mechanical properties and *in vitro* osteogenic response of human mesenchymal stem cells. *Biomacromolecules* **14,** 2179–2188 (2013).

139. Wu, C., Zhang, Y., Zhu, Y., Friis, T. & Xiao, Y. Structure-property relationships of silk-modified mesoporous bioglass scaffolds. *Biomaterials* **31,** 3429–3438 (2010).

140. R., G., Kumar, G. S. & Girija, E. K. Polymer coated phosphate glass/hydroxyapatite composite scaffolds for bone tissue engineering applications. *RSC Adv.* **5,** 60188–60198 (2015).

141. Erol, M., Özyuğuran, A., Özarpat, Ö. & Küçükbayrak, S. 3D Composite scaffolds using strontium containing bioactive glasses. *J. Eur. Ceram. Soc.* **32,** 2747–2755 (2012).

142. Desimone, D. *et al.* Biosilicate ® –gelatine bone scaffolds by the foam replica technique: development and characterization. *Sci. Technol. Adv. Mater.* **14,** 045008 (2013).

143. Hum, J. *et al.* Stiffness improvement of 45S5 bioglass??-based scaffolds through natural and synthetic biopolymer coatings: An ultrasonic study. *Strain* **49,** 431–439 (2013).
144. Metze, A. L. *et al.* Gelatin Coated 45S5 Bioglass®-Derived Scaffolds for Bone Tissue Engineering. in *Key Engineering Materials* **541,** 31–39 (2013).
145. Chen, Q. Z. *et al.* Collagen release kinetics of surface functionalized 45S5 Bioglass??-based porous scaffolds. *J. Biomed. Mater. Res. - Part A* **86,** 987–995 (2008).
146. Erol, M. M. *et al.* Copper-releasing, boron-containing bioactive glass-based scaffolds coated with alginate for bone tissue engineering. *Acta Biomater.* **8,** 792–801 (2012).
147. Yang, G. *et al.* Counterionic biopolymers-reinforced bioactive glass scaffolds with improved mechanical properties in wet state. *Mater. Lett.* **75,** 80–83 (2012).
148. Li, W. *et al.* 45S5 bioactive glass-based scaffolds coated with cellulose nanowhiskers for bone tissue engineering. *RSC Adv.* 56156–56164 (2014). doi:10.1039/c4ra07740g
149. Liu, B., Lin, P., Shen, Y. & Dong, Y. Porous bioceramics reinforced by coating gelatin. *J. Mater. Sci. Mater. Med.* **19,** 1203–1207 (2008).
150. Ratanavaraporn, J., Damrongsakkul, S., Sanchavanakit, Neeracha Banaprasert, T. & Kanokpanont, S. Comparison of Gelatin and Collagen Scaffolds for Fibroblast Cell Culture. *J. Met. Mater. Miner.* **16,** 31–36 (2006).
151. Ratanavaraporn, J., Rangkupan, R., Jeeratawatchai, H., Kanokpanont, S. & Damrongsakkul, S. Influences of physical and chemical crosslinking techniques on electrospun type A and B gelatin fiber mats. *Int. J. Biol. Macromol.* **47,** 431–8 (2010).
152. Bhat, R. & Karim, A. A. Ultraviolet irradiation improves gel strength of fish gelatin. *Food Chem.* **113,** 1160–1164 (2009).
153. Bessho, M., Kojima, T., Okuda, S. & Hara, M. Radiation-Induced Cross-Linking of Gelatin by Using γ-Rays: Insoluble Gelatin Hydrogel Formation. *Bull. Chem. Soc. Jpn.* **80,** 979–985 (2007).
154. Correia, D. M. *et al.* Thermal and hydrolytic degradation of electrospun fish gelatin membranes. *Polym. Test.* **32,** 995–1000 (2013).

155. Cicuéndez, M., Izquierdo-Barba, I., Sánchez-Salcedo, S., Vila, M. & Vallet-Regí, M. Biological performance of hydroxyapatite-biopolymer foams: *in vitro* cell response. *Acta Biomater.* **8,** 802–10 (2012).

156. Amadori, S. *et al.* Effect of sterilization and crosslinking on gelatin films. *J. Mater. Sci. Mater. Med.* **26,** 69 (2015).

157. Li, W. *et al.* Antibacterial 45S5 Bioglass®-based scaffolds reinforced with genipin cross-linked gelatin for bone tissue engineering. *J. Mater. Chem. B* **3,** 3367–3378 (2015).

158. Gil-Albarova, J. *et al. In vivo* osteointegration of three-dimensional crosslinked gelatin-coated hydroxyapatite foams. *Acta Biomater.* **8,** 3777–83 (2012).

159. Bellucci, D., Sola, A., Gentile, P., Ciardelli, G. & Cannillo, V. Biomimetic coating on bioactive glass-derived scaffolds mimicking bone tissue. *J. Biomed. Mater. Res. A* **100,** 3259–66 (2012).

160. Yao, Q. *et al.* Bioglass®-based scaffolds incorporating polycaprolactone and chitosan coatings for controlled vancomycin delivery. *Ceram. Int.* **39,** 7517–7522 (2013).

161. Roohani-Esfahani, S. I. *et al.* Effect of self-assembled nanofibrous silk/polycaprolactone layer on the osteoconductivity and mechanical properties of biphasic calcium phosphate scaffolds. *Acta Biomater.* **8,** 302–312 (2012).

162. Tierney, M. J. in *Handbook of Chemical and Biological Sensors* (eds. Taylor, I. F. & Schultz, J. .) 359 (CRC Press, 1996).

163. Kokubo, T., Kushitani, H., Sakka, S., Kitsugi, T. & Yamamuro, T. Solutions able to reproduce *in vivo* surface-structure changes in bioactive glass-ceramic A-W3. *J. Biomed. Mater. Res.* **24,** 721–734 (1990).

164. Eqtesadi, S. Design and development of bioactive glass/ ceramic scaffolds fabricated by robocasting for bone tissue engineering. (University of Extremadura, 2015).

165. El-Ghannam, A., Hamazawy, E. & Yehia, A. Effect of thermal treatment on bioactive glass microstructure, corrosion behavior, zeta potential, and protein adsorption. *J. Biomed. Mater. Res.* **55,** 387–395 (2001).

166. Erol, M., Küçükbayrak, S. & Ersoy-Meriçboyu, A. Influence of particle size on the crystallization kinetics of glasses produced from waste materials. *J. Non. Cryst. Solids* **357,** 211–219 (2011).

167. Chen, Q. & Boccaccini, A. R. Coupling Mechanical Competence and Bioresorbability in Bioglass®-Derived Tissue Engineering Scaffolds. *Adv. Eng. Mater.* **8,** 285–289 (2006).
168. Boccaccini, A. R., Chen, Q., Lefebvre, L., Gremillard, L. & Chevalier, J. Sintering, crystallisation and biodegradation behaviour of Bioglass-derived glass-ceramics. *Faraday Discuss.* **136,** 27–44; discussion 107–123 (2007).
169. Chen, Q. Z., Xu, J. L., Yu, L. G., Fang, X. Y. & Khor, K. A. Spark plasma sintering of sol–gel derived 45S5 Bioglass®-ceramics: Mechanical properties and biocompatibility evaluation. *Mater. Sci. Eng. C* **32,** 494–502 (2012).
170. Lefebvre, L. *et al.* Structural transformations of bioactive glass 45S5 with thermal treatments. *Acta Mater.* **55,** 3305–3313 (2007).
171. Bretcanu, O. *et al.* Sintering and crystallisation of 45S5 Bioglass?? powder. *J. Eur. Ceram. Soc.* **29,** 3299–3306 (2009).
172. Chen, Q. Z., Xu, J. L., Yu, L. G., Fang, X. Y. & Khor, K. A. Spark plasma sintering of sol-gel derived 45S5 Bioglass®-ceramics: Mechanical properties and biocompatibility evaluation. *Mater. Sci. Eng. C* **32,** 494–502 (2012).
173. Guillon, O., Cao, S., Chang, J., Wondraczek, L. & Boccaccini, A. R. Effect of uniaxial load on the sintering behaviour of 45S5 Bioglass® powder compacts. *J. Eur. Ceram. Soc.* **31,** 999–1007 (2011).
174. Chen, Q. Z., Thompson, I. D. & Boccaccini, A. R. 45S5 Bioglass??-derived glass-ceramic scaffolds for bone tissue engineering. *Biomaterials* **27,** 2414–2425 (2006).
175. Miranda, P., Pajares, A., Saiz, E., Tomsia, A. P. & Guiberteau, F. Fracture modes under uniaxial compression in hydroxyapatite scaffolds fabricated by robocasting. *J. Biomed. Mater. Res. - Part A* **83,** 646–655 (2007).
176. Miranda, P., Pajares, A. & Guiberteau, F. Finite element modeling as a tool for predicting the fracture behavior of robocast scaffolds. *Acta Biomater.* **4,** 1715–1724 (2008).
177. Gibson, L. J. Cellular Solids. *MRS Bulletin* **28,** 270–274 (2003).
178. Chen, Q., Mohn, D. & Stark, W. J. Optimization of Bioglass® scaffold fabrication process. *J. Am. Ceram. Soc.* **94,** 4184–4190 (2011).

179. Meng, D. *et al. In vitro* evaluation of 45S5 Bioglass??-derived glass-ceramic scaffolds coated with carbon nanotubes. *J. Biomed. Mater. Res. - Part A* **99 A,** 435–444 (2011).

180. Hench, L. L. Bioceramics. *J. Am. Ceram. Soc.* **81,** 1705–1728 (1998).

181. Jones, J. R. *et al.* Optimising bioactive glass scaffolds for bone tissue engineering. *Biomaterials* **27,** 964–973 (2006).

182. Abarrategi, A. *et al.* Biological properties of solid free form designed ceramic scaffolds with bmp-2: *In vitro* and *in vivo* evaluation. *PLoS One* **7,** 1–10 (2012).

183. Lan Levengood, S. K. *et al.* Multiscale osteointegration as a new paradigm for the design of calcium phosphate scaffolds for bone regeneration. *Biomaterials* **31,** 3552–3563 (2010).

184. Abarrategi, a *et al.* Label-free magnetic resonance imaging to locate live cells in three-dimensional porous scaffolds. *J. R. Soc. Interface* **9,** 2321–31 (2012).

185. Miranda, P., Pajares, A., Guiberteau, F., Cumbrera, F. L. & Lawn, B. R. Role of flaw statistics in contact fracture of brittle coatings. *Acta Mater.* **49,** 3719–3726 (2001).

186. Kim, H.-W. *et al.* Effect of Flaw State on the Strength of Brittle Coatings on Soft Substrates. *J. Am. Ceram. Soc.* **84,** 2377–2384 (2004).

187. Hench, L. in *Biomaterials, Artificial Organs and Tissue Engineering* (eds. Hench, L. & Jones, J.) 79–89 (Woodhead Publishing Limited and CRC Press LLC, 2005).

188. Martínez-Vázquez, F. J. *et al.* Impregnation of β-tricalcium phosphate robocast scaffolds by in situ polymerization. *J. Biomed. Mater. Res. - Part A* **101,** 3086–3096 (2013).

189. Weibull, W. A statistical distribution function of wide applicability. *J. Appl. Mech.* **18,** 293–297 (1951).

190. Martínez-Vázquez, F. J., Pajares, A., Guiberteau, F. & Miranda, P. Effect of polymer infiltration on the flexural behavior of β-tricalcium phosphate robocast scaffolds. *Materials (Basel).* **7,** 4001–4018 (2014).

191. Rajkumar, M., Meenakshisundaram, N. & Rajendran, V. Development of nanocomposites based on hydroxyapatite/sodium alginate: Synthesis and characterisation. *Mater. Charact.* **62,** 469–479 (2011).

192. Darder, M. & Ruiz-Hitzky, E. in *Workshop Lectures Series* (eds. Carrado, K. A. & Bergaya, F.) 233–257 (The Clay Minerals Society, 2007).
193. Coradin, T., Allouche, J., Boissiere, M. & Livage, J. Sol-Gel Biopolymer/Silica Nanocomposites in Biotechnology. *Current Nanoscience* **2,** 219–230 (2006).
194. Gupta, M. K., Vanwert, A. & Bogner, R. H. Formation of physically stable amorphous drugs by milling with Neusilin. *J. Pharm. Sci.* **92,** 536–51 (2003).
195. Oudadesse, H., Bui, X.-V., Gal, Y. Le, Mostafa, A. & Cathelineau, G. Chitosan Effects on Bioactive Glass for Application as Biocopmosite Biomaterial. *Int. J. Biol. Biomed. Eng.* **5,** 49–56 (2011).
196. Rashidova, S. S. *et al.* Bionanocompositional chitosan-silica sorbent for liquid chromatography. *J. Chromatogr. B* **800,** 49–53 (2004).
197. Al-Sagheer, F. & Muslim, S. Thermal and mechanical properties of chitosan/SiO2 hybrid composites. *J. Nanomater.* **2010,** 1–7 (2010).
198. Nilsen-Nygaard, J., Strand, S., Vårum, K., Draget, K. & Nordgård, C. Chitosan: Gels and Interfacial Properties. *Polymers (Basel).* **7,** 552–579 (2015).
199. Budnyak, T. M., Pylypchuk, I. V, Tertykh, V. A., Yanovska, E. S. & Kolodynska, D. Synthesis and adsorption properties of chitosan-silica nanocomposite prepared by sol-gel method. *Nanoscale Res. Lett.* **10,** 87 (2015).
200. Kevadiya, B. D., Patel, H. A., Joshi, G. V, Abdi, S. H. R. & Bajaj, H. C. Montmorillonite-Alginate Composites as a Drug delivery System: Intercalation and *In vitro* Release of Diclofenac sodium. *Indian J. Pharm. Sci.* **72,** 732–737 (2010).
201. Pongjanyakul, T. & Puttipipatkhachorn, S. Sodium alginate-magnesium aluminum silicate composite gels: characterization of flow behavior, microviscosity, and drug diffusivity. *AAPS PharmSciTech* **8,** E72 (2007).
202. Dandoy, P., Meunier, C. F., Michiels, C. & Su, B. L. Hybrid shell engineering of animal cells for immune protections and regulation of drug delivery: Towards the design of 'Artificial Organs'. *PLoS One* **6,** (2011).
203. Bingel, L., Groh, D., Karpukhina, N. & Brauer, D. S. Influence of dissolution medium pH on ion release and apatite formation of Bioglass® 45S5. *Mater. Lett.* **143,** 279–282 (2015).

204. Loosli, F., Le Coustumer, P. & Stoll, S. Effect of natural organic matter on the disagglomeration of manufactured TiO2 nanoparticles. *Environ. Sci. Nano* **1,** 154 (2014).

205. Harnsilawat, T., Pongsawatmanit, R. & Mcclements, D. Characterization of β-lactoglobulin–sodium alginate interactions in aqueous solutions: A calorimetry, light scattering, electrophoretic mobility and solubility study. *Food Hydrocoll.* **20,** 577–585 (2006).

206. Gioffre, M., Torricelli, P., Panzavolta, S., Rubini, K. & Bigi, A. Role of pH on stability and mechanical properties of gelatin films. *Journal of Bioactive and Compatible Polymers* **27,** 67–77 (2012).

207. Allo, B. A., Rizkalla, A. S. & Mequanint, K. Synthesis and electrospinning of ε-polycaprolactone-bioactive glass hybrid biomaterials via a sol-gel process. *Langmuir* **26,** 18340–8 (2010).

208. Joubert, M., Delaite, C., Bourgeat-Lami, E. & Dumas, P. Ring-opening polymerization of ?-caprolactone andL-lactide from silica nanoparticles surface. *J. Polym. Sci. Part A Polym. Chem.* **42,** 1976–1984 (2004).

209. Yan, S. *et al.* Surface-grafted silica linked with l-lactic acid oligomer: A novel nanofiller to improve the performance of biodegradable poly(l-lactide). *Polymer (Guildf).* **48,** 1688–1694 (2007).

210. Moon, J.-H., Ramaraj, B., Lee, S. M. & Yoon, K. R. Direct grafting of ε-caprolactone on solid core/mesoporous shell silica spheres by surface-initiated ring-opening polymerization. *J. Appl. Polym. Sci.* **107,** 2689–2694 (2008).

211. Hench, L. L. & Wilson, J. Surface-active biomaterials. *Science* **226,** 630–636 (1984).

212. Huang, W., Day, D. E., Kittiratanapiboon, K. & Rahaman, M. N. Kinetics and mechanisms of the conversion of silicate (45S5), borate, and borosilicate glasses to hydroxyapatite in dilute phosphate solutions. *J. Mater. Sci. Mater. Med.* **17,** 583–596 (2006).

213. Fu, Q., Rahaman, M. N., Fu, H. & Liu, X. Silicate, borosilicate, and borate bioactive glass scaffolds with controllable degradation rate for bone tissue engineering applications. I. Preparation and *in vitro* degradation. *J. Biomed. Mater. Res. - Part A* **95,** 164–171 (2010).

214. Khawam, A. & Flanagan, D. R. Solid-state kinetic models: Basics and mathematical fundamentals. *J. Phys. Chem. B* **110,** 17315–17328 (2006).

215. Xin, R., Zhang, Q. & Gao, J. Identification of the wollastonite phase in sintered 45S5 bioglass and its effect on *in vitro* bioactivity. *J. Non. Cryst. Solids* **356,** 1180–1184 (2010).

216. Kashyap, S., Griep, K. & Nychka, J. A. Crystallization kinetics, mineralization and crack propagation in partially crystallized bioactive glass 45S5. *Mater. Sci. Eng. C* **31,** 762–769 (2011).

217. Sung, H.-J., Meredith, C., Johnson, C. & Galis, Z. S. The effect of scaffold degradation rate on three-dimensional cell growth and angiogenesis. *Biomaterials* **25,** 5735–5742 (2004).

218. Blaker, J. J., Nazhat, S. N., Maquet, V. & Boccaccini, A. R. Long-term *in vitro* degradation of PDLLA/Bioglass?? bone scaffolds in acellular simulated body fluid. *Acta Biomater.* **7,** 829–840 (2011).

219. Nair, L. S. & Laurencin, C. T. Biodegradable polymers as biomaterials. *Progress in Polymer Science (Oxford)* **32,** 762–798 (2007).

220. Mohamed, K. R., Beherei, H. H. & El-Rashidy, Z. M. *In vitro* study of nano-hydroxyapatite/chitosan-gelatin composites for bio-applications. *J. Adv. Res.* **5,** 201–8 (2014).

221. in *Pharmaceutical Capsules* (eds. Podczeck, F. & Jones, B. E.) 95 (Pharmaceutical Press, 2004).

222. Draget, K. I., Smidsrød, O. & Skjåk-Bræk, G. in *Polysaccharides and Polyamides in the Food Industry* (eds. Steinbuchel, A. & Rhee, S. K.) 1–30 (Wiley-VCH-Verlag, 2005).

223. Despond, S., Espuche, E., Cartier, N. & Domard, A. Hydration mechanism of polysaccharides: A comparative study. *J. Polym. Sci. Part B Polym. Phys.* **43,** 48–58 (2005).

224. Zhang, R. & Ma, P. X. Porous poly(L-lactic acid)/apatite composites created by biomimetic process. *J. Biomed. Mater. Res.* **45,** 285–293 (1999).

225. Saïed, N. & Aider, M. Zeta Potential and Turbidimetry Analyzes for the Evaluation of Chitosan/Phytic Acid Complex Formation. *J. Food Res.* **3,** p71 (2014).

226. Fu, Q., Rahaman, M. N., Sonny Bal, B., Brown, R. F. & Day, D. E. Mechanical and *in vitro* performance of 13-93 bioactive glass scaffolds prepared by a polymer foam replication technique. *Acta Biomater.* **4,** 1854–1864 (2008).

227. Gibson LJ, A. M. Cellular Solids Structure and Properties | Materials science | Cambridge University Press. *Cambridge University Press* (1997).

228. Keller, T. S., Mao, Z. & Spengler, D. M. Young's modulus, bending strength, and tissue physical properties of human compact bone. *J. Orthop. Res.* **8,** 592–603 (1990).